



ATLAS Note

ATL-COM-PHYS-2019-962

17th June 2021



Draft version 11

1

2 WZ + Heavy Flavor Production in pp collisions 3 at $\sqrt{s} = 13$ TeV

4

The ATLAS Collaboration¹, Aaron Webb^a, Peter Onyisi^a

5

^a*Univ. of Texas at Austin*

6

A measurement of the cross-section for production of WZ with an associated heavy flavor jet
7 is performed using 140 fb^{-1} of proton-proton collision data at $\sqrt{s} = 13$ TeV from the ATLAS
8 experiment at the LHC. A measurement of the fully leptonic decay mode, $WZ \rightarrow l\nu ll$, is
9 performed. The cross-section of $WZ + b$ and $WZ + \text{charm}$ in various fiducial regions is
10 measured.

11

© 2021 CERN for the benefit of the ATLAS Collaboration.

Reproduction of this article or parts of it is allowed as specified in the CC-BY-4.0 license.

12 **Contents**

13	1 Changes and outstanding items	4
14	1.1 Changelog	4
15	1.1.1 Changes relative to v11	4
16	1.1.2 Changes relative to v10	4
17	1.1.3 Changes relative to v9	4
18	1.1.4 Changes relative to v8	5
19	1.1.5 Changes relative to v7	5
20	1.1.6 Changes relative to v5	5
21	1.1.7 Changes relative to v4	6
22	1.1.8 Changes relative to v3	6
23	1.1.9 Changes relative to v2	7
24	1.1.10 Changes relative to v1	7
25	1.2 Outstanding Items	7
26	2 Executive Summary	8
27	3 Data and Monte Carlo Samples	9
28	3.1 Data Samples	10
29	3.2 Monte Carlo Samples	10
30	4 Object Reconstruction	12
31	4.1 Trigger	12
32	4.2 Light leptons	13
33	4.3 Jets	14
34	4.4 B-tagged Jets	14
35	4.5 Missing transverse energy	16
36	4.6 Overlap removal	16
37	5 tZ Separation Multivariate Analysis	16
38	5.1 Top Mass Reconstruction	17
39	5.2 tZ BDT	17
40	5.3 tZ Interference Studies	22
41	6 Event Selection and Signal Region Definitions	25
42	6.1 Event Preselection	25
43	6.2 Fit Regions	29
44	6.3 Non-Prompt Lepton Estimation	45
45	6.3.1 $t\bar{t}$ Validation	45
46	6.3.2 Z+jets Validation	48
47	7 Systematic Uncertainties	53
48	8 Results	63

49	8.1	Fit Procedure	63
50	8.2	Results of the Simultaneous Fit	64
51	8.3	Inclusive 1+2 Jet Fit	75
52	8.4	Alternative tZ Inclusive Fit	79
53	8.4.1	tZ Inclusive Fit	79
54	8.4.2	Floating tZ	79
55	9	Conclusion	80
56	A	Appendices	83
57	Appendices		83
58	A.1	Non-prompt lepton MVA	83
59	A.2	Non-prompt CR Modelling	85
60	A.3	DSID list	89

61 List of contributions

Aaron Webb	Main analyser. Responsible for ntuple production, fits, and note writing.
Peter Onyisi	Advisor to Aaron Webb. Analysis design and implementation strategy.

64 **1 Changes and outstanding items**

65 **1.1 Changelog**

66 This is version 12

67 **1.1.1 Changes relative to v11**

- 68 • Added feynman diagrams of WZ+b
69 • Updated text to latest fit results (WZ+c now has asymmetric errors)
70 • Removed yield numbers from some plots to avoid overlap with the legend
71 • Fixed various typos, grammar issues

72 **1.1.2 Changes relative to v10**

- 73 • Included Zjets plots with lep Pt, eta split by flavor
74 • Clarified the text on a few points regarding systematics, results
75 • Fixed an outdated yield table, combined rare top with ttbar
76 • resolved a high Vgamma uncertainty caused by a single large weight event
77 • included correlation plots for the tZ BDT inputs

78 **1.1.3 Changes relative to v9**

- 79 • Reordered note to put fiducial region definition in the intro, tZ BDT before the event
80 selection
81 • moved alternative fit strategies from the appendix into the main text of the note
82 • removed correlation matrix plot from results
83 • added c/light rejection rates for each DL1r WP
84 • updated OR procedure - previously had an outdated algorithm
85 • Updated results section to include latest fits, table summarizing results
86 • Replaced correlation table with a plot

87 **1.1.4 Changes relative to v8**

- 88 • Included more references to appendices in the text
89 • Expanded explanation of fiducial region definition
90 • Previous draft claimed that both standard and custom PLVs were used. Text is fixed to
91 state that a custom PLV is used for lepton iso, but standard lepton id is used
92 • Included plots of PLV output, included WPs used
93 • specified that non-prompt CR plots are post correction
94 • changed title of results section

95 **1.1.5 Changes relative to v7**

- 96 • Moved from LO to NLO tZ sample
97 • Add additional plots of Z+jets and ttbar CRs in Section A.2
98 • Clarified CDI file used, MC ptag, PFlow jet algorithm
99 • Included overlap removal procedure
100 • Included details on PLV
101 • Added plots of missing tZ BDT input features for each fit region
102 • Changed reference on PLV to recent ttH/ttW note
103 • Included alternate fits with WZ+1-2 jet inclusive, tZ floating

104 **1.1.6 Changes relative to v5**

- 105 • added list of DSIDs to an appendix
106 • included systematics on jet migrations
107 • Updated results section to include simultaneous fit over 1-jet and 2-jet bins, describe
108 unfolding procedure
109 • Updated other sections to account for this change
110 • Included info about migrations in Section 5.2

111 **1.1.7 Changes relative to v4**

- 112 • Fixed various typos, clarified wording
 113 • Expanded info about JER uncertainties, electron systematics, theory uncertainties
 114 • removed a table on lepton selection, included information in the text instead
 115 • Plotted lepton Pt Z and W for Zjet CR, rather than lep 1 and 2
 116 • fixed binning in kinematic plots
 117 • Included prefit and postfit yield tables
 118 • added signal modelling systematics
 119 • included alternate fit studies with tZ included in signal

120 **1.1.8 Changes relative to v3**

- 121 • Merged introduction into executive summary, including unblinding details and list of
 122 SRs/CRs used
 123 • listed ptag used (p4133), and release (AB 21.2.127)
 124 • Included table reftab:xsecUnc listing x-sec uncertainties used
 125 • Removed selection criteria listed in table ?? (QMisID, AmbiguityType) that were removed
 126 from the analysis
 127 • specified variable used to make truth jet flavor determination (HadronConeExclTruthLa-
 128 belIID)
 129 • fixed bug in MtLepMet calculation, updated selection/fits to account for this
 130 • Included plots of MtLepMet and PtZ, swapped lep 1 and 2 p_T plots for lep W and lep Z
 131 plots
 132 • updated tZ BDT training to reduce overfitting, updated plots to include error bars, feature
 133 importance
 134 • updated table 8 to clarify selection, fix the tZ_BDT cut used
 135 • replace a few broken ntuples which included large weight events
 136 • include DL1r distribution for Z+jets and t \bar{t} VRs
 137 • Expanded section on fakes, included information on derived scale factors from VRs.
 138 • Changed the kinematic plots to include $p_T(Z)$ and $m_T(W)$, list lepton p_T based on W and
 139 Z candidates.

140 **1.1.9 Changes relative to v2**

- 141 • Added alternate VBS samples to include missing b-jet diagrams
142 • Included a section on tZ interference effects, ??.
143 • Updated to reflect changes for 2018, including the move to PFlow jets, DL1r, updated
144 trigger, and updated AnalysisBase version (now 21.2.127)
145 • Revised fit regions, using separate 1-jet and 2-jet fits, with all 2-j regions included
146 • updated plots for tZ BDT, added details about the model
147 • Included truth jet information

148 **1.1.10 Changes relative to v1**

- 149 • Added GRL list
150 • Fixed latex issue in line 92, typo in line 172
151 • Added tables 6 and ??, summarizing the event and object selection
152 • Added table 2, which includes the DSID of samples used
153 • Included reference to WZ inclusive paper in introduction

154 **1.2 Outstanding Items**

- 155 • Unblind, update plots and fits to include data
156 • Add cross-section, significance once unblinded

157 2 Executive Summary

158 The production of WZ in association with a heavy flavor jet represents an important background
 159 for many major analyses. This includes any process with multiple leptons and b-jets in the final
 160 state, such as $t\bar{t}H$, $t\bar{t}W$, and $t\bar{t}Z$. While precise measurements have been made of inclusive WZ
 161 production [1], $WZ +$ heavy flavor remains poorly understood. This is largely because the QCD
 162 processes involved in the production of the b-jet make it difficult to simulate accurately. This
 163 introduces a large uncertainty for analyses that include this process as a background.

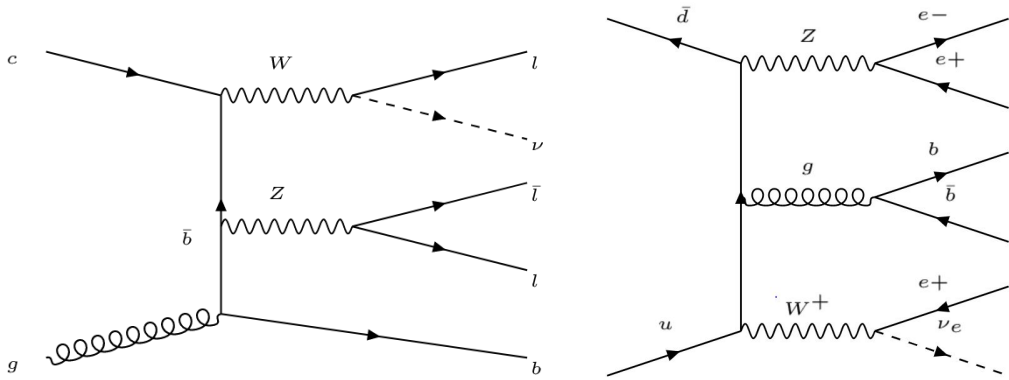


Figure 1: Example Feynman diagrams of $WZ +$ heavy flavor production

164 We perform a study of the fully leptonic decay mode of this channel; that is, events where both
 165 the W and Z decay leptonically. Because WZ has no associated jets at leading order, while the
 166 major backgrounds for this channel tend to have high jet multiplicity, events with more than two
 167 jets are rejected. This gives a final state signature of three leptons and one or two jets.

168 Events that meet a preselection criteria are sorted into regions based on the b-tagging score of
 169 their associated jets. This is done to separate $WZ +$ b-jet events from $WZ +$ charm and WZ
 170 + light jets. These regions are fit to data in order to make a more accurate estimate of the
 171 contribution of $WZ +$ heavy-flavor, where heavy-flavor jets include b-jets and charm jets. The
 172 full Run-2 dataset collected by the ATLAS detector, representing 139 fb^{-1} of data from pp
 173 collisions at $\sqrt{s} = 13 \text{ TeV}$, is used for this study.

174 The fiducial volume at particle level is defined based on the number of stable leptons and jets in
 175 each event. Three light leptons with total charge ± 1 and one or two associated jets are required.
 176 Only leptons which do not originate from hadron or τ decays are considered. The phase space
 177 definitions use dressed kinematics of the final state particles. Leptons are dressed by summing
 178 the momentum of photons within a cone of $\Delta R < 0.1$ of the lepton to correct the leptons energy.
 179 Particle level jets are reconstructed using the anti- k_t algorithm with a radius of $R = 0.4$. The
 180 kinematic selection applied to these objects is summarized below:

- 181 • Three light leptons with total charge ± 1 , $|\eta| < 2.5$

- 182 • OS lepton with $p_T > 10$ GeV, SS leptons with $p_T > 20$ GeV
- 183 • One OSSF lepton pair with $|M(l\bar{l}) - 91.2 \text{ GeV}| < 10 \text{ GeV}$
- 184 • One or two associated truth jets with $p_T > 25 \text{ GeV}, |\eta| < 2.5, R < 0.4$

185 The result of the fit is used to extract the cross-section in this fiducial region for WZ + b and
 186 WZ + c with one associated jet, and WZ + b and WZ + c with two associated jets, where the
 187 number and flavor of the jets is determined at particle level. Events with both charm and b-jets
 188 are counted as WZ + b. The analysis reports a cross-section measurement of WZ + b and WZ +
 189 c, along with their correlations, for both 1-jet and 2-jet exclusive regions. Normalization factors,
 190 representing how the MC prediction differs from the observed result in the fit regions, are also
 191 reported.

192 Section 3 details the data and Monte Carlo (MC) samples used in the analysis. The reconstruction
 193 of various physics objects is described in Section 4. Section 6 describes the event selection applied
 194 to these samples, along with the definitions of the various regions used in the fit. The multivariate
 195 analysis techniques used to separate the tZ background from WZ + heavy flavor are described in
 196 Section 5. Section 7 describes the various sources of systematic uncertainties considered in the
 197 fit. Finally, the results of the analysis are summarized in Section 8, followed by a brief conclusion
 198 in Section 9.

199 **3 Data and Monte Carlo Samples**

200 Both data and Monte Carlo samples used in this analysis were prepared in the xAOD format,
 201 which was used to produce a Dx AOD sample in the HIGG8D1 derivation framework. The HIGG8D1
 202 framework is designed for the $t\bar{t}H$ multi-lepton analysis, which targets events with multiple
 203 leptons as well as tau hadrons. This framework reduces the size of the dataset by removing
 204 events based on event topology and only keeping useful information for each event. Events are
 205 removed from the derivations that do not meet one of the following selections:

- 206 • at least two light leptons within a range $|\eta| < 2.6$, with leading lepton $p_T > 15$ GeV and
 207 subleading lepton $p_T > 5$ GeV
- 208 • OR at least one light lepton with $p_T > 15$ GeV within a range $|\eta| < 2.6$, and at least two
 209 hadronic taus with $p_T > 15$ GeV.

210 Samples were then generated from these HIGG8D1 derivations with p-tag of p4134 for data
 211 and p4133 for Monte Carlo using AnalysisBase version 21.2.127 modified to include custom
 212 variables.

213 3.1 Data Samples

214 The study uses a sample of proton-proton collision data collected by the ATLAS detector from
215 2015 through 2018 at an energy of $\sqrt{s} = 13$ TeV, which represents an integrated luminosity of
216 139 fb^{-1} [2]. This data set was collected with a bunch-crossing spacing of 25 ns. All data used
217 in this analysis was verified by data quality checks [3], having been included in the following
218 Good Run Lists:

- 219** • data15_13TeV.periodAllYear_DetStatus-v79-repro20-02_DQDefects-00-02-02
220 _PHYS_StandardGRL_All_Good_25ns.xml
- 221** • data16_13TeV.periodAllYear_DetStatus-v88-pro20-21_DQDefects-00-02-04
222 _PHYS_StandardGRL_All_Good_25ns.xml
- 223** • data17_13TeV.periodAllYear_DetStatus-v97-pro21-13_Unknown_PHYS_StandardGRL
224 _All_Good_25ns_Triggerno17e33prim.xml
- 225** • data18_13TeV.periodAllYear_DetStatus-v102-pro22-04_Unknown_PHYS_StandardGRL
226 _All_Good_25ns_Triggerno17e33prim.xml

227 Runs included from the AllYear period containers are included.

228 3.2 Monte Carlo Samples

229 Several different generators were used to produce Monte Carlo simulations of the signal and
230 background processes. For all samples, the response of the ATLAS detector is simulated using
231 GEANT4 [4]. The WZ signal samples are simulated using Sherpa 2.2.2 [5]. Signal events are
232 generated using the NNPDF30NNLO PDF set with up to one parton at NLO and 2 to 3 partons
233 at LO [6].

234 The tZ background is simulated at NLO with MADGRAPH5_AMC@NLO, with PYTHIA8 used to
235 perform parton showering and fragmentation. The NNPDF30NNLO PDF set is used.

236 Specific information about the Monte Carlo samples being used can be found in Table 1. A list
237 of the specific samples used by data set ID is shown in Table 2.

Table 1: The configurations used for event generation of signal and background processes, including the event generator, matrix element (ME) order, parton shower algorithm, and parton distribution function (PDF).

Process	Event generator	ME order	Parton Shower	PDF
WZ, VV	SHERPA 2.2.2	MEPS NLO	SHERPA	CT10 [7]
tZ	MG5_AMC [8]	NLO	PYTHIA 8	CTEQ6L1
t̄W	MG5_AMC (SHERPA 2.1.1)	NLO (LO multileg)	PYTHIA 8 (SHERPA)	NNPDF 3.0 NLO (NNPDF 3.0 NLO)
t̄t(Z/γ* → ll)	MG5_AMC	NLO	PYTHIA 8	NNPDF 3.0 NLO
t̄tH	MG5_AMC (MG5_AMC)	NLO (NLO)	PYTHIA 8 (HERWIG++) [9]	NNPDF 3.0 NLO [6] (CT10 [7])
tHqb	MG5_AMC	LO	PYTHIA 8	CT10
tHW	MG5_AMC (SHERPA 2.1.1)	NLO (LO multileg)	HERWIG++ (SHERPA)	CT10 (NNPDF 3.0 NLO)
tWZ	MG5_AMC	NLO	PYTHIA 8	NNPDF 2.3 LO
t̄t̄t, t̄t̄t̄	MG5_AMC	LO	PYTHIA 8	NNPDF 2.3 LO [10]
t̄tW+W-	MG5_AMC	LO	PYTHIA 8	NNPDF 2.3 LO
t̄t	POWHEG-BOX v2 [11]	NLO	PYTHIA 8	NNPDF 3.0 NLO
t̄t̄γ	MG5_AMC	LO	PYTHIA 8	NNPDF 2.3 LO
s-, t-channel, Wt single top	POWHEG-BOX v1 [12]	NLO	PYTHIA 6	CT10
qqVV, VVV Z → l+l-	SHERPA 2.2.1	MEPS NLO	SHERPA	NNPDF 3.0 NLO

Sample	DSID
WZ	364253, 364739-42
VV	364250, 364254, 364255, 363355-60, 364890
t̄W	410155
t̄Z	410156, 410157, 410218-20
low mass t̄Z	410276-8
Rare Top	410397, 410398, 410399
single Top	410658-9, 410644-5
three Top	304014
four Top	410080
t̄WW	410081
Z + jets	364100-41
low mass Z + jets	364198-215
W + jets	364156-97
Vγ	364500-35
tZ	412063-5
tW	410013-4
WtZ	410408
VVV	364242-9
VH	342284-5
WtH	341998
t̄tγ	410389
t̄t	410470
t̄tH	345873-5, 346343-5

Table 2: List of Monte Carlo samples by data set ID used in the analysis.

238 4 Object Reconstruction

239 All regions defined in this analysis share a common lepton, jet, and overall event preselection.
 240 The selection applied to each physics object is detailed here; the event preselection, and the
 241 selection used to define the various fit regions, is described in Section 6.

242 4.1 Trigger

243 Events are required to be selected by dilepton triggers, as summarized in Table 3.

Dilepton triggers (2015)	
$\mu\mu$ (asymm.)	HLT_mu18_mu8noL1
ee (symm.)	HLT_2e12_lhloose_L12EM10VH
$e\mu, \mu e$ (\sim symm.)	HLT_e17_lhloose_mu14
Dilepton triggers (2016)	
$\mu\mu$ (asymm.)	HLT_mu22_mu8noL1
ee (symm.)	HLT_2e17_lhvloose_nod0
$e\mu, \mu e$ (\sim symm.)	HLT_e17_lhloose_nod0_mu14
Dilepton triggers (2017)	
$\mu\mu$ (asymm.)	HLT_mu22_mu8noL1
ee (symm.)	HLT_2e24_lhvloose_nod0
$e\mu, \mu e$ (\sim symm.)	HLT_e17_lhloose_nod0_mu14
Dilepton triggers (2018)	
$\mu\mu$ (asymm.)	HLT_mu22_mu8noL1
ee (symm.)	HLT_2e24_lhvloose_nod0
$e\mu, \mu e$ (\sim symm.)	HLT_e17_lhloose_nod0_mu14

Table 3: List of lowest p_T -threshold, un-prescaled dilepton triggers used for 2015-2018 data taking.

244 4.2 Light leptons

245 Electron candidates are reconstructed from energy clusters in the electromagnetic calorimeter
 246 that are associated with charged particle tracks reconstructed in the inner detector [13]. Electron
 247 candidates are required to have $p_T > 10$ GeV and $|\eta_{\text{cluster}}| < 2.47$. Muon candidates are
 248 reconstructed by combining inner detector tracks with track segments or full tracks in the muon
 249 spectrometer [14]. Muon candidates are required to have $p_T > 10$ GeV and $|\eta| < 2.5$. Candidates
 250 in the transition region between different electromagnetic calorimeter components, $1.37 <$
 251 $|\eta_{\text{cluster}}| < 1.52$, are rejected. A multivariate likelihood discriminant combining shower shape
 252 and track information is used to distinguish real electrons from hadronic showers (fake electrons).
 253 To further reduce the non-prompt electron contribution, the track is required to be consistent
 254 with originating from the primary vertex; requirements are imposed on the transverse impact
 255 parameter significance ($|d_0|/\sigma_{d_0} < 5$) and the longitudinal impact parameter ($|\Delta z_0 \sin \theta_\ell| < 0.5$
 256 mm). Electron candidates are required to pass TightLH identification.

257 Muon candidates are reconstructed by combining inner detector tracks with track segments or
 258 full tracks in the muon spectrometer [14]. Muon candidates are required to have $p_T > 10$ GeV
 259 and $|\eta| < 2.5$. The longitudinal impact parameter is the same for both electrons and muons, while
 260 muons are required to pass a slightly tighter transverse impact parameter, $|d_0|/\sigma_{d_0} < 3$. Muons
 261 are also required to pass Medium ID requirements.

262 Leptons are additionally required to pass a non-prompt BDT selection developed by the $t\bar{t}H$
263 multilepton/ $t\bar{t}W$ analysis group. This BDT and the WPs used are summarized in Appendix A.1,
264 and described in detail in [15]. Optimized working points and scale factors for this BDT are
265 taken from that analysis.

266 **4.3 Jets**

267 Jets are reconstructed from calibrated topological clusters built from energy deposits in the
268 calorimeters [16], as well as information from the inner tracking detector, using the anti- k_t
269 algorithm with a radius parameter $R = 0.4$. Particle Flow, or PFlow, jets are used in the analysis.
270 Jets with energy contributions likely arising from noise or detector effects are removed from
271 consideration [17], and only jets satisfying $p_T > 25$ GeV and $|\eta| < 2.5$ are used in this analysis.
272 For jets with $p_T < 60$ GeV and $|\eta| < 2.4$, a jet-track association algorithm is used to confirm
273 that the jet originates from the selected primary vertex, in order to reject jets arising from pileup
274 collisions [18].

275 **4.4 B-tagged Jets**

276 In order to make a measurement of $WZ +$ heavy flavor it is necessary to distinguish these events
277 from $WZ +$ light jets. For this purpose, the DL1r b-tagging algorithm is used to distinguish
278 heavy flavor jets from lighter ones. The DL1r algorithm [19] uses jet kinematics, particularly
279 jet vertex information, as input for a neural network which assigns each jet a score designed to
280 reflect how likely that jet is to have originated from a b-quark.

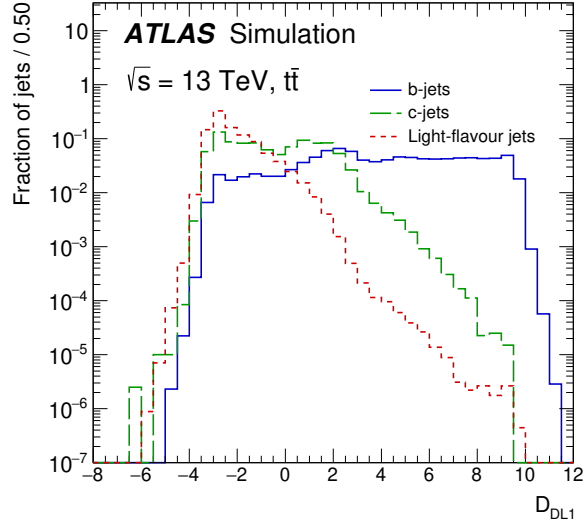


Figure 2: Output distribution of the DL1r algorithm for pure samples of b-jets, charm jets, and light jets, with each normalized to unity [19]

From the output of the BDT, working points (WPs) are developed based on the efficiency of truth b-jets at particular values of the DL1r algorithm. These WPs are taken from the March 2020 CDI file, 2020-21-13TeV-MC16-CDI-2020-03-11_v2.root. The working points used in this analysis are summarized in Table 4.

WP	Rejection		
	b-jet eff.	c-jet	light jet
85%	2.6	29	
77%	4.9	130	
70%	9.4	390	
60%	27	1300	

Table 4: c-jet and light-flavor jet rejections corresponding to each b-tagging Working Point by b-jet efficiency, evaluated on $t\bar{t}$ events.

As shown in table 4, a tighter WP will accept fewer b-jets, but reject a higher fraction of charm and light jets. Generally, analyses that include b-jets will use a fixed working point, for example, requiring that a jet pass the 70% threshold. By instead treating these working points as bins, e.g. events with jets that fall between the 85% and 77% WPs fall into one bin, while events with jets passing the 60% WP fall into another, additional information can be gained. This analysis uses each of these working points to form orthogonal regions in order to provide separation between $WZ + b$, $WZ + c$, and $WZ + \text{light}$.

292 **4.5 Missing transverse energy**

293 Missing transverse momentum (E_T^{miss}) is used as part of the event selection. The missing
 294 transverse momentum vector is defined as the negative of the vector sum of the transverse
 295 momenta of all reconstructed physics objects as well as remaining unclustered energy, the latter
 296 of which is estimated from low- p_T tracks associated with the primary vertex but not assigned
 297 to a hard object, with object definitions taken from [20]. Light leptons considered in the E_T^{miss}
 298 reconstruction are required to have $p_T > 10 \text{ GeV}$, while jets are required to have $p_T > 20 \text{ GeV}$.

299 **4.6 Overlap removal**

300 To avoid double counting objects and remove leptons originating from decays of hadrons, overlap
 301 removal is performed in the following order: any electron candidate within $\Delta R = 0.1$ of another
 302 electron candidate with higher p_T is removed; any electron candidate within $\Delta R = 0.1$ of a muon
 303 candidate is removed; any jet within $\Delta R = 0.2$ of an electron candidate is removed; if a muon
 304 candidate and a jet lie within $\Delta R = \min(0.4, 0.04 + 10[\text{GeV}]/p_T(\text{muon}))$ of each other, the jet
 305 is kept and the muon is removed if the jet has at least three associated tracks, otherwise the jet is
 306 removed and the muon is kept.

307 This algorithm is applied to the preselected objects. The overlap removal procedure is summarized
 308 in Table 5.

Keep	Remove	Cone size (ΔR)
electron	electron (low p_T)	0.1
muon	electron	0.1
electron	jet	0.2
jet	muon	$\min(0.4, 0.04 + 10[\text{GeV}]/p_T(\text{muon}))$, $n_{\text{track}} > 3$
muon	jet	$\min(0.4, 0.04 + 10[\text{GeV}]/p_T(\text{muon}))$, $n_{\text{track}} < 3$

Table 5: Summary of the overlap removal procedure between electrons, muons, and jets.

309 **5 tZ Separation Multivariate Analysis**

310 Because tZ produces a final state identical to the signal, it represents a predominant background
 311 in the most signal enriched regions. That is, the region with one jet passing the 60% DL1r WP.
 312 Therefore, a boosted decision tree (BDT) algorithm is trained to separate WZ + heavy flavor
 313 from tZ.

314 Separation between tZ and WZ + heavy flavor is achieved in part by reconstructing the invariant
 315 mass of the top candidate, which clusters more closely to the top mass for tZ than WZ + heavy

316 flavor. The result of this BDT is used to create a tZ enriched region in the fit, reducing its impact
 317 on the measurement of WZ + heavy flavor.

318 5.1 Top Mass Reconstruction

319 The reconstruction of the top mass follows the procedure described in detail in section 6.1 of
 320 [21]. The mass of the top quark candidate is reconstructed from the jet, the lepton not included
 321 in the Z-candidate, and a reconstructed neutrino. In the case that there is one jet in the event,
 322 there is only one possible b-jet candidate. For events with two jets, the jet with the highest DL1r
 323 score is used.

324 The neutrino from the W decay is expected to be the only source of E_T^{miss} . Therefore, the E_T
 325 and ϕ of the neutrino are taken from the E_T^{miss} measurement. This leaves the z-component of
 326 the neutrino momentum, $p_{\nu z}$ as the only unknown.

327 This unknown is solved for by taking the combined invariant mass of the lepton and neutrino to
 328 give the invariant mass of the W boson:

$$329 \quad (p_l + p_\nu)^2 = m_W^2$$

330 Expanding this out into components, this equation gives:

$$331 \quad \sqrt{p_{T\nu}^2 + p_{z\nu}^2} E_l = \frac{m_W^2 - m_l^2}{2} + p_{T\nu}(p_{lx}\cos\phi_\nu + p_{ly}\sin\phi_\nu) + p_{lz}p_{\nu z}$$

332 This equation gives two solutions for $p_{\nu z}$. For cases where only one of these solutions is real,
 333 that is taken as the value of $p_{\nu z}$. For instances with two real solutions, the one which is shown
 334 to be correct in the largest fraction of simulations is taken. For cases when no real solution is
 335 found, often because of detector effects, the value of E_T^{miss} is varied in decreasing increments of
 336 100 MeV until a real solution is found.

337 The reconstructed top mass distribution for tZ and WZ + b can be seen in figure 3.

338 5.2 tZ BDT

339 A Boosted Decision Tree (BDT), specifically XGBoost [22], is used to provide separation between
 340 tZ and WZ+b. The following kinematic variables are used as inputs:

- 341 • The invariant mass of the reconstructed top candidate
- 342 • p_T of each of the leptons, jet
- 343 • The invariant mass of each combination of lepton pairs, $M(l\bar{l})$

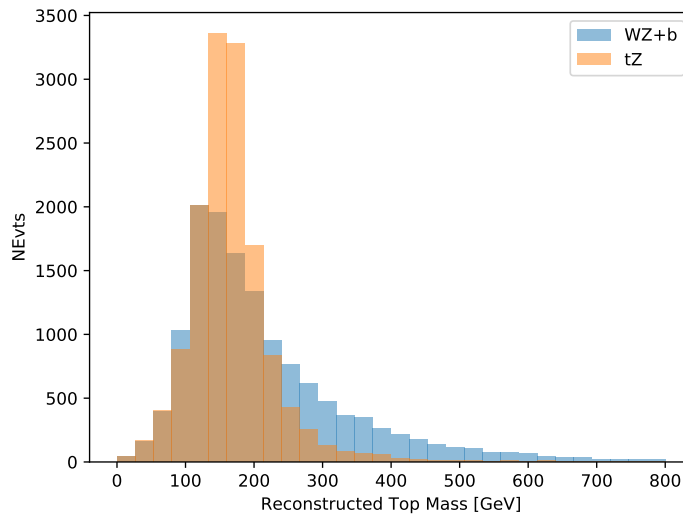


Figure 3: Reconstructed top mass distributions for tZ and WZ + b, measured in MeV.

344 • E_T^{miss}

345 • Distance between each combination of leptons, $\Delta R(ll)$

346 • Distance between each lepton and the jet, $\Delta R(lj)$

347 The training samples included only events meeting the requirements of the 1-jet, 60% b-tag
 348 region, i.e. passing all the selection described in section 6 and having exactly one jet which
 349 passes the tightest (60%) DL1r working point.

350 The distributions of a few of these features for both signal and background are shown in figure
 351 4.

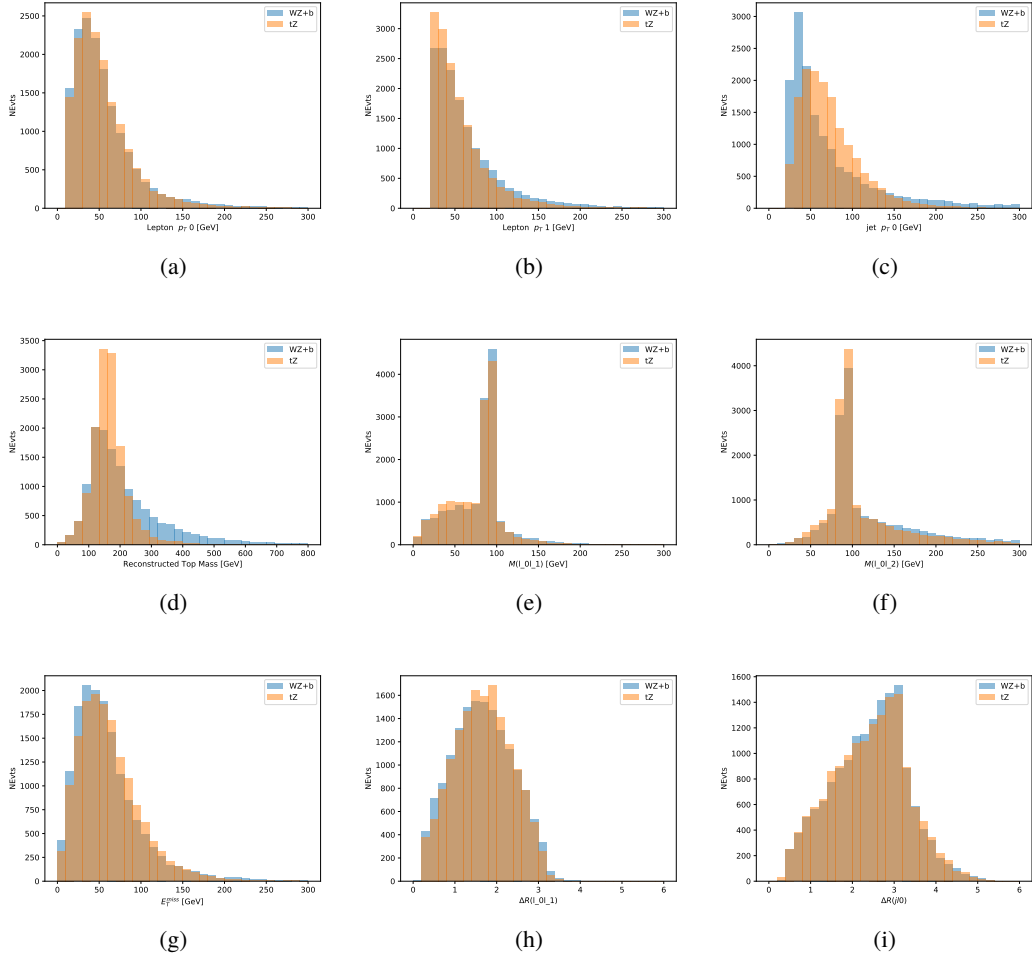


Figure 4: Distribution of input features of the BDT for signal (WZ) and background (tZ). Both are scaled to an equal number of events. (a), (b) and (c) show the p_T of lepton 0, lepton 1, and the jet, (d) shows the reconstructed top mass, (e) and (f) show the invariant mass of leptons 0 and 1, leptons 0 and 2. (g) shows the E_T^{miss} of each event. (h) and (i) show the ΔR between lepton 0 and lepton 1, and the jet. See section 6.1 for definitions of lepton numbering.

352 Correlations between the input features are shown in figure 5.

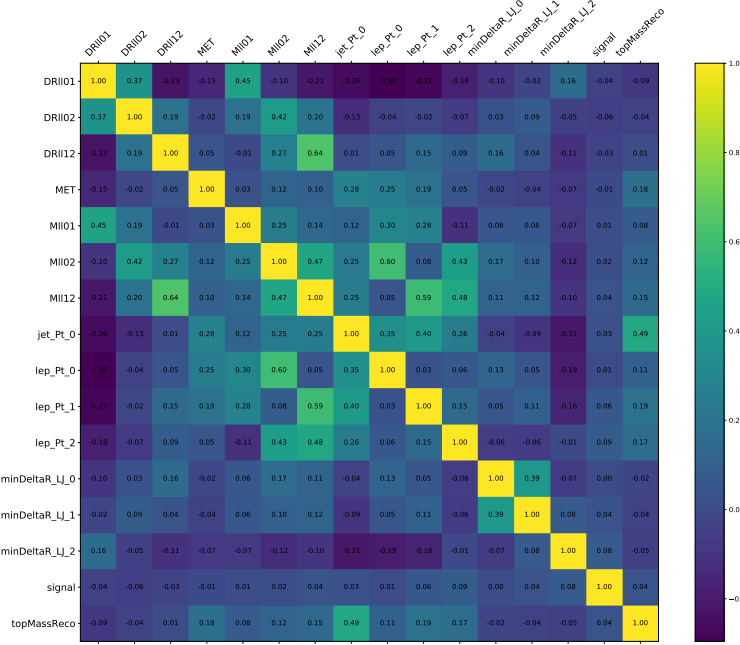


Figure 5: Correlation matrix of the input features of the tZ separation BDT.

353 A sample of 20,000 background (tZ) and signal (WZ+b) Monte Carlo events each are used to
 354 train the BDT. And additional 5,000 events are reserved for testing the model, in order to prevent
 355 over-fitting. A total of 750 decision trees with a maximum depth of 6 branches are used to build
 356 the model. These parameters are chosen empirically, by training several models with different
 357 parameters and selecting the one that gave the best separation for the test sample.

358 The results of the BDT training are shown in figure 6. The output scores for both signal and
 359 background events is shown on the left. The right shows the receiving operating characteristic
 360 (ROC) curve that results from the MVA. The ROC curve represents the background rejection
 361 as a function of signal rejection, where each point on the curve represents a different response
 362 score.

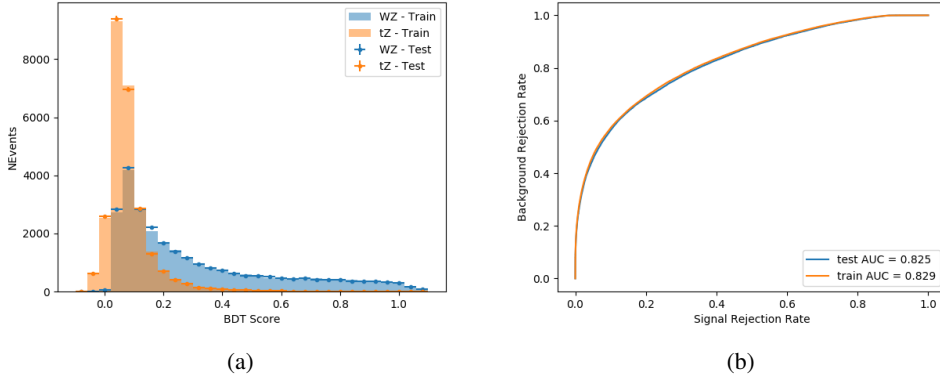


Figure 6: Distribution of the BDT response for signal and background events on the left, the ROC curve for the BDT on the right.

363 The relative importance of each input feature in the model, measured by how often they appeared
 364 in the decision trees, is shown in figure 7.

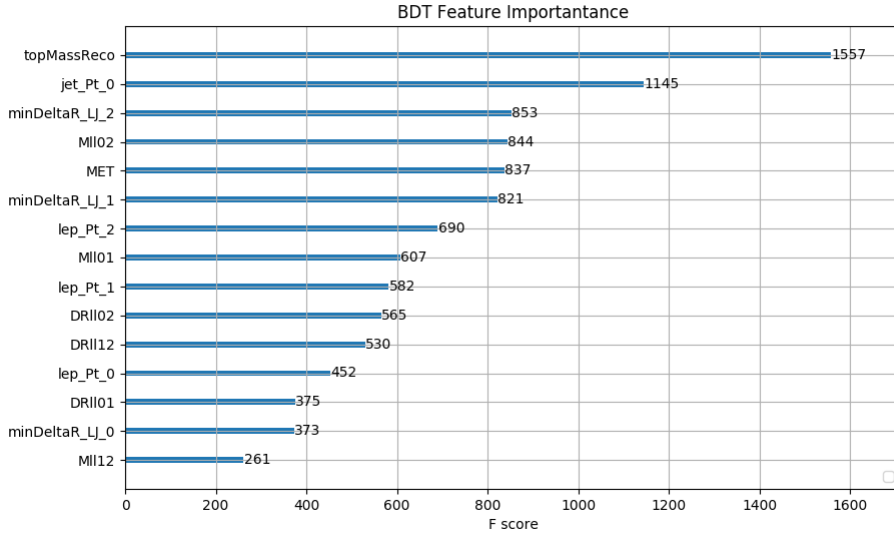


Figure 7: Relative importance of each input feature in the model.

365 These results suggest that some amount of separation can be achieved between these two pro-
 366 cesses, with a high BDT score selecting a set of events that is pure in WZ + b. A BDT score
 367 of 0.12 is selected as a cutoff, where events with scores higher than this form a signal enriched
 368 region, and events with scores lower than this form a tZ control region. This cutoff is selected

369 by varying its value in stat-only Asimov fits, and selecting the one that minimizes the statistical
 370 uncertainty on $\text{WZ} + \text{b}$. A working point of 0.12 produces a background rejection rate of 74%,
 371 compared to a signal acceptance of 78%.

372 The possibility of using solely the reconstructed top mass shown in Figure 3 to separate tZ
 373 and $\text{WZ} + \text{b}$ was considered, and produced the ROC curve shown in Figure 8. This shows
 374 significantly reduced separation compared to the BDT, justifying the use of the more complex
 375 BDT in the analysis.

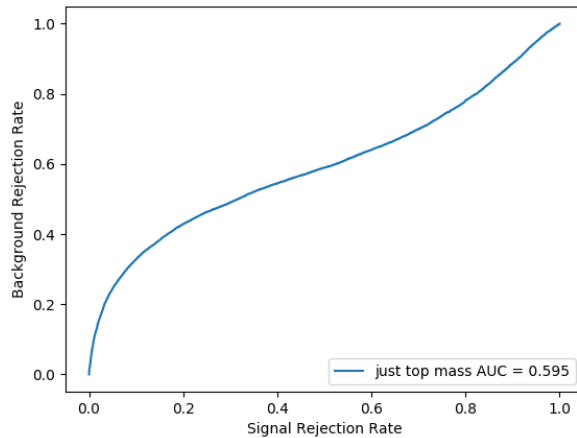


Figure 8: ROC for the separation of tZ and $\text{WZ} + \text{b}$ produced from the distribution of the reconstructed top mass.

376 5.3 tZ Interference Studies

377 Because it includes an on-shell Z boson as well as a b-jet and W from the top decay, tZ production
 378 represents an identical final state to $\text{WZ} + \text{b}$ -jet. This implies the possibility of matrix-element
 379 level interference between these two processes not accounted for in the Monte Carlo simulations,
 380 which consider the two processes independently. Truth level studies are performed in order to
 381 estimate the impact of these interference effects.

382 In order to estimate the matrix-element level interference effects between tZ and $\text{WZ} + \text{b}$ -jet, two
 383 different sets of simulations are produced using MadGraph 5 [23] - one which simulates these
 384 two processes independently, and another where they are produced simultaneously, such that
 385 interference effects are present. These two sets of samples are then compared, and the difference
 386 between them can be taken to represent any interference effects.

387 MadGraph simulations of 10,000 tZ and 10,000 $\text{WZ} + \text{b}$ -jet events are produced, along with
 388 20,000 events where both are present, in the fiducial region where three leptons and at least one
 389 jet are produced.

390 A selection mimicking the preselection used in the main analysis is applied to the samples: The
391 SS leptons are required to have $p_T > 20$ GeV, and > 10 GeV is required for the OS lepton. The
392 associated b-jet is required to have $p_T > 25$ GeV, and all physics objects are required to fall in a
393 range of $|\eta| < 2.5$.

394 The kinematics of these samples after the selection has been applied are shown below:

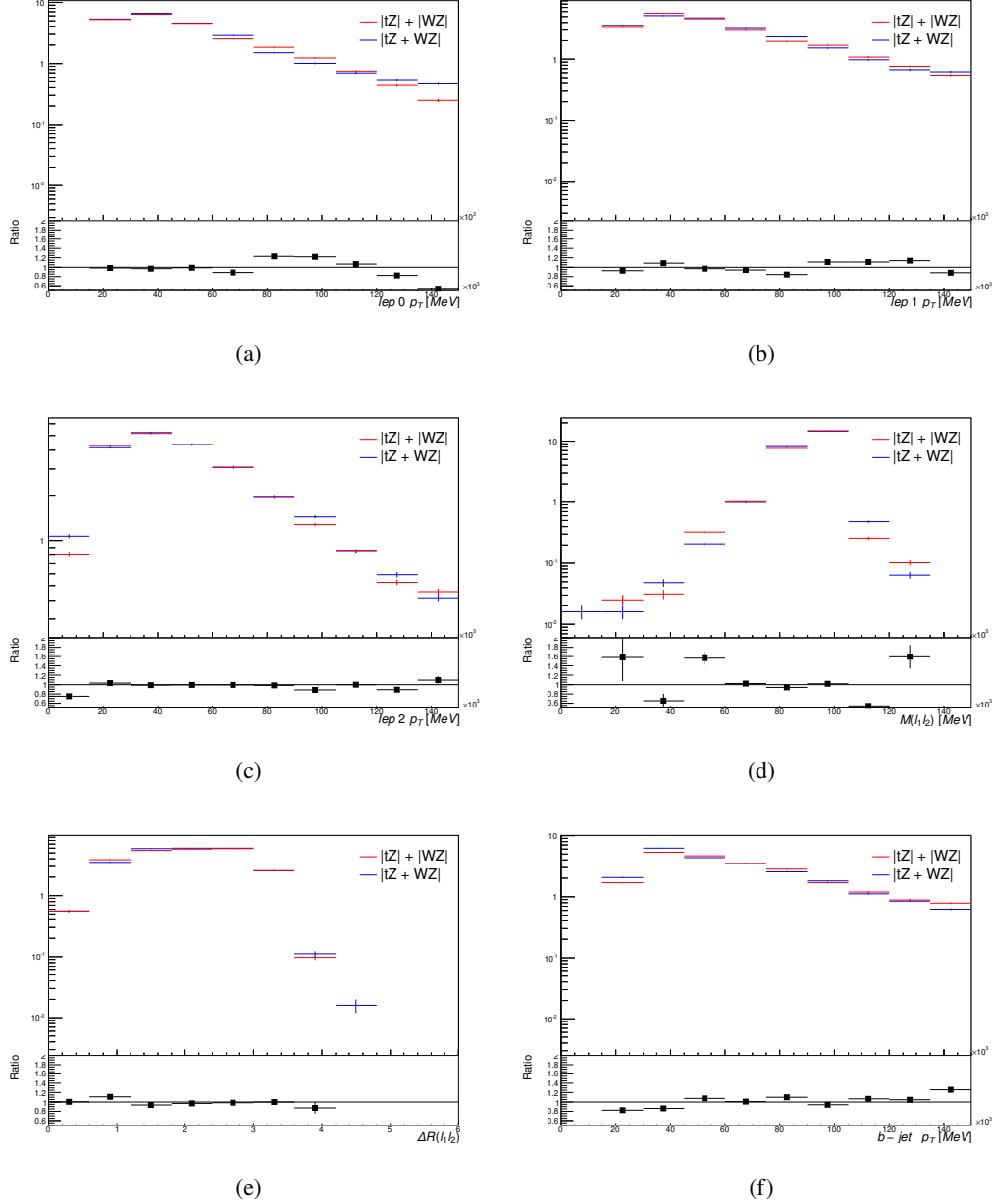


Figure 9: Comparisons between (a) the p_T of the lepton from the W, (b) and (c) show the p_T of the lepton from the Z, (d) the invariant mass of the Z-candidate, (e) ΔR of the leptons from the Z, and (f) the p_T of the b-jet, for WZ and tZ events generated with interference effects (blue) and without interference effects (red).

395 The overall cross-sections of the two methods agree within error, and no significant differences
 396 in the kinematic distributions are seen. It is therefore concluded that interference effects do not

397 significantly impact the results.

398 6 Event Selection and Signal Region Definitions

399 Events are required to pass a preselection described in Section 6.1 and summarized in Table 6.
400 Those that pass this preselection are divided into various fit regions described in Section 6.2,
401 based on the number of jets in the event, and the b-tag score of those jets.

402 6.1 Event Preselection

403 Events are required to include exactly three reconstructed light leptons passing the requirements
404 described in 4.2, which have a total charge of ± 1 .

405 The leptons are ordered in the analysis code as 0, 1, and 2. Lepton 0 is the lepton whose charge
406 is opposite the other two. Lepton 1 is the lepton closest to the opposite charge lepton, i.e. the
407 smallest ΔR , leaving lepton 2 as the lepton further from the opposite charge lepton. Lepton 0 is
408 required to have $p_T > 10$ GeV, as it is found to be prompt the vast majority of the time, while
409 the same sign leptons, 1 and 2, are required to have $p_T > 20$ GeV to reduce the contribution of
410 non-prompt leptons, as non-prompt leptons tend to be soft.

411 The invariant mass of at least one pair of opposite sign, same flavor leptons is required to fall
412 within 10 GeV of the mass of the Z boson, 91.2 GeV. Events where one of the opposite sign pairs
413 has an invariant mass less than 12 GeV are rejected in order to suppress low mass resonances.

414 An additional requirement is placed on the missing transverse energy, $E_T^{\text{miss}} > 20$ GeV, and the
415 transverse mass of the W candidate, $m(E_T^{\text{miss}} + l_{\text{other}}) > 30$ GeV, defined as

416 $\sqrt{2p_T^{\text{lep}} E_T^{\text{miss}} * (1 - \cos(\phi_{\text{lep}} - \phi_{E_T^{\text{miss}}}))}$. Here E_T^{miss} is the missing transverse energy, and
417 l_{other} is the lepton not included in the Z-candidate.

418 Events are required to have one or two reconstructed jets passing the selection described in
419 Section 4.3. Events with more than two jets are rejected in order to reduce the contribution of
420 backgrounds such as $t\bar{t}Z$ and $t\bar{t}W$, which tend to have higher jet multiplicity.

Event Selection
Exactly three leptons with total charge ± 1
Two same-charge leptons with $p_T > 20$ GeV
One opposite charge lepton with $p_T > 10$ GeV
$m(l^+l^-)$ within 10 GeV of 91.2 GeV
Transverse mass of W-candidate, $\sqrt{2p_T^{lep}E_T^{\text{miss}} * (1 - \cos(\phi_{lep} - \phi_{E_T^{\text{miss}}}))} > 30$ GeV
Missing transverse energy, $E_T^{\text{miss}} > 20$ GeV
One or two jets with $p_T > 25$ GeV

Table 6: Summary of the selection applied to events for inclusion in the fit

421 The event yields in the preselection region for both data and Monte Carlo are summarized in
 422 Table 6.1, which shows good agreement between data and Monte Carlo, and demonstrates that
 423 this region consists primarily of WZ + jets events. The WZ events are split into WZ + b, WZ
 424 + c, and WZ + l based on the truth flavor of the associated jet in the event. Specifically, this
 425 determination is made based on the HadronConeExclTruthLabelID of the jet, as recommended
 426 by the b-tagging working group [24]. In this ordering a b-jet identification supersedes charm,
 427 which supersedes light. That is, WZ + light events contain no charm and no b jets at truth level,
 428 WZ + c contain at least one truth charm and no b-jets, and WZ + b contains at least one truth
 429 b-jet.

Process	Events
WZ + b	143 ± 43
WZ + c	930 ± 280
WZ + l	6250 ± 1900
Other VV	16.6 ± 4.1
ZZ	460 ± 55
t̄W	14.8 ± 2.1
t̄tZ	96 ± 14
Single top	0.1 ± 0.2
Three top	0.003 ± 0.002
Four top	0.01 ± 0.01
t̄tWW	0.20 ± 0.04
Z + jets	320 ± 70
V + γ	75 ± 43
tZ	164 ± 37
tW	4.9 ± 1.2
WtZ	21 ± 11
VVV	23 ± 11
VH	67 ± 6
t̄t	84 ± 9
t̄tH	3.6 ± 0.4
Total	8700 ± 2300
Data	8696

Table 7: Event yields in the preselection region at 139.0 fb^{-1} . Includes the full set of systematic uncertainties

⁴³⁰ Here Other VV represents diboson processes other than WZ, and consists predominantly of
⁴³¹ $ZZ \rightarrow ll\bar{l}\bar{l}$ events where one of the leptons is not reconstructed.

⁴³² Simulations are further validated by comparing the kinematic distributions of the Monte Carlo
⁴³³ with data, which are shown in Figure 10. Here, bins with 5% or more WZ+b are blinded.

WZ Fit Region - Inclusive

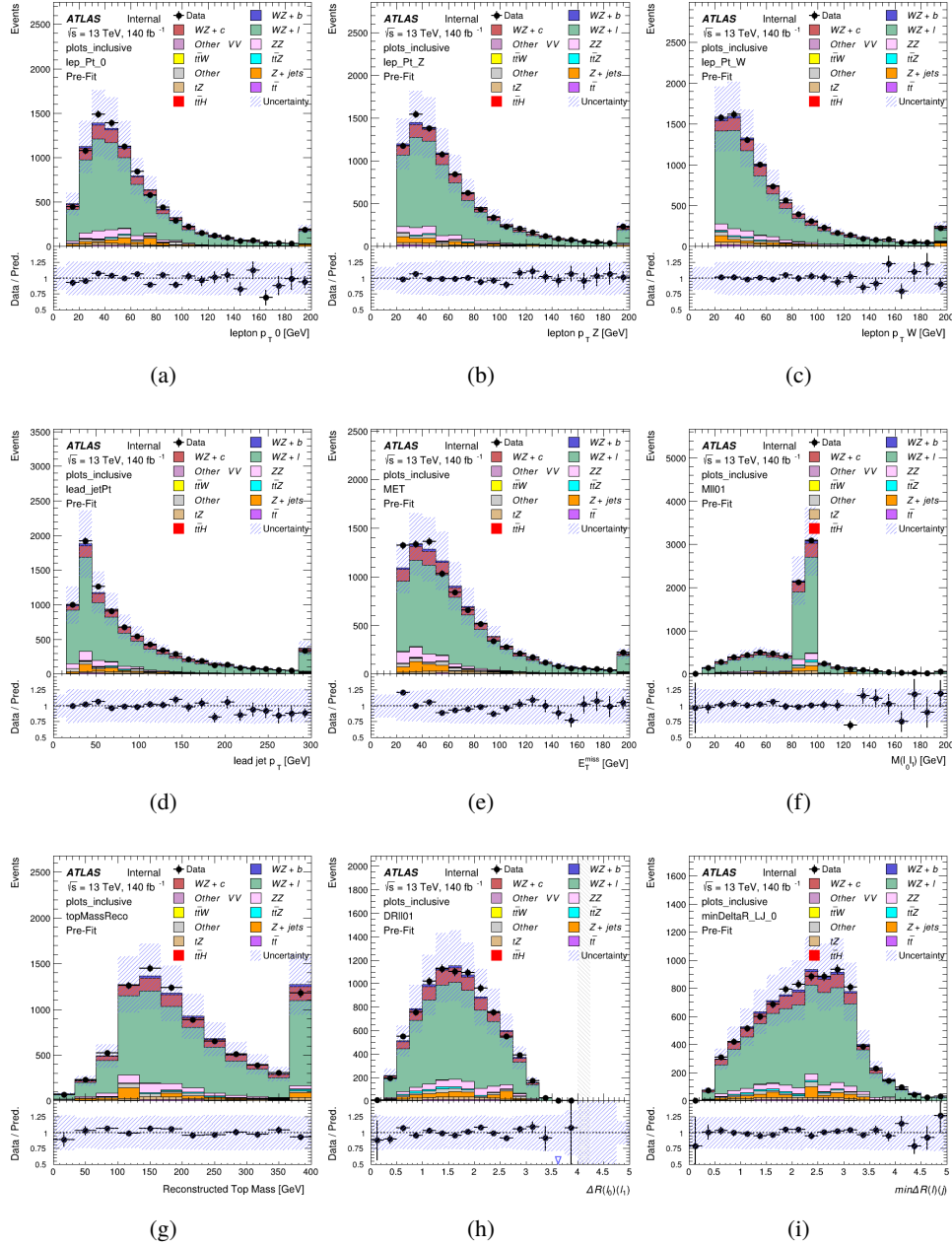


Figure 10: Comparisons between the data and MC distributions in the preselection region for (a) the p_T of the opposite sign lepton, (b) the p_T of the other lepton from the Z candidate, (c) the p_T of the lepton from the W candidate, (d) the leading jet p_T , (e) the E_T^{miss} , and (f) the invariant mass of leptons 0 and 1, (g) the reconstructed top mass, (h) $\Delta(R)$ between lepton 0 and 1, (i) the $\Delta(R)$ between the closest lepton and jet.

434 **6.2 Fit Regions**

435 Once preselection has been applied, the remaining events are categorized into one of twelve
 436 orthogonal regions. The regions used in the fit are summarized in Table 8.

Table 8: A list of the regions used in the fit and the selection used for each. In the two jet regions, only one of the jets is required to pass the corresponding b-tagging WP.

Region	Selection
1j, <85%	$N_{\text{jets}} = 1, n_{\text{Jets_DL1r_85}} = 0$
1j, 85%-77%	$N_{\text{jets}} = 1, n_{\text{Jets_DL1r_85}} = 1, n_{\text{Jets_DL1r_77}} = 0$
1j, 77%-70%	$N_{\text{jets}} = 1, n_{\text{Jets_DL1r_77}} = 1, n_{\text{Jets_DL1r_70}} = 0$
1j, 70%-60%	$N_{\text{jets}} = 1, n_{\text{Jets_DL1r_70}} = 1, n_{\text{Jets_DL1r_60}} = 0$
1j, 60%	$N_{\text{jets}} = 1, n_{\text{Jets_DL1r_60}} = 1, tZ \text{ BDT} > 0.12$
1j tZ CR	$N_{\text{jets}} = 1, n_{\text{Jets_DL1r_60}} = 1, tZ \text{ BDT} < 0.12$
2j, <85%	$N_{\text{jets}} = 2, n_{\text{Jets_DL1r_85}} = 0$
2j, 85%-77%	$N_{\text{jets}} = 2, n_{\text{Jets_DL1r_85}} \geq 1, n_{\text{Jets_DL1r_77}} = 0$
2j, 77%-70%	$N_{\text{jets}} = 2, n_{\text{Jets_DL1r_77}} \geq 1, n_{\text{Jets_DL1r_70}} = 0$
2j, 70%-60%	$N_{\text{jets}} = 2, n_{\text{Jets_DL1r_70}} \geq 1, n_{\text{Jets_DL1r_60}} = 0$
2j, 60%	$N_{\text{jets}} = 2, n_{\text{Jets_DL1r_60}} \geq 1, tZ \text{ BDT} > 0.12$
2j tZ CR	$N_{\text{jets}} = 2, n_{\text{Jets_DL1r_60}} \geq 1, tZ \text{ BDT} < 0.12$

437 The working points discussed in Section 4.4 are used to separate events into fit regions based on
 438 the highest working point reached by a jet in each event. Because the background composition
 439 differs significantly based on the number of b-jets, events are further subdivided into 1-jet and
 440 2-jet regions in order to minimize the impact of background uncertainties.

441 An unfolding procedure is performed to account for differences in the number of reconstructed
 442 jets compared to the number of truth jets in each event. The `AntiKt4TruthDressedWZJets`
 443 truth jet collection is used to make this determination. In order to account for migration of
 444 WZ+1-jet and WZ+2-jet events between the 1-jet and 2-jet bins at reco level, the signal samples
 445 are separated based on the number of truth jets. Events with 0 jets or more than 3 jets at truth
 446 level, yet fall within one of the categories listed in Table 8, are categorized as WZ + other, and
 447 treated as a background. The migration matrix in the number of jets at truth level versus reco
 448 level is shown in Figure 11. The composition of the number of truth jets in each reco jet bin is
 449 taken from MC, with uncertainties in these estimates described in detail in Section 7.

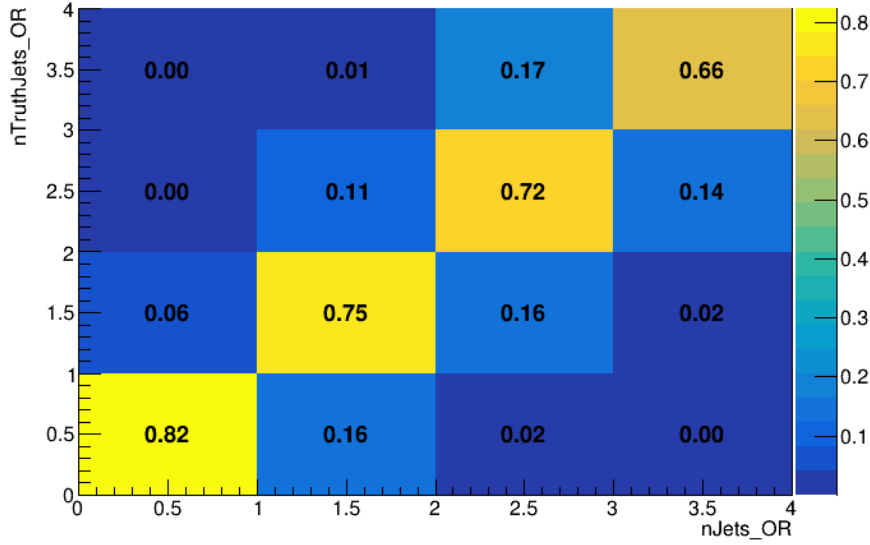


Figure 11: Number of truth jets compared to the number of reconstructed jets in each WZ event falling in the preselection region. Each row is normalized to unity, with overflow bins not shown included in the normalization. That is, each bin represents the absolute fraction of events with a particular truth jet multiplicity that include the corresponding number of reconstructed jets.

450 An additional tZ control region is created based on the BDT described in Section 5. The region
 451 with 1-jet passing the 60% working point is split in two - a signal enriched region of events with
 452 a BDT score greater than 0.12, and a tZ control region including events with a score less than
 453 0.12. This cutoff is arrived at by performing a fit to an Asimov dataset with a variety of cutoffs,
 454 and selecting the value that produces the highest significance for the measurement of WZ + b.

455 The modeling in each region is validated by comparing data and MC predictions for various
 456 kinematic distributions. Events containing 5% or more WZ + b are blinded. These plot are
 457 shown in Figures 12-25.

WZ Fit Region - 1j Inclusive

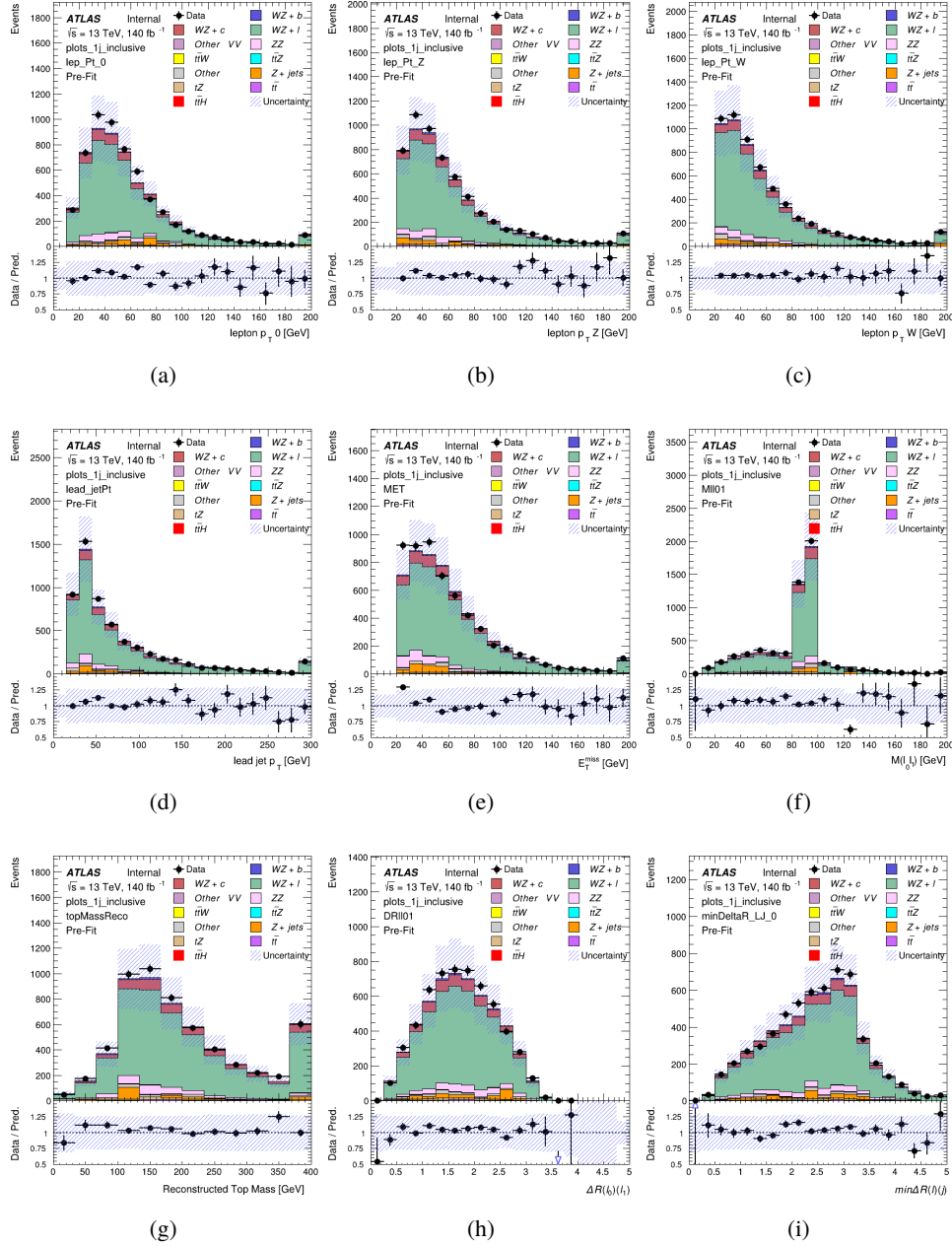


Figure 12: Comparisons between the data and MC distributions in the preselection region for (a) the p_T of the opposite sign lepton, (b) the p_T of the other lepton from the Z candidate, (c) the p_T of the lepton from the W candidate, (d) the leading jet p_T , (e) the E_T^{miss} , and (f) the invariant mass of leptons 0 and 1, (g) the reconstructed top mass, (h) $\Delta(R)$ between lepton 0 and 1, (i) the $\Delta(R)$ between the closest lepton and jet.

WZ Fit Region - 1j < 85% WP

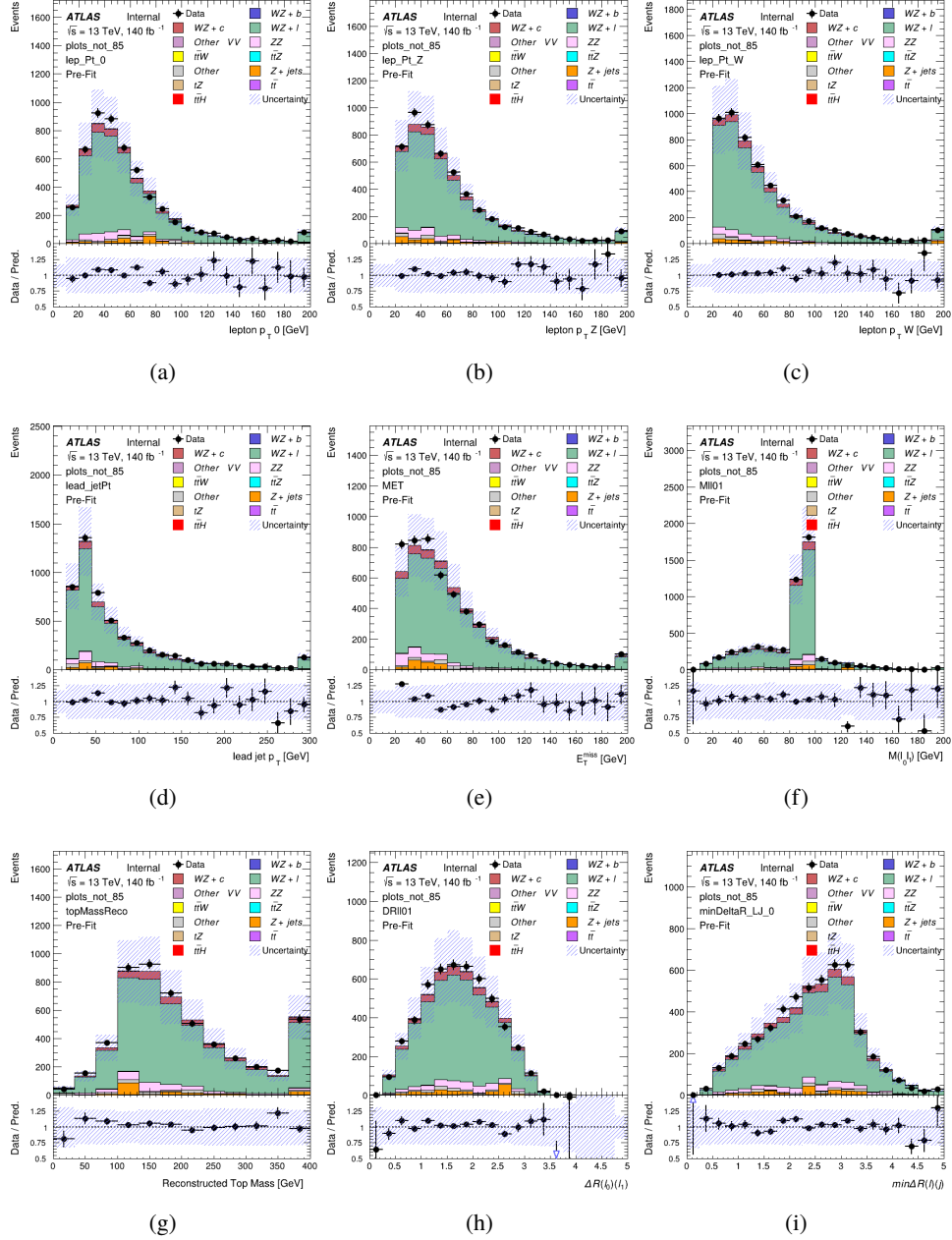


Figure 13: Comparisons between the data and MC distributions in the preselection region for (a) the p_T of the opposite sign lepton, (b) the p_T of the other lepton from the Z candidate, (c) the p_T of the lepton from the W candidate, (d) the leading jet p_T , (e) the E_T^{miss} , and (f) the invariant mass of leptons 0 and 1, (g) the reconstructed top mass, (h) $\Delta(R)$ between lepton 0 and 1, (i) the $\Delta(R)$ between the closest lepton and jet.

WZ Fit Region - 1j 77-85% WP

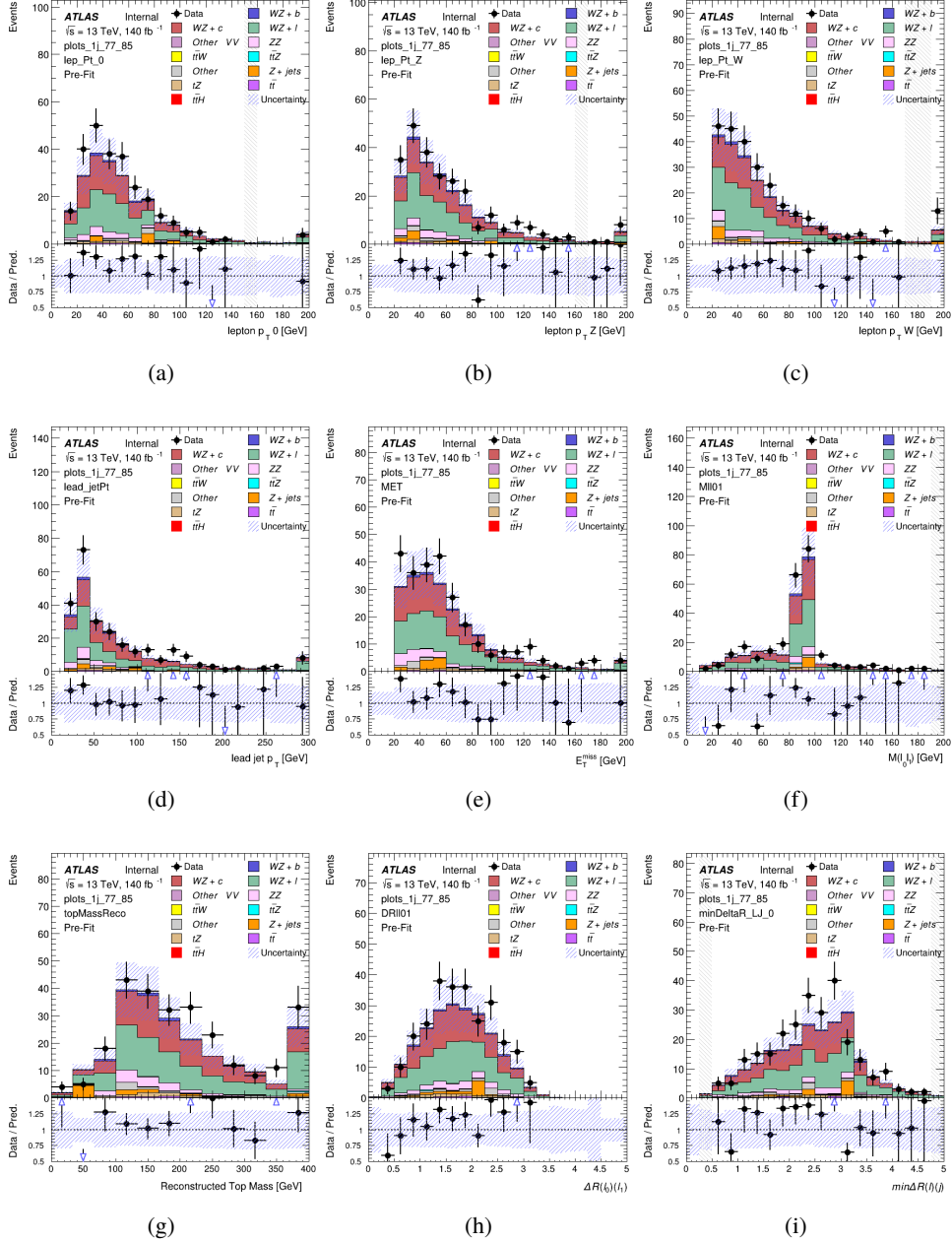


Figure 14: Comparisons between the data and MC distributions in the preselection region for (a) the p_T of the opposite sign lepton, (b) the p_T of the other lepton from the Z candidate, (c) the p_T of the lepton from the W candidate, (d) the leading jet p_T , (e) the E_T^{miss} , and (f) the invariant mass of leptons 0 and 1, (g) the reconstructed top mass, (h) $\Delta(R)$ between lepton 0 and 1, (i) the $\Delta(R)$ between the closest lepton and jet.

WZ Fit Region - 1j 70-77% WP

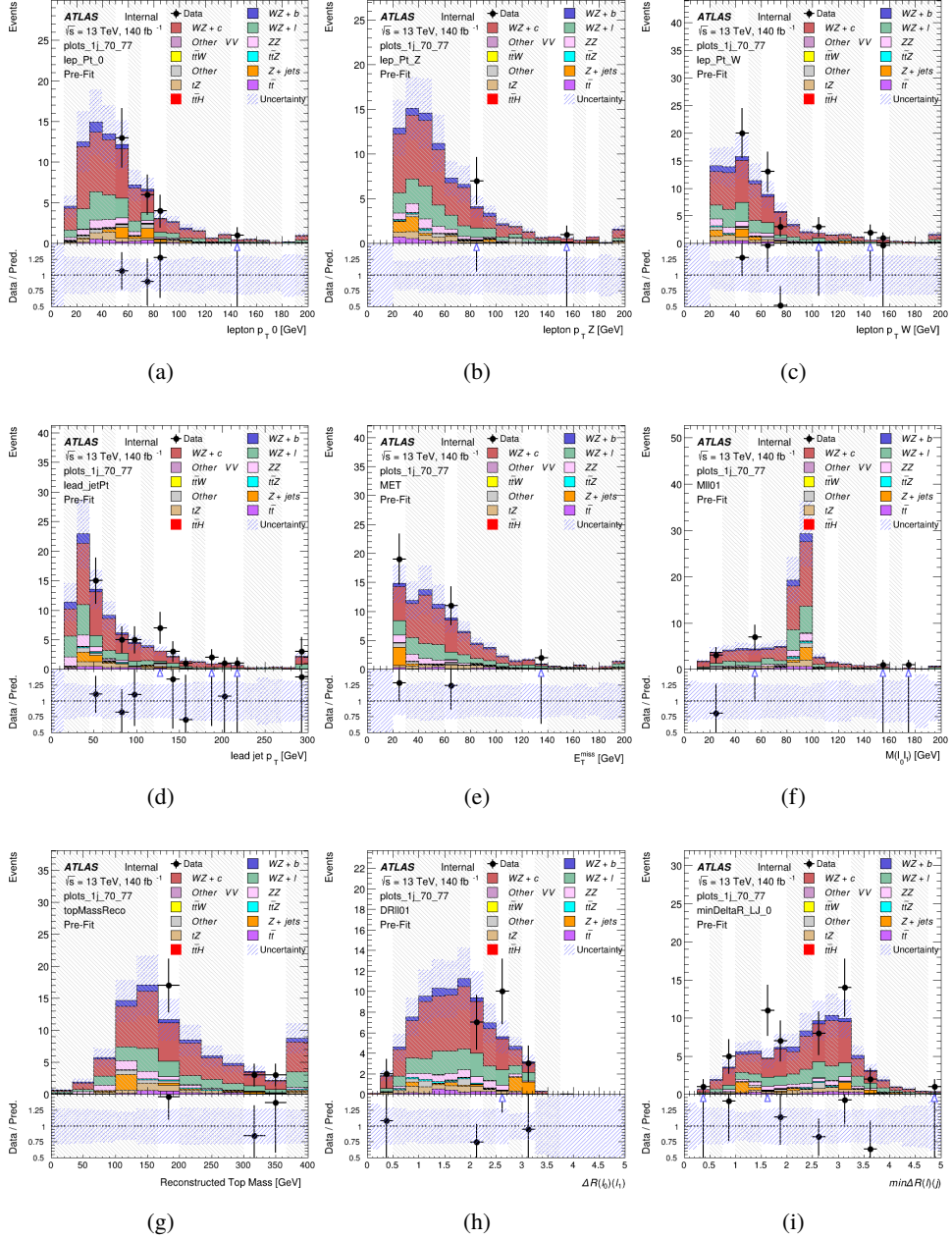


Figure 15: Comparisons between the data and MC distributions in the preselection region for (a) the p_T of the opposite sign lepton, (b) the p_T of the other lepton from the Z candidate, (c) the p_T of the lepton from the W candidate, (d) the leading jet p_T , (e) the E_T^{miss} , and (f) the invariant mass of leptons 0 and 1, (g) the reconstructed top mass, (h) $\Delta(R)$ between lepton 0 and 1, (i) the $\Delta(R)$ between the closest lepton and jet.

WZ Fit Region - 1j 60-70% WP

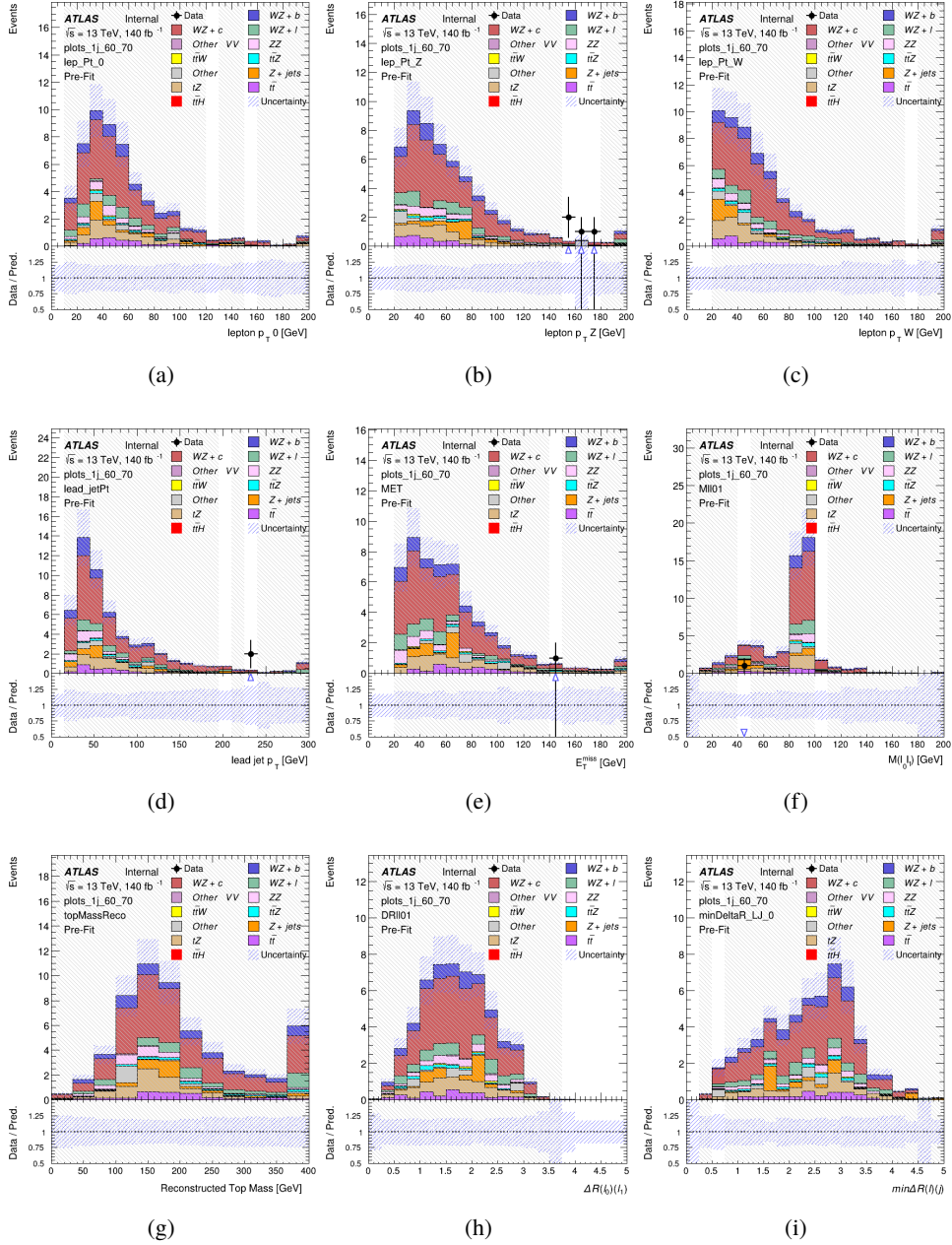


Figure 16: Comparisons between the data and MC distributions in the preselection region for (a) the p_T of the opposite sign lepton, (b) the p_T of the other lepton from the Z candidate, (c) the p_T of the lepton from the W candidate, (d) the leading jet p_T , (e) the E_T^{miss} , and (f) the invariant mass of leptons 0 and 1, (g) the reconstructed top mass, (h) $\Delta(R)$ between lepton 0 and 1, (i) the $\Delta(R)$ between the closest lepton and jet.

WZ Fit Region - 1j 60% WP

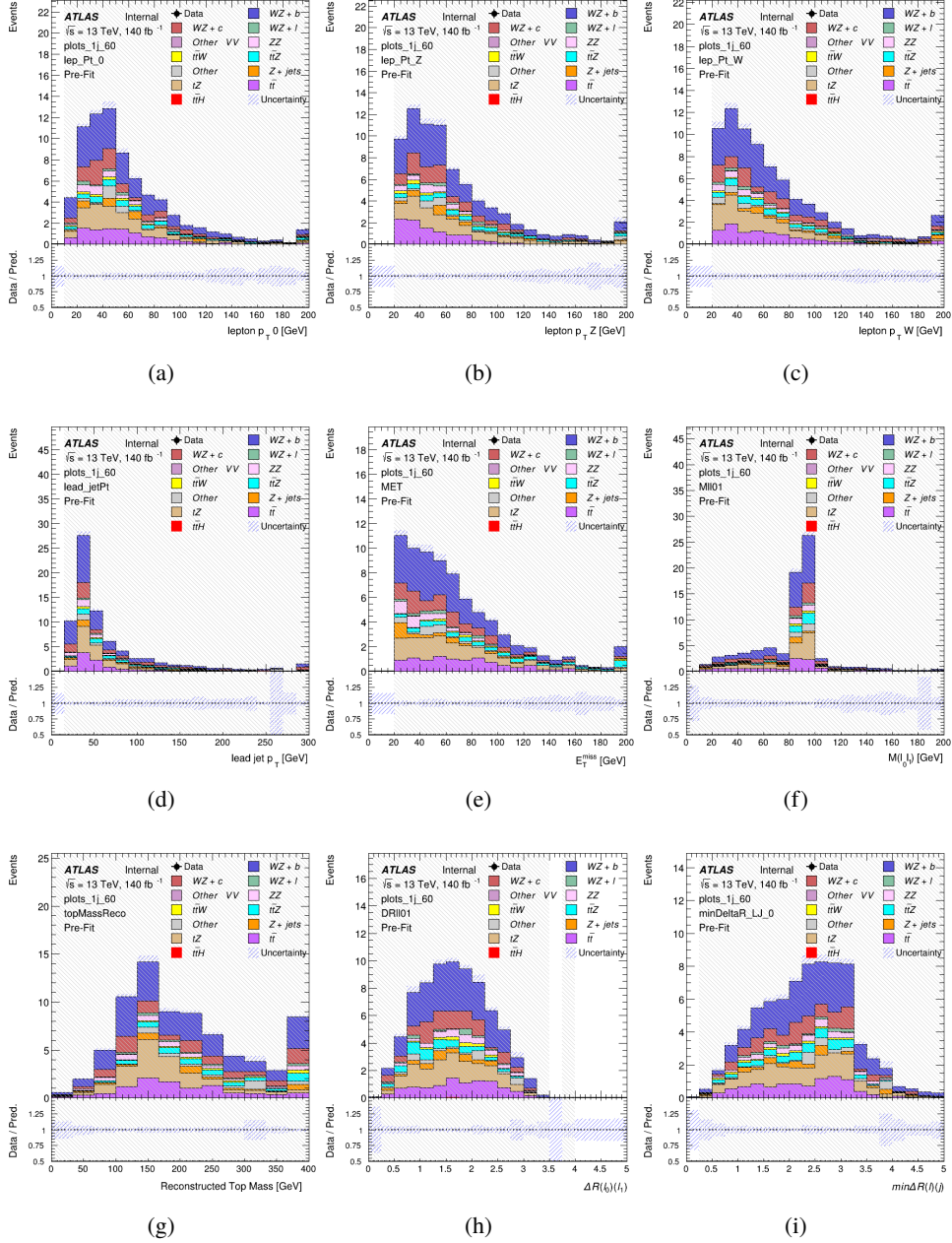


Figure 17: Comparisons between the data and MC distributions in the preselection region for (a) the p_T of the opposite sign lepton, (b) the p_T of the other lepton from the Z candidate, (c) the p_T of the lepton from the W candidate, (d) the leading jet p_T , (e) the E_T^{miss} , and (f) the invariant mass of leptons 0 and 1, (g) the reconstructed top mass, (h) $\Delta(R)$ between lepton 0 and 1, (i) the $\Delta(R)$ between the closest lepton and jet.

WZ Fit Region - tZ-CR

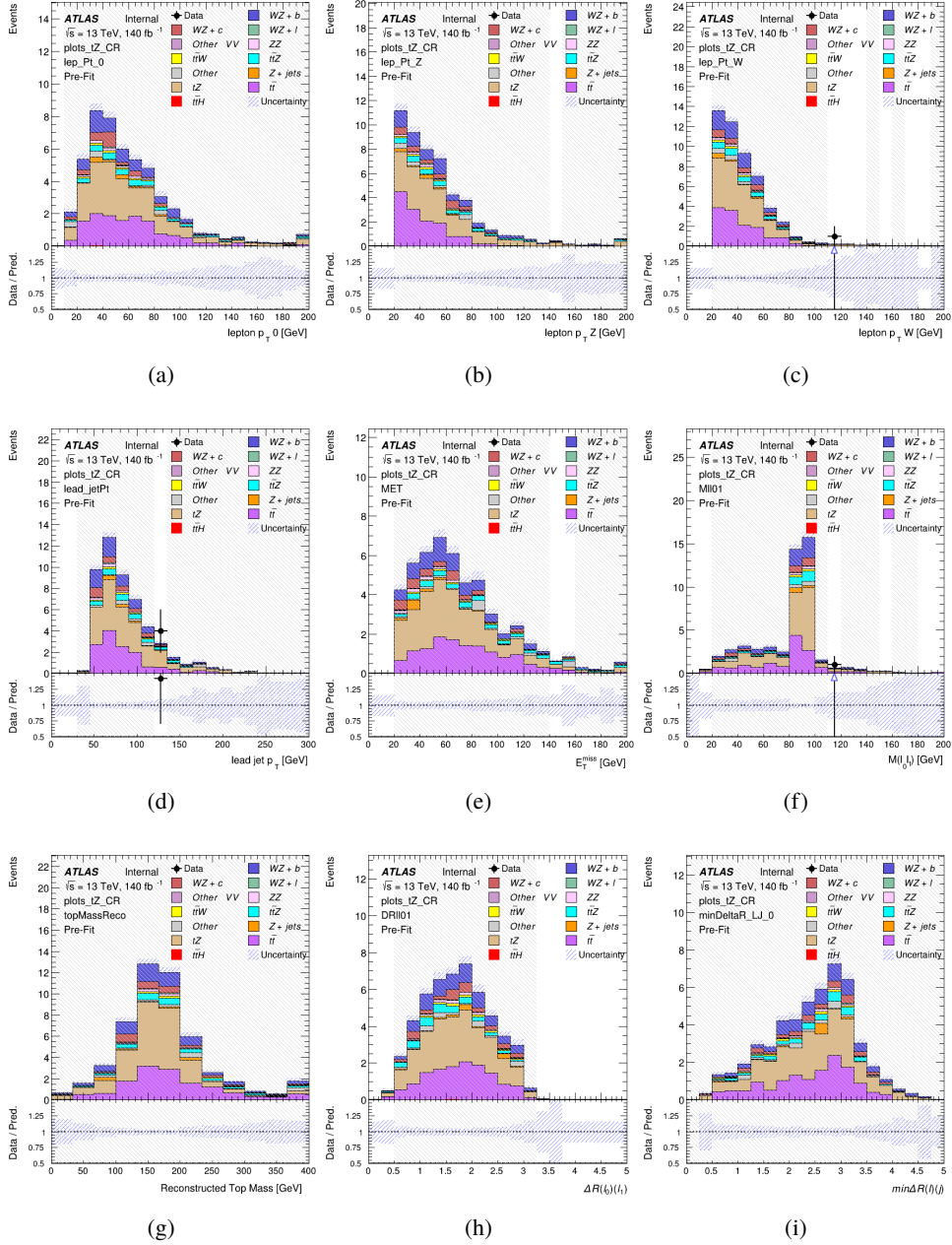


Figure 18: Comparisons between the data and MC distributions in the preselection region for (a) the p_T of the opposite sign lepton, (b) the p_T of the other lepton from the Z candidate, (c) the p_T of the lepton from the W candidate, (d) the leading jet p_T , (e) the E_T^{miss} , and (f) the invariant mass of leptons 0 and 1, (g) the reconstructed top mass, (h) $\Delta(R)$ between lepton 0 and 1, (i) the $\Delta(R)$ between the closest lepton and jet.

WZ Fit Region - 2j Inclusive

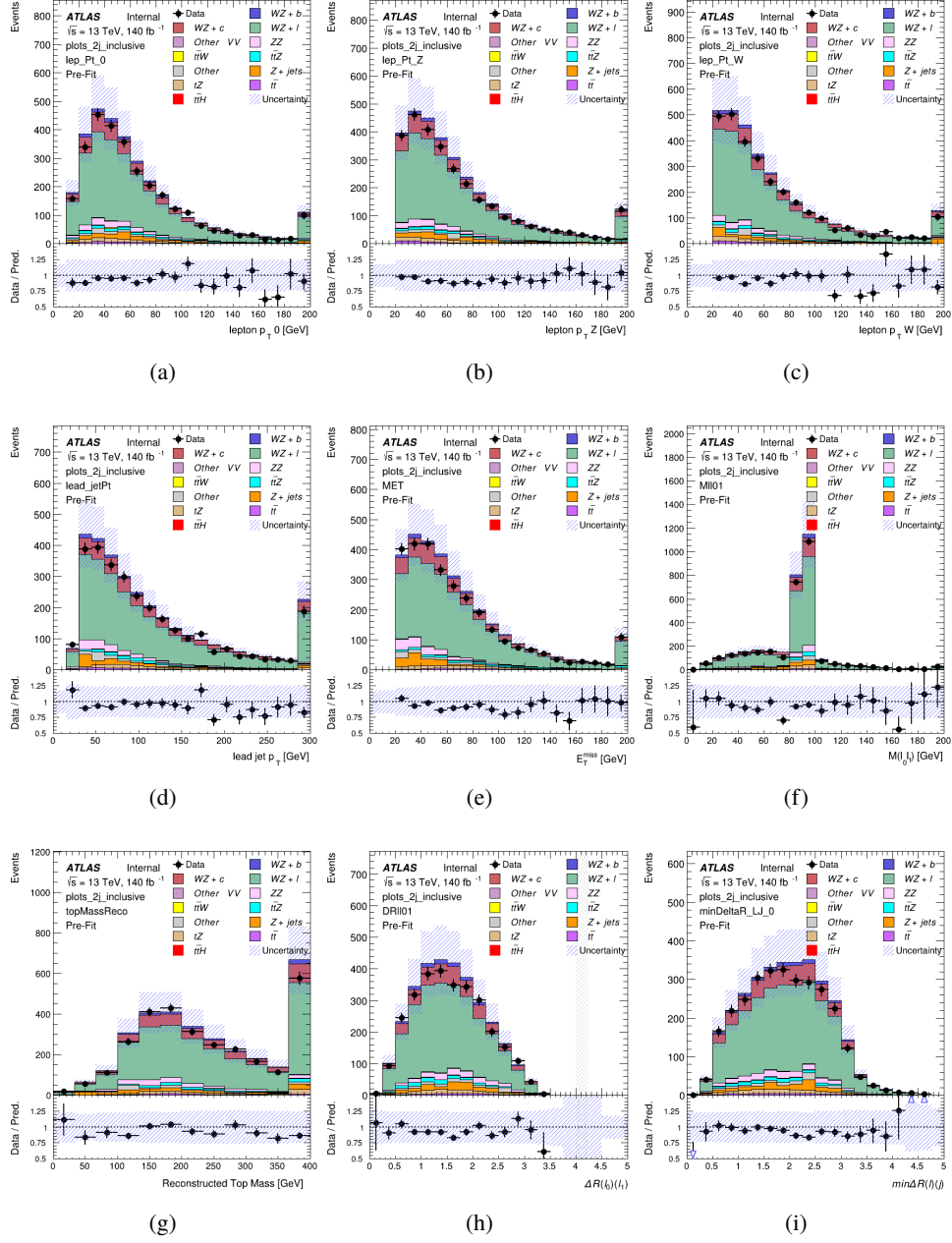


Figure 19: Comparisons between the data and MC distributions in the preselection region for (a) the p_T of the opposite sign lepton, (b) the p_T of the other lepton from the Z candidate, (c) the p_T of the lepton from the W candidate, (d) the leading jet p_T , (e) the E_T^{miss} , and (f) the invariant mass of leptons 0 and 1, (g) the reconstructed top mass, (h) $\Delta(R)$ between lepton 0 and 1, (i) the $\Delta(R)$ between the closest lepton and jet.

WZ Fit Region - 2j < 85% WP

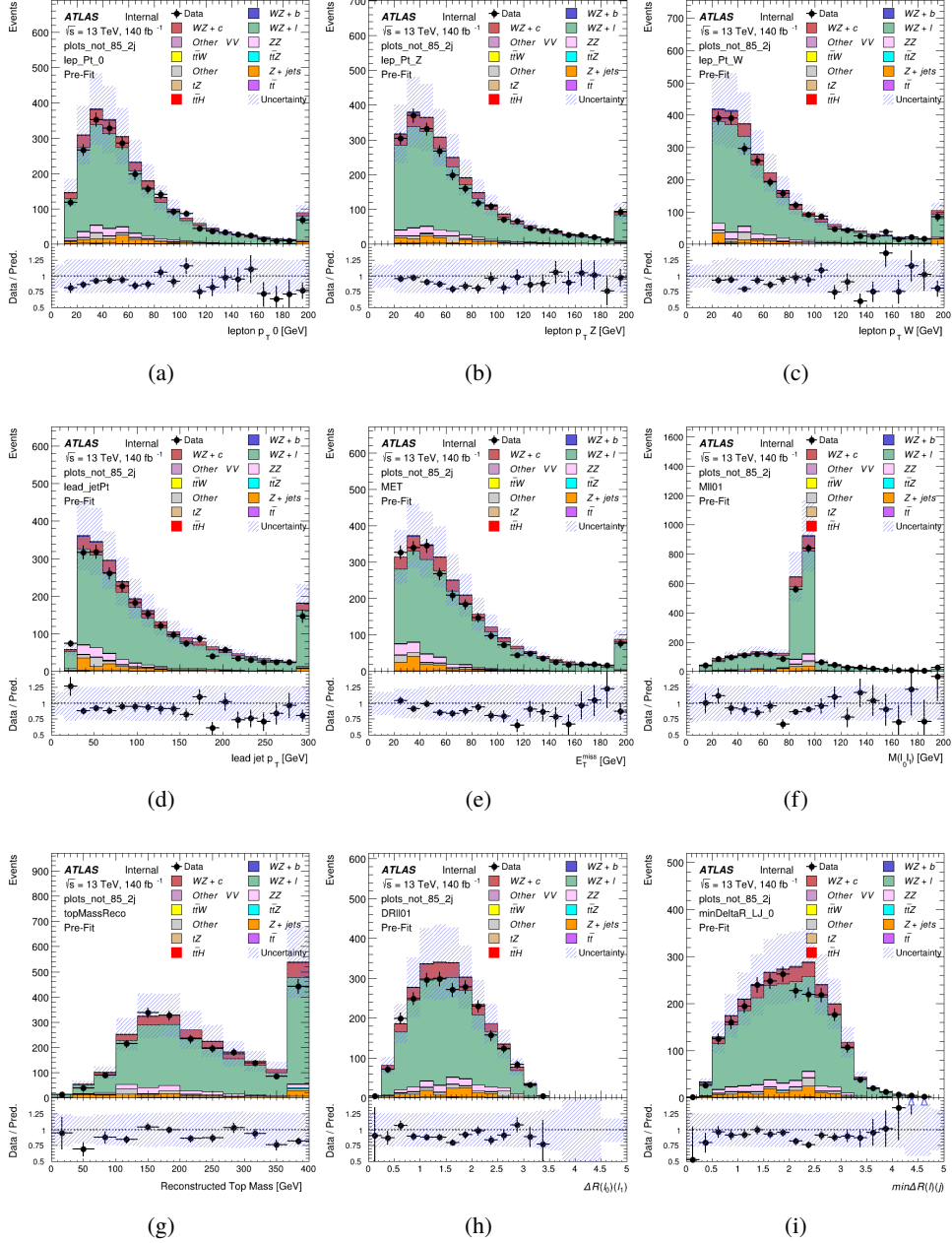


Figure 20: Comparisons between the data and MC distributions in the preselection region for (a) the p_T of the opposite sign lepton, (b) the p_T of the other lepton from the Z candidate, (c) the p_T of the lepton from the W candidate, (d) the leading jet p_T , (e) the E_T^{miss} , and (f) the invariant mass of leptons 0 and 1, (g) the reconstructed top mass, (h) $\Delta(R)$ between lepton 0 and 1, (i) the $\Delta(R)$ between the closest lepton and jet.

WZ Fit Region - 2j 77-85% WP

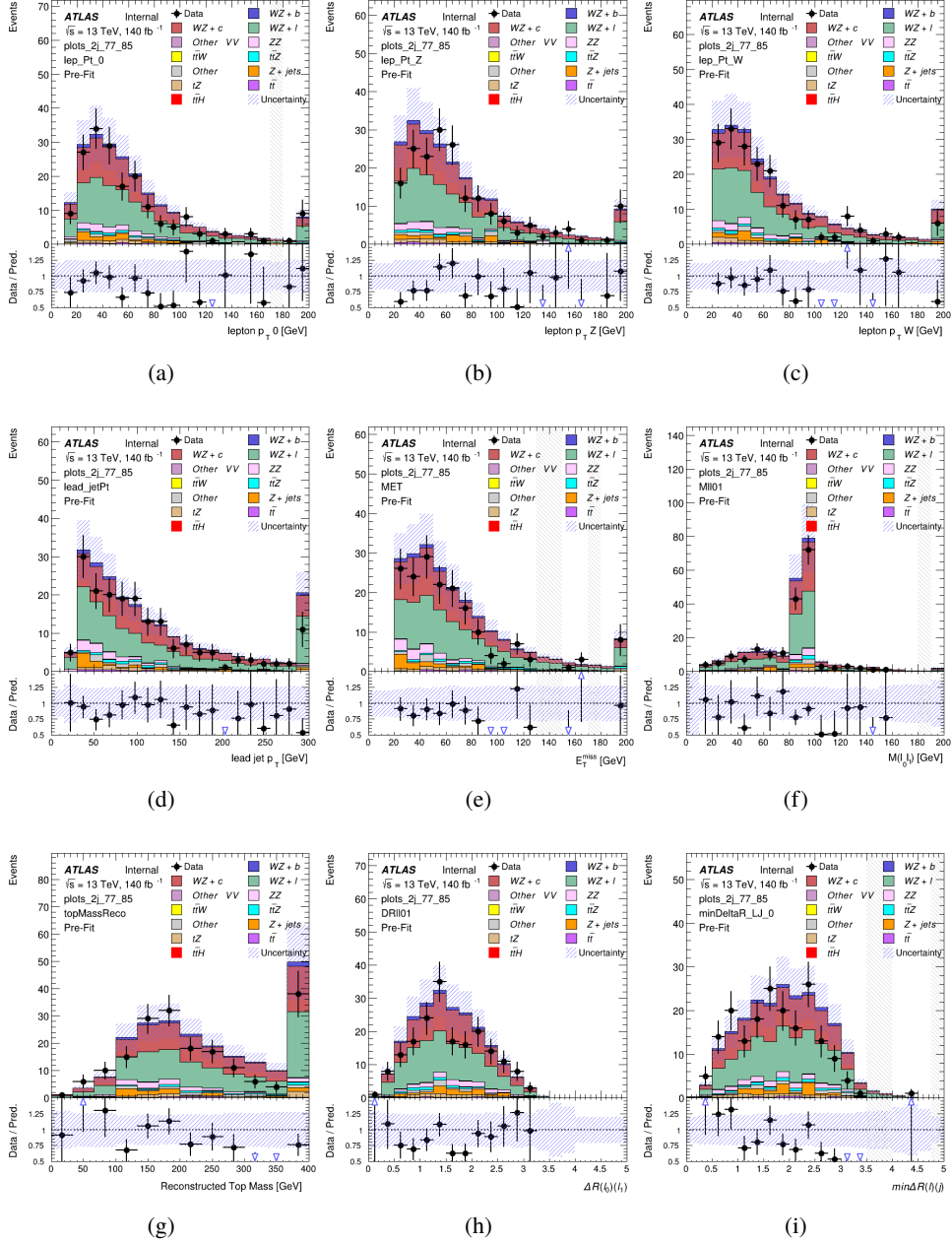


Figure 21: Comparisons between the data and MC distributions in the preselection region for (a) the p_T of the opposite sign lepton, (b) the p_T of the other lepton from the Z candidate, (c) the p_T of the lepton from the W candidate, (d) the leading jet p_T , (e) the E_T^{miss} , and (f) the invariant mass of leptons 0 and 1, (g) the reconstructed top mass, (h) $\Delta(R)$ between lepton 0 and 1, (i) the $\Delta(R)$ between the closest lepton and jet.

WZ Fit Region - 2j 70-77% WP

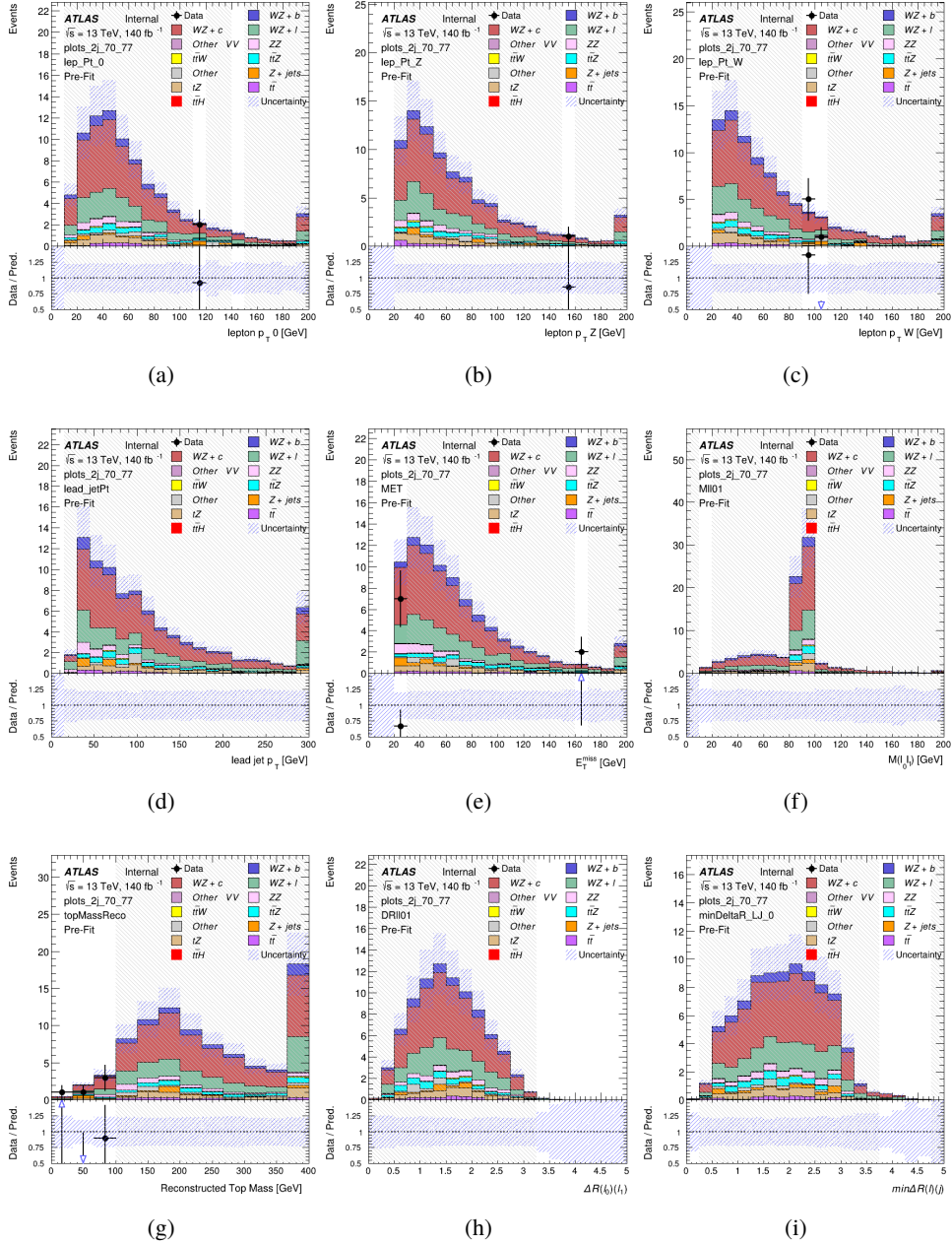


Figure 22: Comparisons between the data and MC distributions in the preselection region for (a) the p_T of the opposite sign lepton, (b) the p_T of the other lepton from the Z candidate, (c) the p_T of the lepton from the W candidate, (d) the leading jet p_T , (e) the E_T^{miss} , and (f) the invariant mass of leptons 0 and 1, (g) the reconstructed top mass, (h) $\Delta(R)$ between lepton 0 and 1, (i) the $\Delta(R)$ between the closest lepton and jet.

WZ Fit Region - 2j 60-70% WP

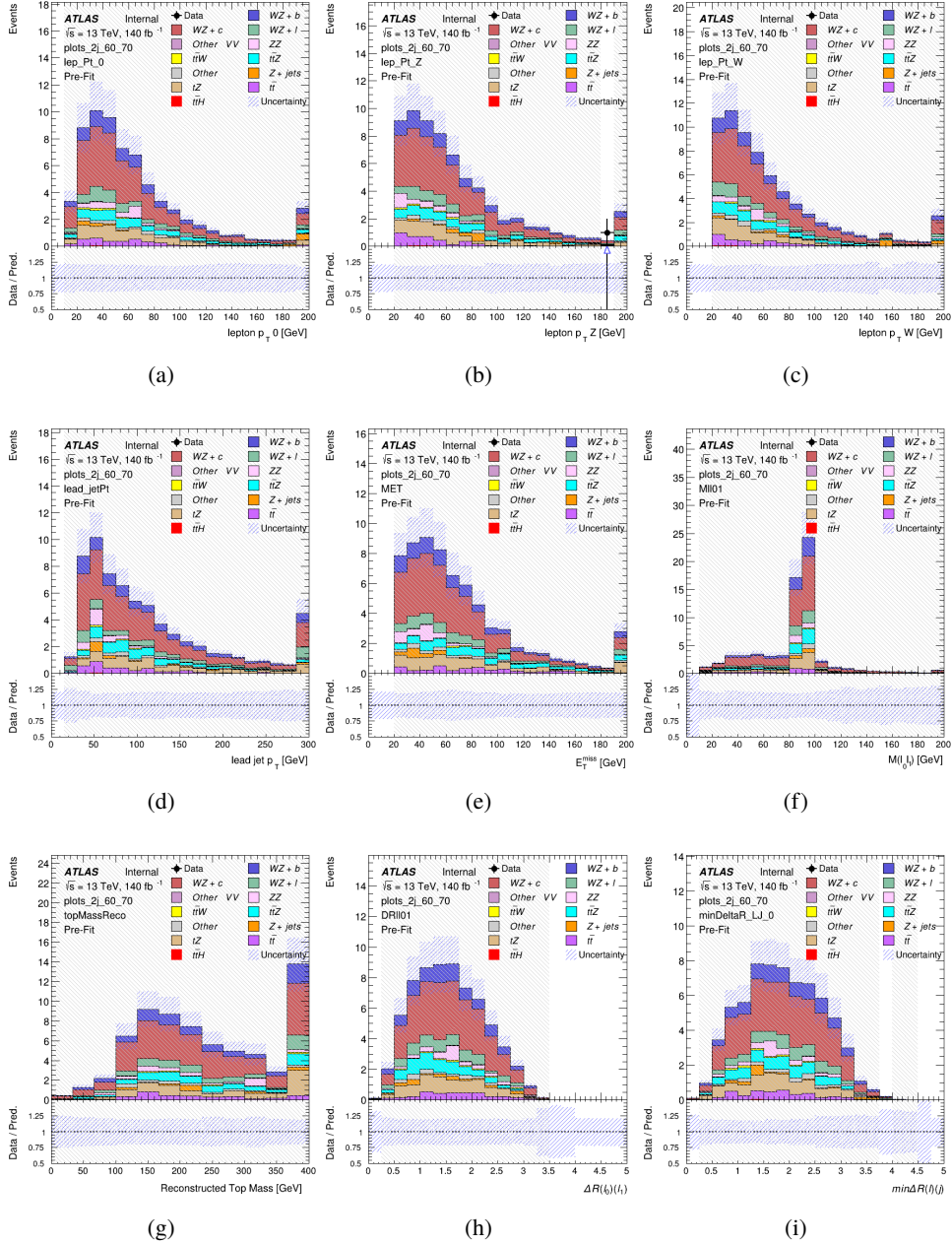


Figure 23: Comparisons between the data and MC distributions in the preselection region for (a) the p_T of the opposite sign lepton, (b) the p_T of the other lepton from the Z candidate, (c) the p_T of the lepton from the W candidate, (d) the leading jet p_T , (e) the E_T^{miss} , and (f) the invariant mass of leptons 0 and 1, (g) the reconstructed top mass, (h) $\Delta(R)$ between lepton 0 and 1, (i) the $\Delta(R)$ between the closest lepton and jet.

WZ Fit Region - 2j 60% WP

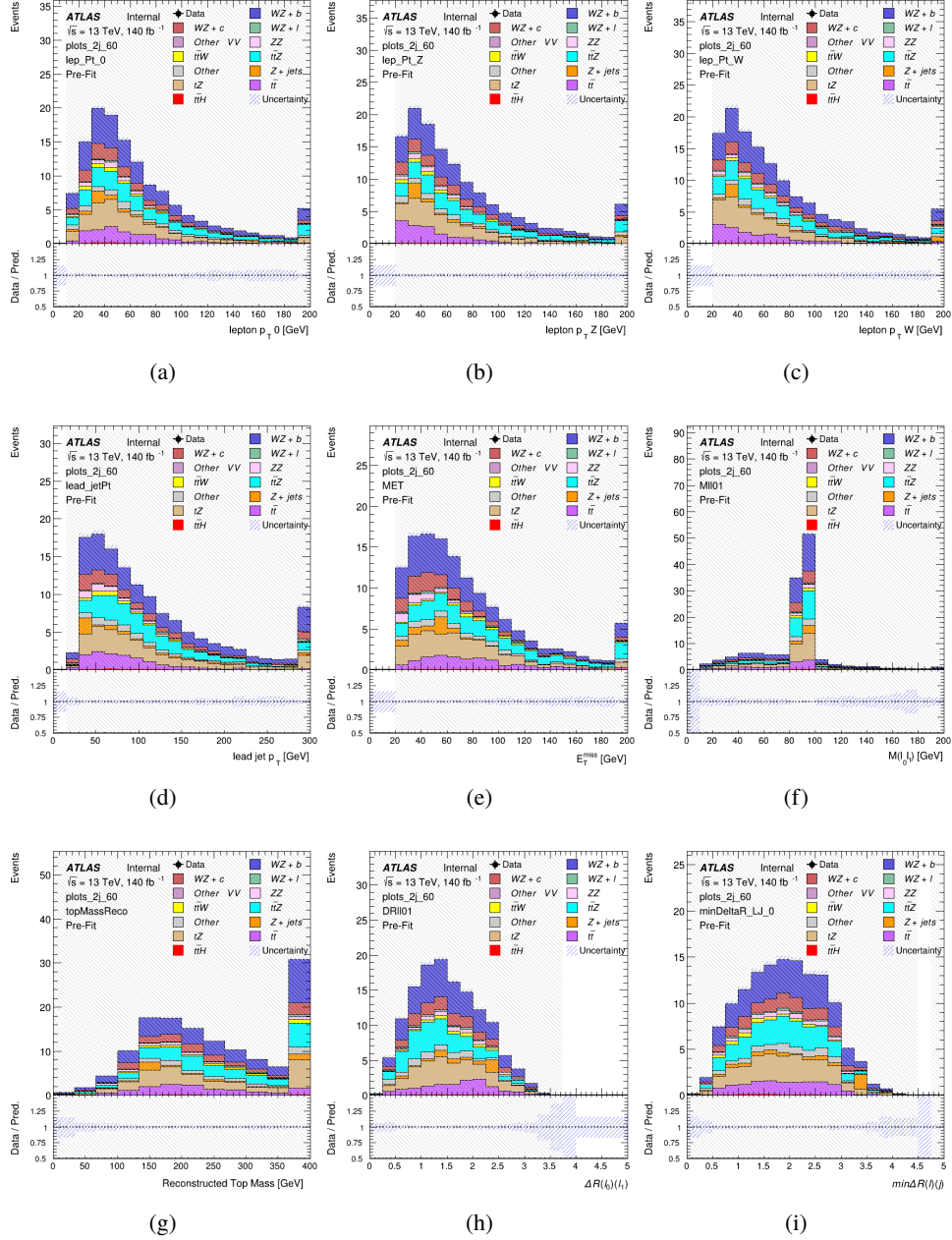


Figure 24: Comparisons between the data and MC distributions in the preselection region for (a) the p_T of the opposite sign lepton, (b) the p_T of the other lepton from the Z candidate, (c) the p_T of the lepton from the W candidate, (d) the leading jet p_T , (e) the E_T^{miss} , and (f) the invariant mass of leptons 0 and 1, (g) the reconstructed top mass, (h) $\Delta(R)$ between lepton 0 and 1, (i) the $\Delta(R)$ between the closest lepton and jet.

WZ Fit Region - tZ-CR-2j

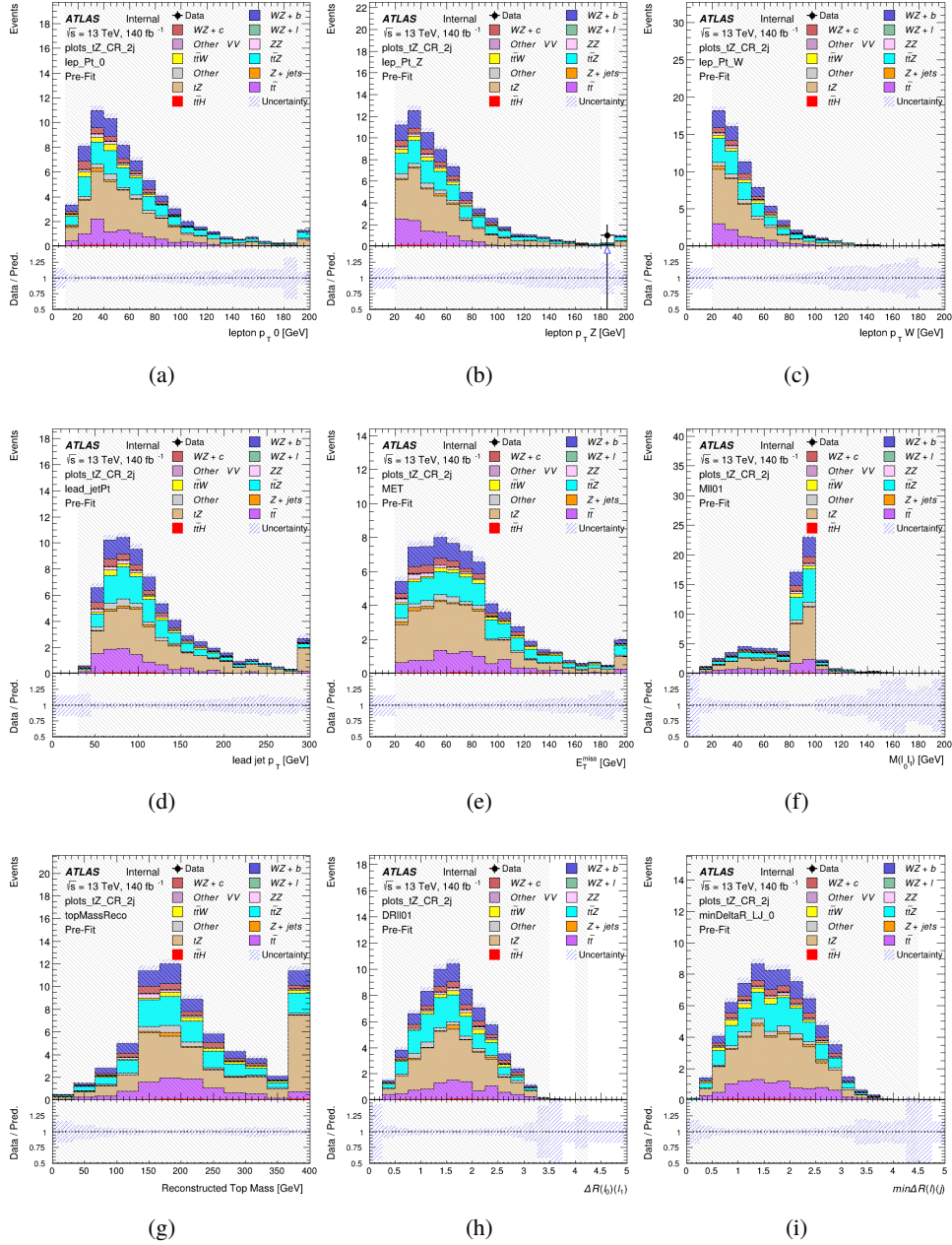


Figure 25: Comparisons between the data and MC distributions in the preselection region for (a) the p_T of the opposite sign lepton, (b) the p_T of the other lepton from the Z candidate, (c) the p_T of the lepton from the W candidate, (d) the leading jet p_T , (e) the E_T^{miss} , and (f) the invariant mass of leptons 0 and 1, (g) the reconstructed top mass, (h) $\Delta(R)$ between lepton 0 and 1, (i) the $\Delta(R)$ between the closest lepton and jet.

458 **6.3 Non-Prompt Lepton Estimation**

459 Two processes that act as sources of non-prompt leptons appear in the analysis: $t\bar{t}$ and Z+jet
 460 production both produce two prompt leptons, and each contribute to the 31 region when an
 461 additional non-prompt lepton appears in the event. The contribution of these processes is
 462 estimated with Monte Carlo simulations, which are validated using enriched validation regions.

463 The modelling in the Z+jets and $t\bar{t}$ CRs is further validated for each of the pseudo-continuous
 464 b-tag regions used in the analysis. The relevant lepton p_T spectrum in each b-tag region is shown
 465 in Appendix A.2 for these CRs after the correction factors derived below have been applied.

466 **6.3.1 $t\bar{t}$ Validation**

467 $t\bar{t}$ events can produce two prompt leptons from the decay of each of the tops. These top decays
 468 produce two b-quarks, the decay of which can produce additional non-prompt leptons, which
 469 occasionally pass the event preselection. In order to validate that the Monte Carlo simulates this
 470 process accurately, the MC prediction in a non-prompt $t\bar{t}$ enriched validation region is compared
 471 to data.

472 The $t\bar{t}$ validation region is similar to the preselection region - three leptons meeting the criteria
 473 described in Section 6 are required, and the requirements on E_T^{miss} remain the same. However,
 474 the selection requiring that a lepton pair form a Z-candidate are reversed. Events where the
 475 invariant mass of any two opposite sign, same flavor leptons falls within 10 GeV of 91.2 GeV are
 476 rejected. This ensures the $t\bar{t}$ validation region is orthogonal to the preselection region.

477 Further, because the jet multiplicity of $t\bar{t}$ events tends to be higher than WZ + jets, the number
 478 of jets in each event is required to be greater than 1. As b-jets are almost invariably produced
 479 from top decays, at least one b-tagged jet passing the 70% DL1r WP in each event is required.
 480 Various kinematic plots of this region are shown in Figure 26.

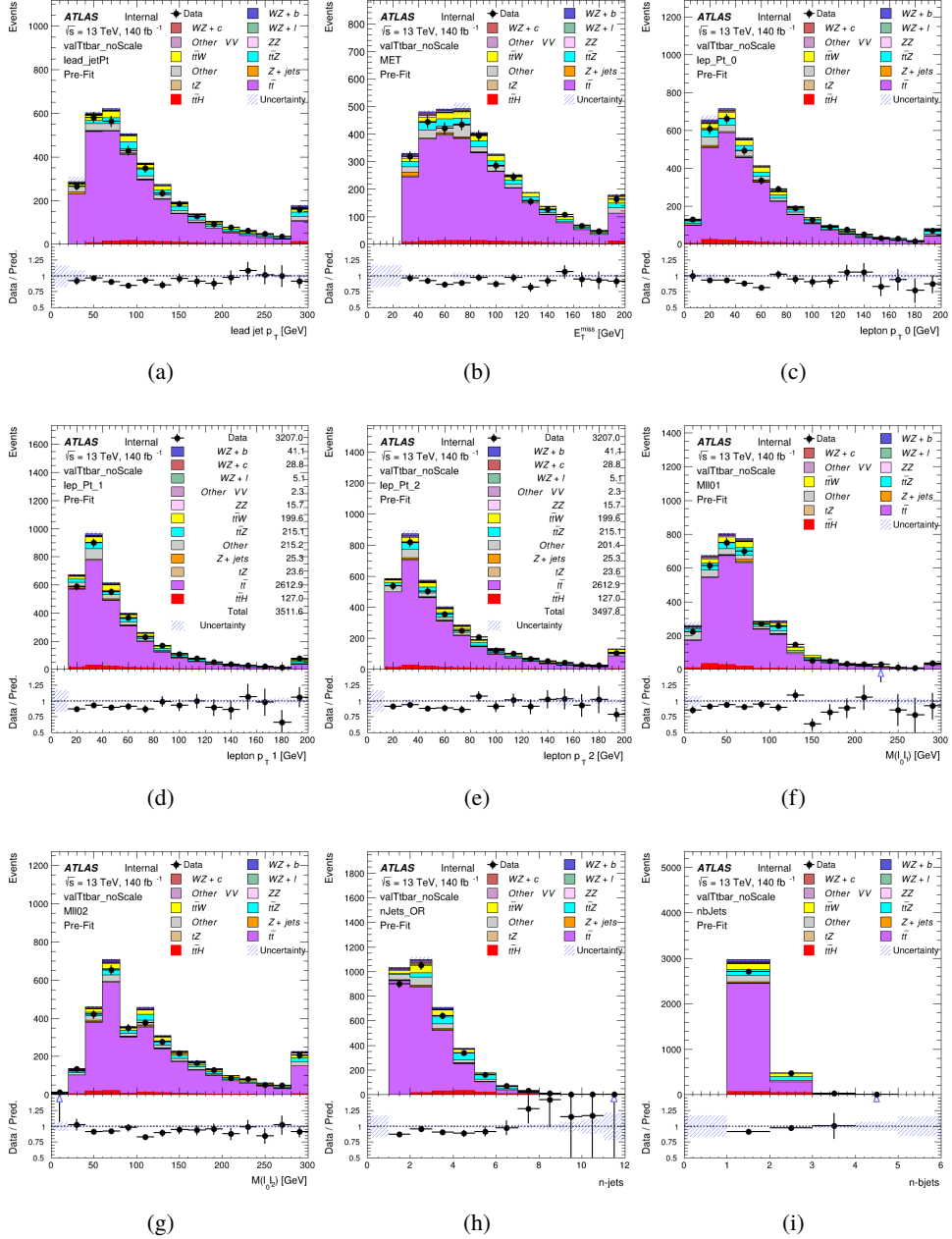


Figure 26: Comparisons between the data and MC distributions in the $t\bar{t}$ validation region for (a) the p_T of the leading jet, (b) the missing transverse energy, (c) the p_T of lepton 0, (d) p_T of lepton 1, (e) p_T of lepton 2, (f) the invariant mass of leptons 0 and 1, (g) the invariant mass of leptons 0 and 2, (h) the number of jets, (i) the number of b-tagged jets.

481 The shape of each distribution agrees quite well between data and MC, with a constant offset
 482 between the two. This is accounted for by applying a constant correction factor of 0.9 to the $t\bar{t}$

483 MC prediction. Plots showing the kinematics of the $t\bar{t}$ VR after this correction factor has been
 484 applied are shown in Figure 27.

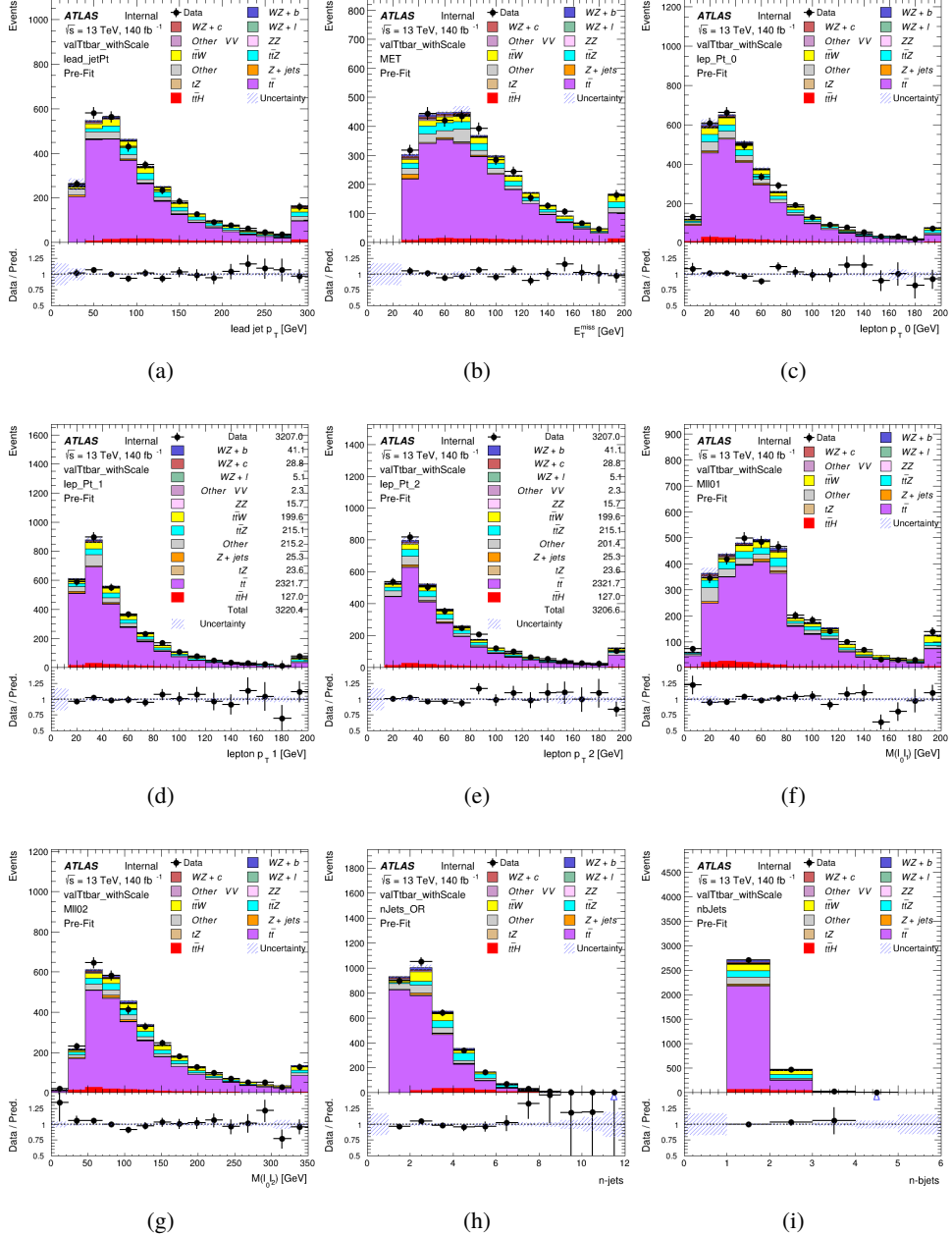


Figure 27: Comparisons between the data and MC distributions in the $t\bar{t}$ validation region after the correction factor has been applied for (a) the p_T of the leading jet, (b) the missing transverse energy, (c) the p_T of lepton 0, (d) p_T of lepton 1, (e) p_T of lepton 2, (f) the invariant mass of leptons 0 and 1, (g) the invariant mass of leptons 0 and 2, (h) the number of jets, (i) the number of b-tagged jets.

485 The modeling is further validated by looking at the yield in the $t\bar{t}$ VR for each DL1r WP, giving
 486 a clearer correspondence to the signal regions used in the fit. For these plots, the requirement
 487 that each event contain at least one b-tagged jet is removed. Each region shown in Figure 28
 488 requires one or more jets pass the listed WP, with no jets passing the next highest WP.

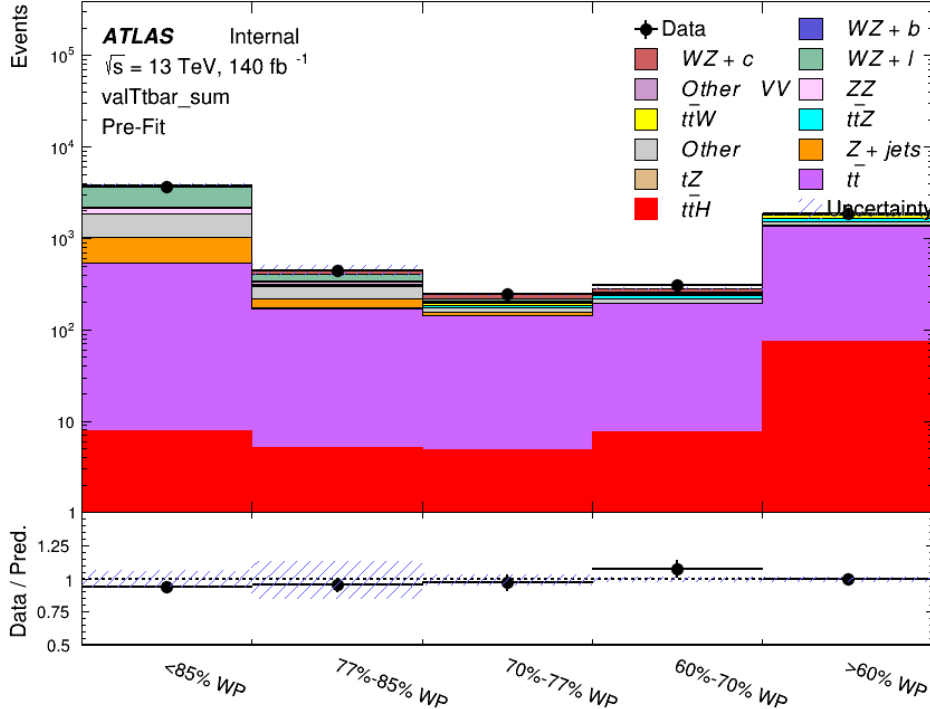


Figure 28: Data and MC comparisons for each DL1r WP for both 1-jet and 2-jet regions, after the $t\bar{t}$ VR selection and correction factor have been applied

489 As data and MC are found to agree within 20% for each of these working points, a 20% systematic
 490 uncertainty on the $t\bar{t}$ prediction is included for the analysis.

491 6.3.2 Z+jets Validation

492 Similar to $t\bar{t}$, a Z+jets validation region is produced in order to validate the MC predictions.
 493 The lepton requirements remain the same as the preselection region. Because no neutrinos are
 494 present for this process, the E_T^{miss} cut is reversed, requiring $E_T^{\text{miss}} < 30 \text{ GeV}$. This also ensures
 495 this validation region is orthogonal to the preselection region. Further, the number of jets in each
 496 event is required to be greater than or equal to one. Various kinematic plots of this region are
 497 shown below. The general agreement between data and MC in each of these suggests that the
 498 contribution of Z+jets is well modeled by Monte Carlo.

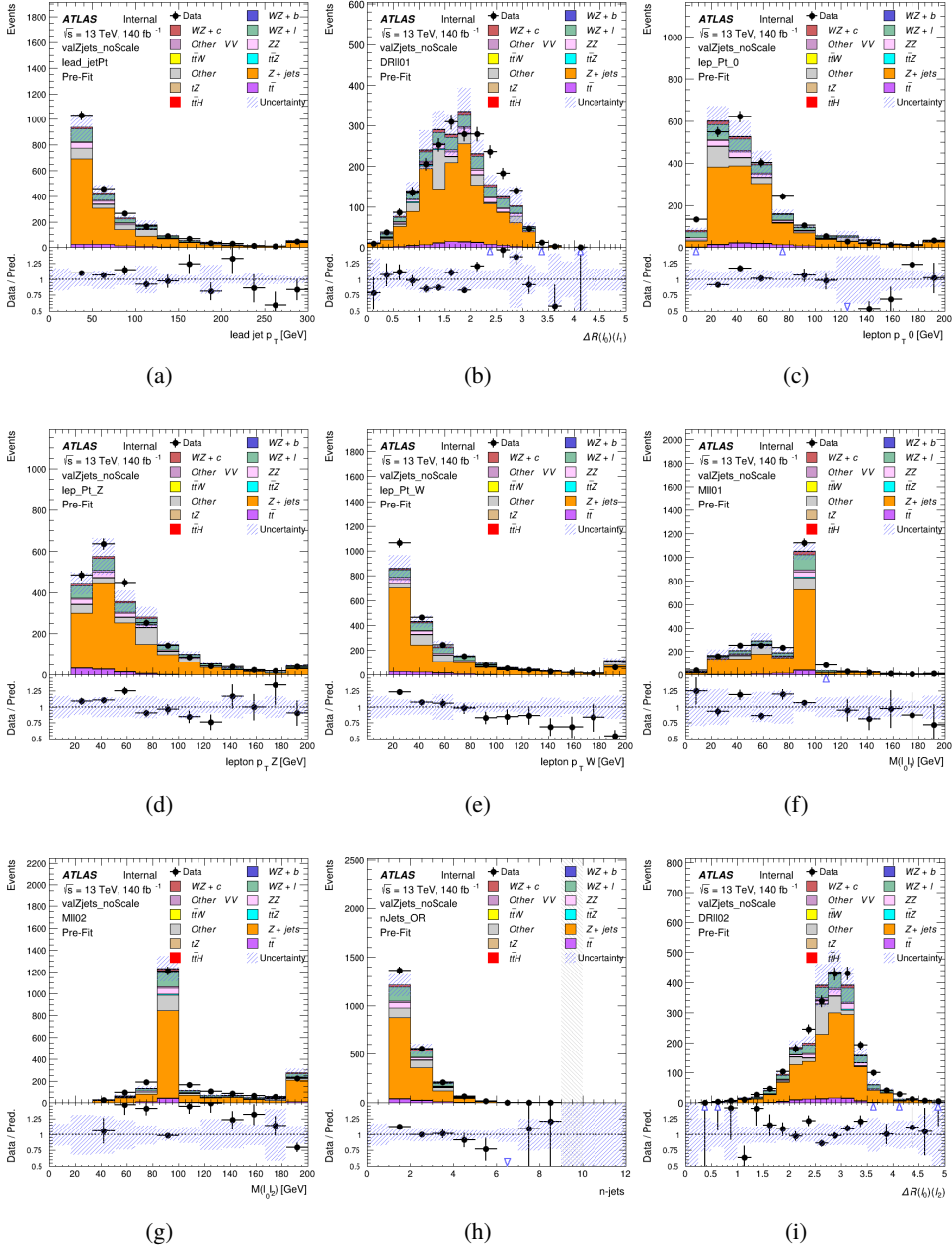


Figure 29: Comparisons between the data and MC distributions in the Z+jets validation region for (a) the p_T of the leading jet, (b) ΔR between leptons 0 and 1, (c) the p_T of lepton 0, (d) p_T of SS lepton from the Z candidate, (e) p_T of the SS lepton from the W candidate, (f) the invariant mass of leptons 0 and 1, (g) the invariant mass of leptons 0 and 2, (h) the number of jets, (i) ΔR between leptons 0 and 2. Includes only statistical uncertainties

499 While there is general agreement between data and MC within statistical uncertainty, the shape

of the p_T spectrum of the lepton from the W candidate is found to differ. As this is the lepton not included in the Z-candidate, in the case of Z+jets, this lepton is most often the non-prompt lepton. A similar effect is seen for both non-prompt muons and electrons in the Z+jets validation region, as shown in Figure 30.

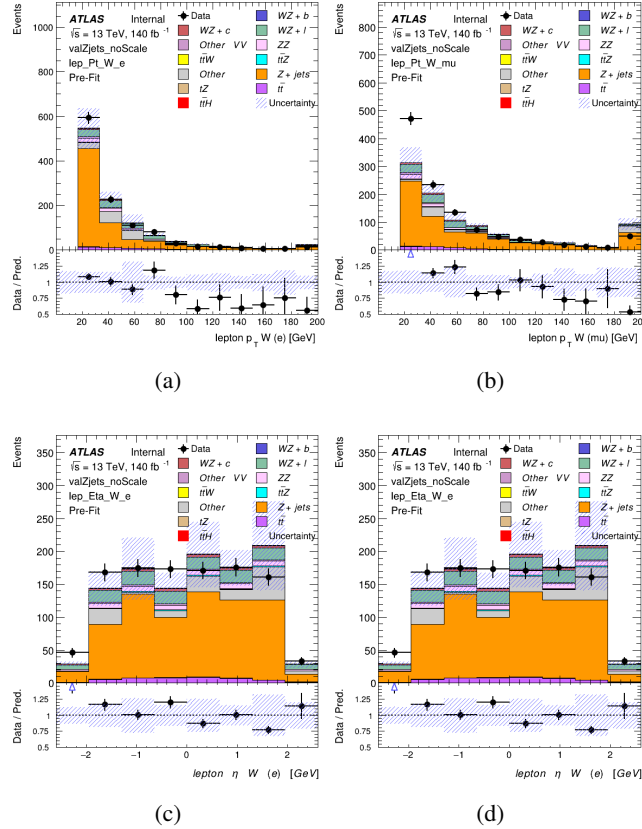


Figure 30: p_T spectrum of the lepton from the W candidate for (a) electrons and (b) muons, as well as η spectrum for (c) electrons and (d) muons, before the correction has been applied

To account for this discrepancy, a variable correction factor is applied to Z+jets. χ^2 minimization of the W lepton p_T spectrum is performed to derive a correction factor as a function of this p_T . Kinematic plots of the Z + jets validation region after this correction factor has been applied are shown in Figure 31.

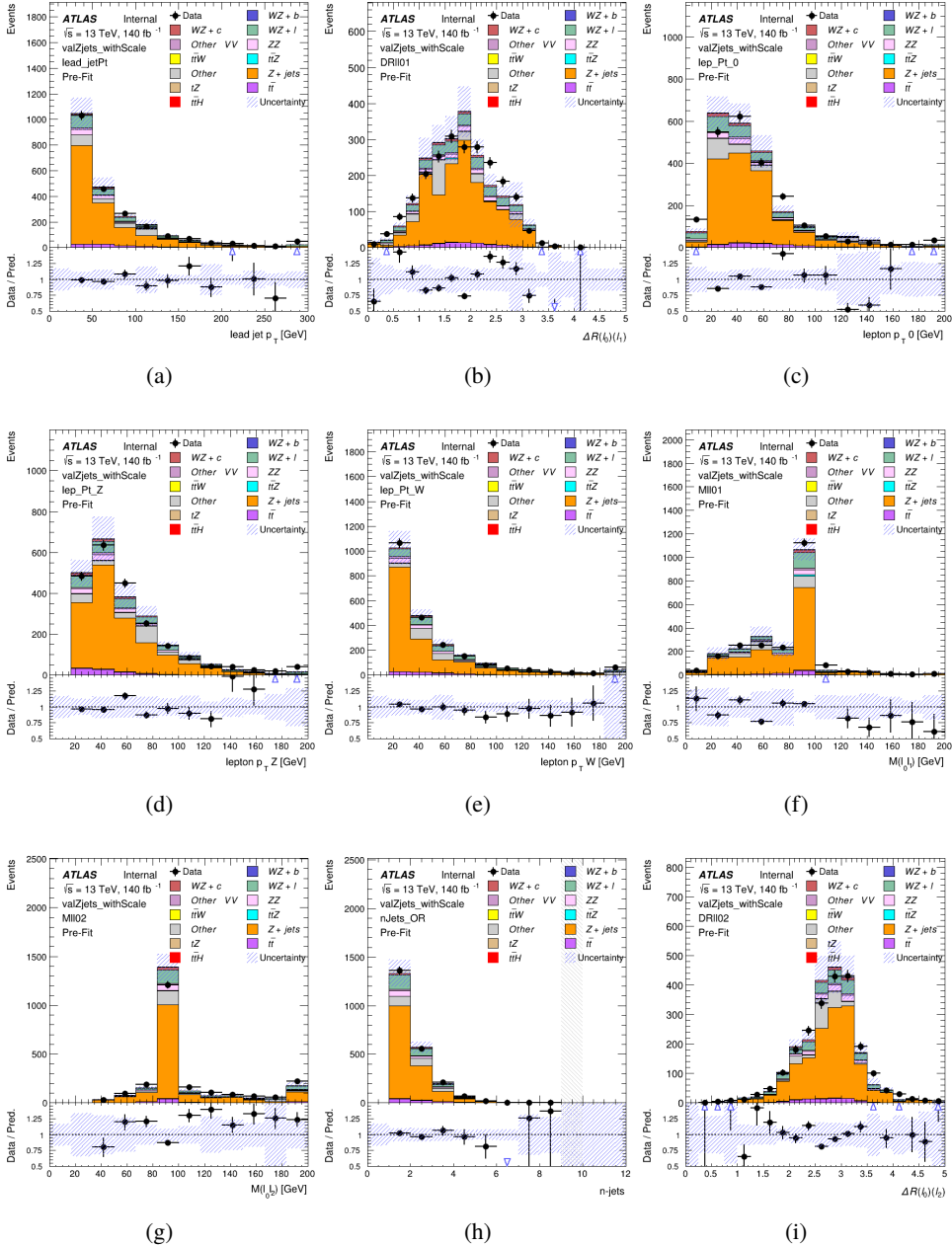


Figure 31: Comparisons between the data and MC distributions in the Z+jets validation region after the correction factor has been applied for (a) the p_T of the leading jet, (b) ΔR between leptons 0 and 1, (c) the p_T of lepton 0, (d) p_T of SS lepton from the Z candidate, (e) p_T of the SS lepton from the W candidate, (f) the invariant mass of leptons 0 and 1, (g) the invariant mass of leptons 0 and 2, (h) the number of jets, (i) ΔR between leptons 0 and 2

508 The p_T and η of the lepton from the W candidate split by lepton flavor after this correction has

been applied is shown in figure 32.

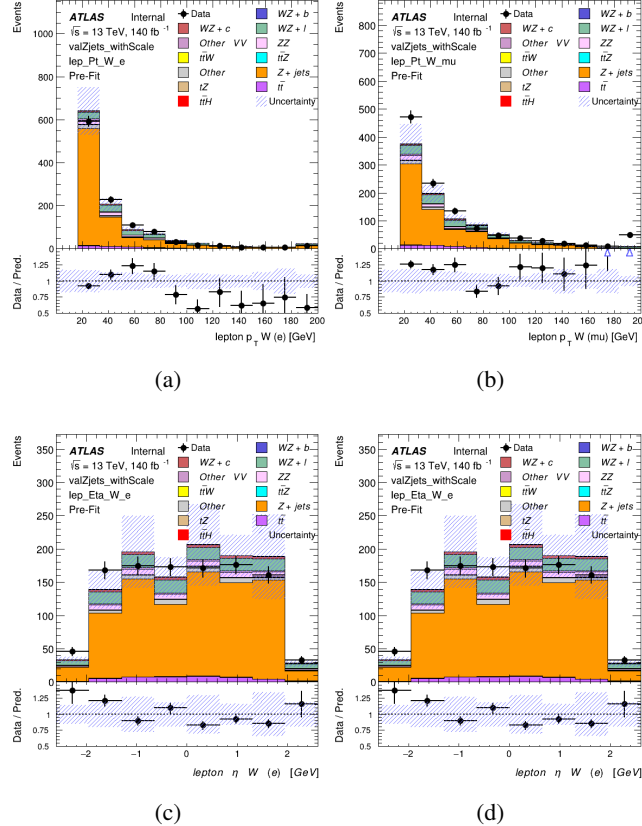


Figure 32: p_T spectrum of the lepton from the W candidate for (a) electrons and (b) muons, as well as η spectrum for (c) electrons and (d) muons, after the correction has been applied

The modeling is further validated by looking at the yield in the Z+jets VR for each DL1r WP, giving a clearer correspondence to the signal regions used in the fit. Each region shown in Figure 33 requires one or more jets pass the listed WP, with no jets passing the next highest WP.

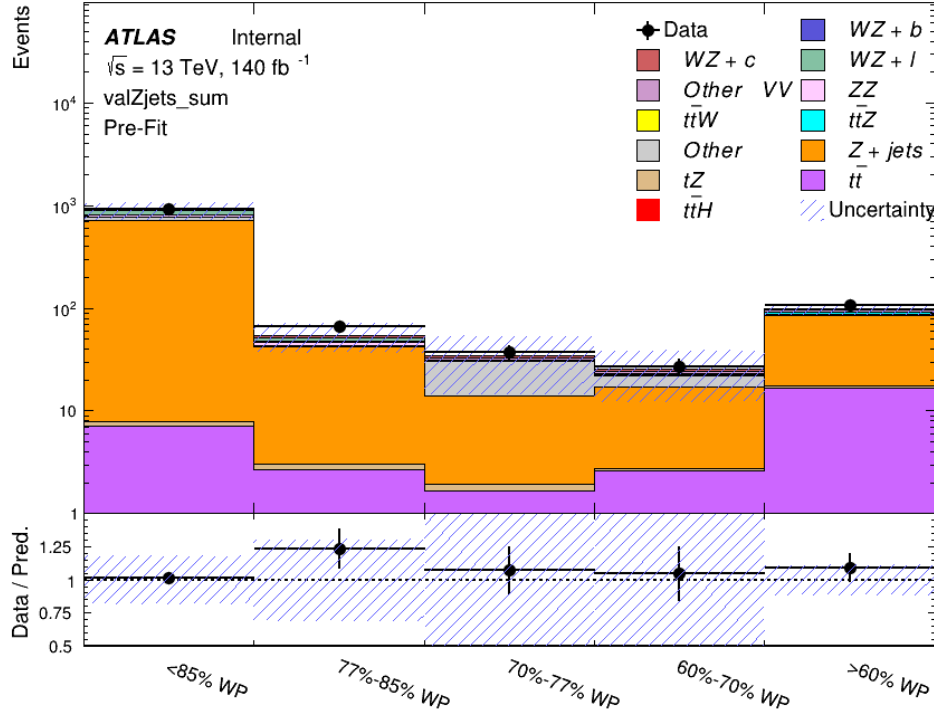


Figure 33: Data and MC comparisons for each DL1r WP for both 1-jet and 2-jet regions, after the Z+jets VR selection and correction factor have been applied

513 For each of the b-tagging working points considered, the data falls within 25% of the MC
 514 prediction once this correction factor has been applied. Therefore, a 25% systematic uncertainty
 515 is applied to Z + jets in the analysis.

516 7 Systematic Uncertainties

517 The systematic uncertainties that are considered are summarized in Table 9. These are imple-
 518 mented in the fit either as a normalization factors or as a shape variation or both in the signal and
 519 background estimations. These systematic uncertainties are treated as independent nuisance
 520 parameters (NPs) in the fit, and are assumed to be gaussian. Each NP is varied up and down by
 521 its uncertainty, and the difference in the result of the fit is taken to be the systematic uncertainty
 522 of that NP. The numerical impact of each of these uncertainties is outlined in Section 8.

Table 9: Sources of systematic uncertainty considered in the analysis.

Systematic uncertainty	Components
Luminosity	1
Pileup reweighting	1
Physics Objects	
Electron	5
Muon	14
Prompt Lepton Veto	1
Jet energy scale	28
Jet energy resolution	8
Jet vertex fraction	1
Jet flavor tagging	131
E_T^{miss}	3
Total (Experimental)	194
Signal Modeling	
Shape modelling	3
Renormalization and factorization scales	5
nJet Migration	5
Background Modeling	
Cross section	15
Renormalization and factorization scales	12
Parton shower and hadronization model	2
Shower tune	4
Total (Signal and background modeling)	41
Total (Overall)	235

523 The uncertainty in the combined 2015–2018 integrated luminosity is 1.7% [25], obtained using
 524 the LUCID-2 detector [26] for the primary luminosity measurements.

525 The experimental uncertainties are related to the reconstruction and identification of light
 526 leptons and b-tagging of jets, and to the reconstruction of E_T^{miss} . The TOTAL electron ID
 527 correlation model is used, corresponding to 1 electron ID systematic [27]. Electron ID is found
 528 to be a subleading systematic that is unconstrained by the fit, making it an appropriate choice for
 529 this analysis.

530 The sources which contribute to the uncertainty in the jet energy scale (JES) [28] are de-
 531 composed into uncorrelated components and treated as independent sources in the analysis.
 532 The CategoryReduction model is used to account for JES uncertainties, which decomposes the
 533 uncertainties into 30 nuisance parameters included in the fit. The SimpleJER model is used

534 to account for jet energy resolution (JER) uncertainties, and 8 JER uncertainty components are
535 included as NPs in the fit.

536 The uncertainties in the b-tagging efficiencies measured in dedicated calibration analyses
537 [19] are also decomposed into uncorrelated components. The large number of components for
538 b-tagging is due to the use of the full continuous b-tagging spectrum: The calibration of the
539 distribution of the MVA discriminant for each of the individual working points considered for
540 b— c— and light jets, and the correlations between them, produces a large number of systematic
541 uncertainties.

542 The full list of systematic uncertainties considered in the analysis is summarized in Tables 10,
543 11 and 12.

544

Experimental Systematics on Leptons and E_T^{miss}			
Type	Description	Systematics Name	Application
Trigger			
Scale Factors	Trigger Efficiency	lepSFTrigTight_MU(EL)_SF_Trigger_STAT(SYST)	Event Weight
Muons			
Efficiencies	Reconstruction and Identification	lepSFObjTight_MU_SF_ID_STAT(SYST)	Event Weight
	Isolation	lepSFObjTight_MU_SF_Isol_STAT(SYST)	Event Weight
	Track To Vertex Association	lepSFObjTight_MU_SF_TTVA_STAT(SYST)	Event Weight
p_T Scale	p_T Scale	MUONS_SCALE	p_T Correction
Resolution	Inner Detector Energy Resolution	MUONS_ID	p_T Correction
	Muon Spectrometer Energy Resolution	MUONS_MS	p_T Correction
Electrons			
Efficiencies	Reconstruction	lepSFObjTight_EL_SF_ID	Event Weight
	Identification	lepSFObjTight_EL_SF_Reco	Event Weight
	Isolation	lepSFObjTight_EL_SF_Isol	Event Weight
Scale Factor	Energy Scale	EG_SCALE_ALL	Energy Correction
Resolution	Energy Resolution	EG_RESOLUTION_ALL	Energy Correction
E_T^{miss}			
Soft Tracks Terms	Resolution	MET_SoftTrk_ResoPerp	p_T Correction
	Resolution	MET_SoftTrk_ResoPara	p_T Correction
	Scale	MET_SoftTrk_ScaleUp	p_T Correction
	Scale	MET_SoftTrk_ScaleDown	p_T Correction

Table 10: Summary of experimental systematics considered for leptons and E_T^{miss} . Includes type, description, name of systematic as used in the fit, and mode of application. The mode of application indicates the systematic evaluation, e.g. as an overall event re-weighting (Event Weight) or rescaling (p_T Correction).

Experimental Systematics on Jets			
Type	Origin	Systematics Name	Application
Jet Vertex Tagger		JVT	Event Weight
Energy Scale	Calibration Method	JET_21NP_ JET_EffectiveNP_1-19	p_T Correction p_T Correction
	η inter-calibration	JET_EtaIntercalibration_Modelling JET_EtaIntercalibration_NonClosure JET_EtaIntercalibration_TotalStat	p_T Correction p_T Correction p_T Correction
	High p_T jets	JET_SingleParticle_HighPt	p_T Correction
	Pile-Up	JET_Pileup_OffsetNPV JET_Pileup_OffsetMu JET_Pileup_PtTerm JET_Pileup_RhoTopology	p_T Correction p_T Correction p_T Correction p_T Correction
	Non Closure	JET_PunchThrough_MC15	p_T Correction
	Flavour	JET_Flavor_Response JET_BJES_Response JET_Flavor_Composition	p_T Correction p_T Correction p_T Correction
Resolution		JET_JER_EffectiveNP_NP_1-8	Event Weight

Table 11: Jet systematics take into account effects of jets calibration method, η inter-calibration, high p_T jets, pile-up, and flavor response. They are all diagonalised into effective parameters.

Experimental Systematics on b-tagging		
Type	Origin	Systematic Name
Scale Factors	DL1r b-tagger efficiency on b originated jets in bins of η	DL1r_Continuous_EventWeight_B0-29
	DL1r b-tagger efficiency on c originated jets in bins of η	DL1r_Continuous_EventWeight_C0-19
	DL1r b-tagger efficiency on light flavoured originated jets in bins of η and p_T	DL1r_Continuous_EventWeight_Light0-79
	DL1r b-tagger extrapolation efficiency	DL1r_Continuous_EventWeight_extrapolation DL1r_Continuous_EventWeight_extrapolation_from_charm

Table 12: Summary of experimental systematics to be included for b-tagging of jets in the analysis, using the continuous DL1r tagging algorithm. All of the b-tagging related systematics are applied as event weights. From left: type, description, and the name of systematic used in the fit.

545 Theoretical uncertainties applied to MC predictions, including cross section, PDF, and scale
 546 uncertainties are taken from theory calculations, with the exception of non-prompt and diboson
 547 backgrounds. The cross-section uncertainty on tZ is taken from [29]. Derivation of the non-
 548 prompt background uncertainties, Z+jets and t \bar{t} , is explained in detail in Section 6.3. These
 549 normalization uncertainties are chosen so as to account for the complete uncertainty in the
 550 non-prompt contribution, and therefore no additional modelling uncertainties are considered for
 551 Z+jets and t \bar{t} .

552 The other VV + heavy flavor processes (namely VV+b and VV+charm, which primarily consist
 553 of ZZ events) are also poorly understood, because these processes involve the same physics as
 554 WZ + heavy flavor, and have also not been measured. Therefore, an arbitrary 50% uncertainty is
 555 applied to those samples, as it is found to have little impact on the significance of the final result:
 556 Fits were performed with this uncertainty decreased to 25% and increased to 75% and no change
 557 in the final result was observed.

558 The theory uncertainties applied to the predominate background estimates are summarized in
 559 Table 13.

Process	X-section [%]
WZ	QCD Scale: $^{+3.7}_{-3.4}$ PDF($+\alpha_S$): ± 3.1
tZ	X-sec: ± 15.2
t̄t H (aMC@NLO+Pythia8)	QCD Scale: $^{+5.8}_{-9.2}$ PDF($+\alpha_S$): ± 3.6
t̄t Z (aMC@NLO+Pythia8)	QCD Scale: $^{+9.6}_{-11.3}$ PDF($+\alpha_S$): ± 4
t̄t W (aMC@NLO+Pythia8)	QCD Scale: $^{+12.9}_{-11.5}$ PDF($+\alpha_S$): ± 3.4
VV + b/charm (Sherpa 2.2.1)	± 50
VV + light (Sherpa 2.2.1)	± 6
t̄t	± 20
Z + jets	± 25
Others	± 50

Table 13: Summary of theoretical uncertainties for MC predictions in the analysis.

560 Due to its importance as a background, additional modelling uncertainties are considered for tZ.
 561 Alternative tZ samples with variations in scale (DSID 412064-5) and shower modelling (DSID
 562 501046) are included as systematics..

563 The fit involves varying the overall normalization of signal templates over the regions de-
 564 scribed in Section 6.2, which are defined by the flavor and number of associated jets at truth-
 565 level. The modelling of these template shapes therefore significantly impacts the final result.
 566 Additional signal uncertainties, probing the shape of the signal templates as well as the rate of
 567 migrations between the number of truth-jets and reconstructed jets, are estimated by comparing
 568 estimates from the nominal Sherpa WZ samples with alternative WZ samples generated with
 569 Powheg+Pythia8 (DSID 361601). Separate systematics are included in the fit for WZ + b, WZ
 570 + c and WZ + light, where the distribution among each of the fit regions is varied based on the
 571 prediction of the Powheg sample.

572 The variations in the signal templates are shown in Figures 34 and 35. Each of these plots is
 573 normalized to unity in order to capture the relevant differences in shape.

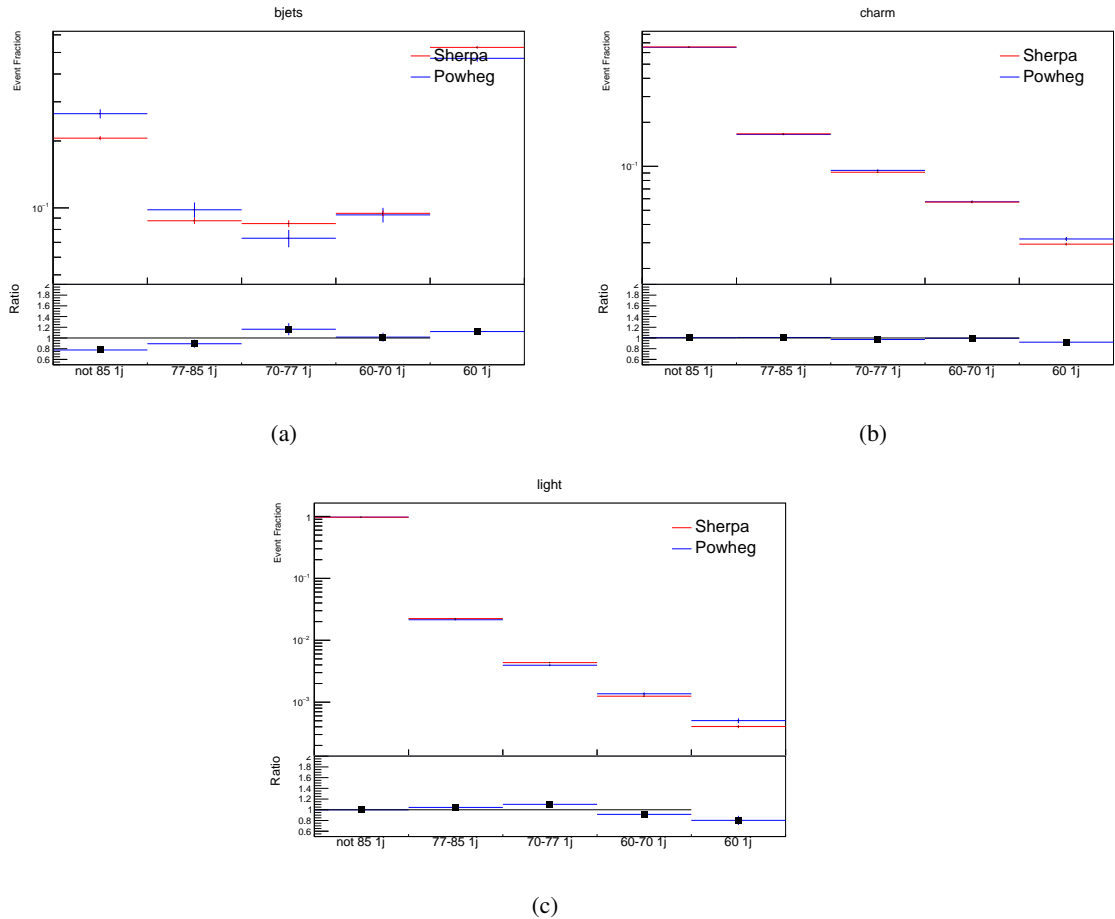


Figure 34: Comparison between Sherpa and Powheg predictions of the distribution of (a) WZ + b, (b) WZ + charm, and (c) WZ + light among the various b-tag WPs used in the 1-jet fit.

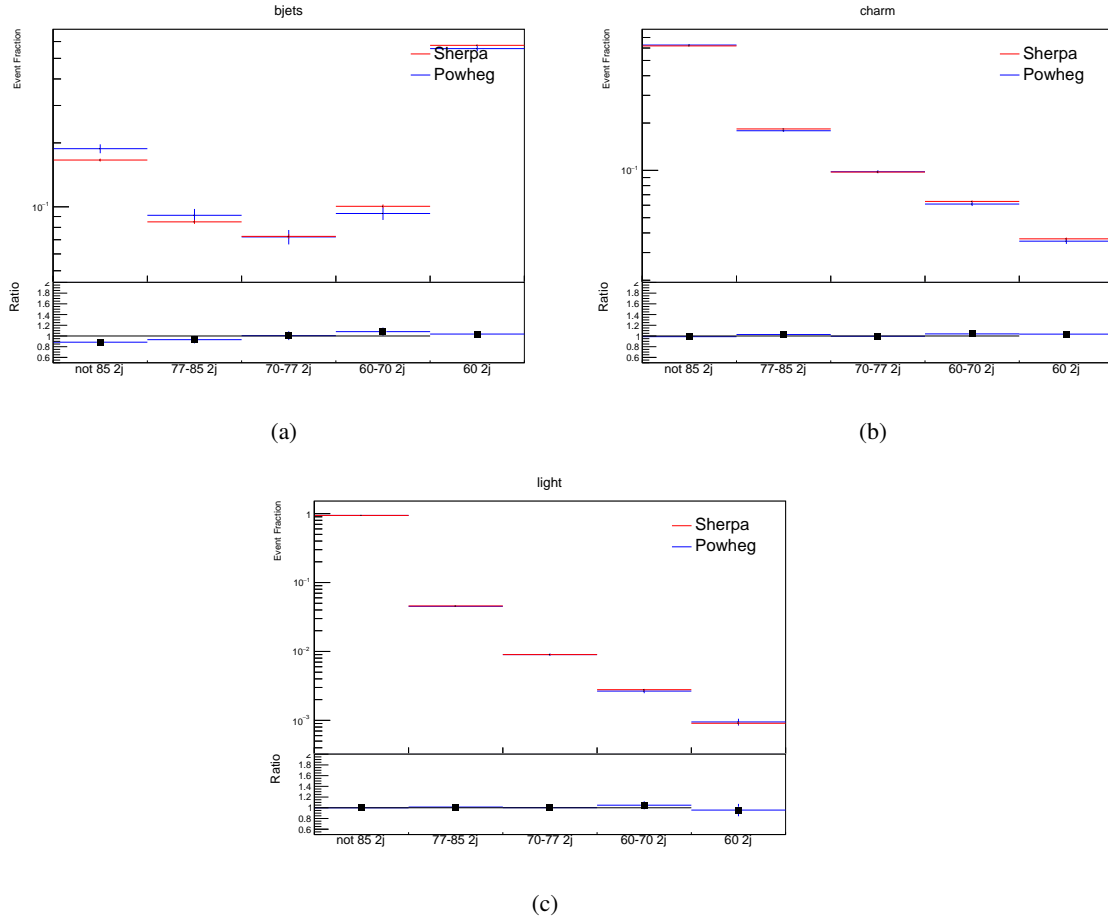


Figure 35: Comparison between Sherpa and Powheg predictions of the distribution of (a) WZ + b, (b) WZ + charm, and (c) WZ + light among the various b-tag WPs used in the 2-jet fit.

574 Separate systematics are included in the fit for WZ + b, WZ + charm and WZ + light, where
 575 the distribution among each of the fit regions is varied based on the prediction of the Powheg
 576 sample.

577 A similar approach is taken to account for uncertainties in migrations between the number of
 578 reco and truth jets. The fraction of events with 1 truth jet which fall into the 1 jet bin versus the
 579 2 jet bin at reco level is compared for Sherpa and Powheg. The same is done for events with 2
 580 truth jets. This comparison is shown in figure 36.

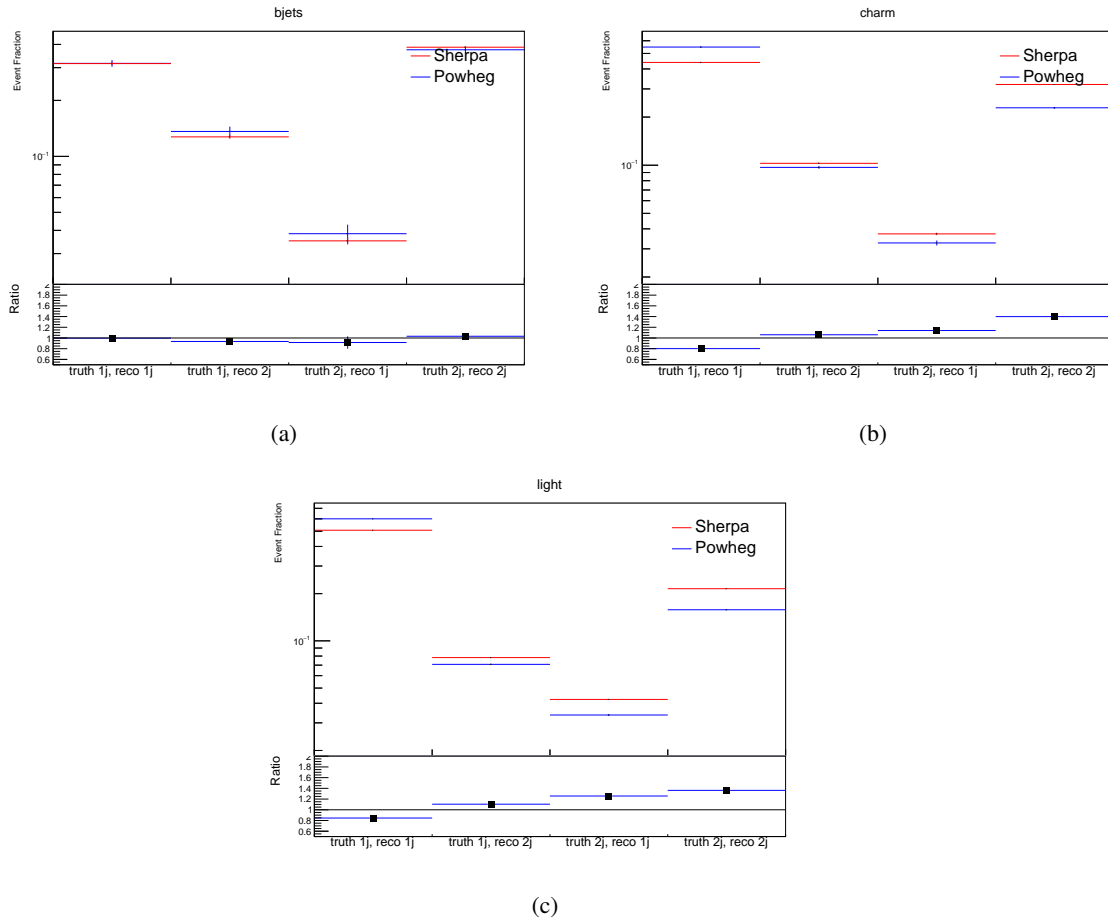


Figure 36: Comparison between Sherpa and Powheg predictions for truth jet migrations between the 1 and 2 jet reco bins for (a) WZ + b, (b) WZ + charm, and (c) WZ + light

581 A systematic is included where events are shifted between the 1-jet and 2-jet regions based on
582 the differences between these two shapes. This is done independently for each of the WZ + b,
583 WZ + charm, and WZ + light templates.

Additional systematics are included to account for the uncertainty in the contamination of 0 jet and 3 or more jet events (at truth level) in the 1 and 2 reco jet bins. Because these events fall outside the scope of this measurement, these events are included as a background. As such, a normalization, rather than a shape, uncertainty is applied for this background.

588 The number of WZ events with 0-jets and $>=3$ -jets in the reconstructed 1-jet and 2-jet regions
 589 are compared for Sherpa and Powheg, as seen in figure 37. These differences are taken as separate
 590 normalization systematics on the yield of WZ+0-jet and WZ+ $>=3$ -jet events.

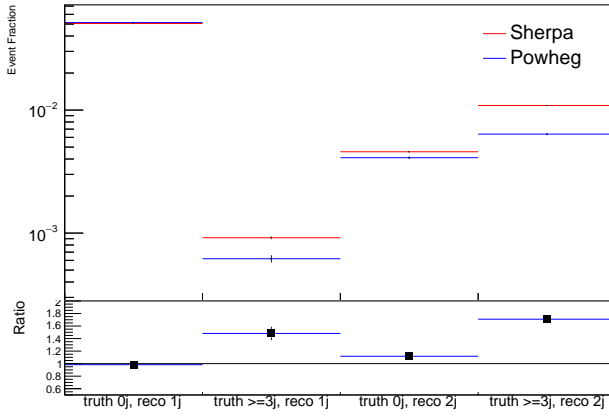


Figure 37: Comparison between Sherpa and Powheg predictions for 0 and ≥ 3 truth jet contributions in the 1 and 2 jet reco bins

8 Results

8.1 Fit Procedure

A maximum-likelihood fit is performed over the unfolded signal templates in the various fit regions described in Section 6 in order to extract the best-fit value of the WZ + b-jet and WZ + charm jet contributions for events with both 1 and 2 associated jets.

Because the fit regions are defined by the number of associated jets at reco-level, an unfolding procedure is applied to the signal in order to account for differences in the number of truth jets compared to the number of reco-jets. The WZ + b, WZ + charm and WZ + light contributions are separated into independent samples based on the number of truth jets in each event. WZ + 1 truth-jet and WZ + 2 truth-jets are treated as signal samples, while WZ + 0 truth-jets and WZ + ≥ 3 truth-jets are treated as an additional background.

A maximum likelihood fit to data is performed simultaneously in the regions described in Section 6, summarized in figure 38. The six signal templates, which include WZ+b 1-jet, WZ+c 1-jet, WZ+l 1-jet, WZ+b 2-jets, WZ+c 2-jets, WZ+l 2-jets, are allowed to float, while the remaining background contributions are held fixed. The parameters $\mu_{WZ+b-1-jet}$, $\mu_{WZ+charm1-jet}$, $\mu_{WZ+light-1-jet}$, $\mu_{WZ+b-2-jet}$, $\mu_{WZ+charm2-jet}$, $\mu_{WZ+light-2-jet}$, where $\mu = \sigma_{\text{observed}}/\sigma_{\text{SM}}$, are extracted from the fit. A simultaneous fit is performed over all 1-jet and 2-jet regions.

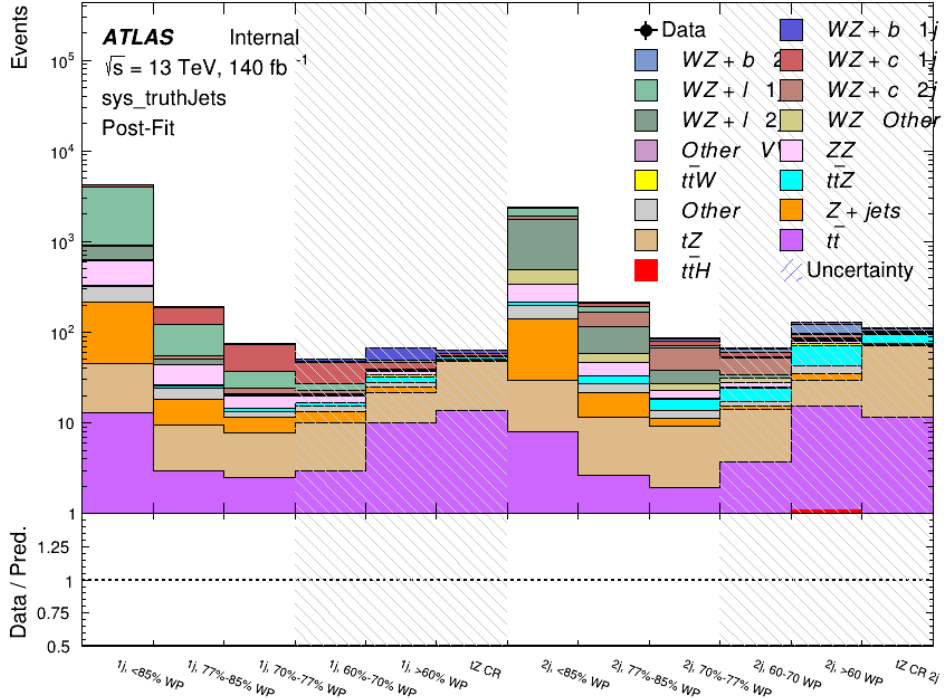


Figure 38: Post-fit summary of the fit regions.

As described in Section 7, there are 235 systematic uncertainties that are considered as NPs in the fit. These NPs are constrained by Gaussian or log-normal probability density functions. The latter are used for normalisation factors to ensure that they are always positive. The expected number of signal and background events are functions of the likelihood. The prior for each NP is added as a penalty term, decreasing the likelihood as it is shifted away from its nominal value.

Several alternative fit strategies are documented in Sections 8.3–8.4.1. These include a measurement of $WZ + 1$ or 2 jets inclusively, a fit where tZ is allowed to float, and a case where tZ is included as part of the signal.

8.2 Results of the Simultaneous Fit

The Asimov fit for 1-jet events gives an expected μ value of $1.00^{+0.47}_{-0.43}(\text{stat})^{+0.30}_{-0.27}(\text{sys})$ for $WZ + b$. The normalization factors extracted from the fit for $WZ + \text{charm}$ and $WZ + \text{light}$ are $1.00^{+0.18}_{-0.17}(\text{stat})^{+0.19}_{-0.17}(\text{sys})$ and $1.00 \pm 0.06 \pm 0.14$, respectively.

The expected cross-section of $WZ+b$ with 1-jet in the fiducial region outlined in Section 2 is $1.74^{+0.82}_{-0.75}(\text{stat})^{+0.53}_{-0.48}(\text{sys}) \text{ fb}$, and $14.6 \pm 2.5(\text{stat}) \pm 2.3(\text{sys}) \text{ fb}$ for $WZ + \text{charm}$, with a

correlation of -0.15 between them. An expected significance of 2.0 is observed for WZ + b in this region.

For 2-jet events, the fit gives an expected μ value of $1.00^{+0.53}_{-0.51}(\text{stat})^{+0.39}_{-0.34}(\text{sys})$ for WZ + b. The fitted cross-section modifiers for WZ + charm and WZ + light are $1.00^{+0.25}_{-0.24}(\text{stat})^{+0.32}_{-0.27}(\text{sys})$ and $1.00 \pm 0.06 \pm 0.16$, respectively.

The expected WZ + b cross-section in the fiducial region with 2 associated jets is $2.5^{+1.3}_{-1.3}(\text{stat})^{+0.95}_{-0.83}(\text{sys})$ fb with an expected significance of 1.7σ . The 2-jet expected cross-section of WZ + charm is $12.7^{+3.3}_{-3.2}(\text{stat})^{+3.9}_{-3.4}(\text{sys}) \pm 3.2(\text{stat}) \pm 2.7(\text{sys})$ fb, and the correlation between WZ + charm and WZ + b is -0.22.

The results of the fit to an Asimov dataset for the fiducial regions considered, including both the normalization factors as well as the expected cross-sections, along with their uncertainties, are summarized in Table 14.

634

Process	μ	σ
WZ + b - 1-jet	$1.00^{+0.47}_{-0.43}(\text{stat})^{+0.30}_{-0.27}(\text{sys})$	$1.74^{+0.82}_{-0.75}(\text{stat})^{+0.53}_{-0.48}(\text{sys})$ fb
WZ + c - 1-jet	$1.00^{+0.18}_{-0.17}(\text{stat})^{+0.19}_{-0.17}(\text{sys})$	$14.6^{+2.5}_{-2.3}(\text{stat})^{+2.6}_{-2.3}(\text{sys})$ fb
WZ + b - 2-jet	$1.00^{+0.53}_{-0.51}(\text{stat})^{+0.39}_{-0.34}(\text{sys})$	$2.5^{+1.3}_{-1.3}(\text{stat})^{+0.95}_{-0.83}(\text{sys})$ fb
WZ + c - 2-jet	$1.00^{+0.25}_{-0.24}(\text{stat})^{+0.32}_{-0.27}(\text{sys})$	$12.7^{+3.3}_{-3.2}(\text{stat})^{+3.9}_{-3.4}(\text{sys})$ fb

Table 14: Normalization factors and cross-sections extracted from the fit for each of the fiducial regions considered

An expected significance of 2.0σ is observed for WZ + b with 1-jet, and 1.7σ for WZ + b with two jets. A summary of the correlations between these various measurements is shown in Figure 39.

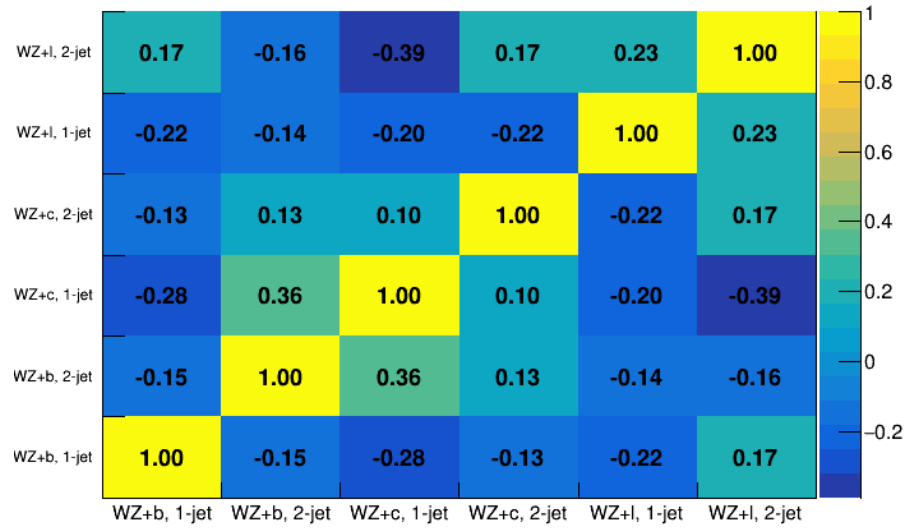


Figure 39: Correlations between the various measured components of WZ.

638 The pre-fit yields in each of the 1-jet regions used in the fit are shown in Table 15.

639

Sample	1j, <85% WP	1j, 77%-85% WP	1j, 70%-77% WP	1j, 60%-70% WP	1j, 60% WP	tZ CR
WZ + b – 1j	8.1 ± 1.6	4.7 ± 0.5	4.6 ± 0.4	5.1 ± 0.4	18.1 ± 2.4	5.0 ± 0.6
WZ + c – 1j	260 ± 22	81 ± 6	43.1 ± 3.6	25.8 ± 2.6	9.4 ± 1.8	2.9 ± 0.6
WZ + l – 1j	3090 ± 250	91 ± 13	17 ± 3	4.9 ± 1.6	1.3 ± 0.4	0.2 ± 0.1
WZ + b – 2j	1.10 ± 0.37	0.44 ± 0.11	0.39 ± 0.06	0.62 ± 0.14	2.1 ± 0.5	0.59 ± 0.14
WZ + c – 2j	21 ± 5	5.6 ± 1.2	3.0 ± 0.7	2.0 ± 0.5	0.70 ± 0.20	0.30 ± 0.08
WZ + l – 2j	250 ± 60	5.7 ± 1.6	0.73 ± 0.53	0.31 ± 0.15	0.07 ± 0.06	0.01 ± 0.01
WZ – Other	13 ± 5	1.4 ± 0.4	0.42 ± 0.08	0.2 ± 0.01	0.30 ± 0.05	0.67 ± 0.15
Other VV	6.2 ± 0.6	0.2 ± 0.4	0.2 ± 0.04	0.07 ± 0.1	0.1 ± 0.1	0.1 ± 0.2
ZZ	336 ± 26	17.8 ± 2.1	4.3 ± 0.6	1.7 ± 0.5	0.36 ± 0.08	0.10 ± 0.03
t <bar>t>W</bar>	1.1 ± 0.2	0.2 ± 0.1	0.3 ± 0.1	0.4 ± 0.1	1.5 ± 0.3	0.7 ± 0.2
t <bar>t>Z</bar>	6.8 ± 1.2	1.4 ± 0.3	1.0 ± 0.2	1.2 ± 0.2	4.4 ± 0.8	3.2 ± 0.6
Z + jets	169 ± 38	8.9 ± 1.9	3.7 ± 0.8	3.3 ± 0.7	3.2 ± 0.7	0.8 ± 0.17
V + γ	45 ± 28	1.9 ± 2.4	0.1 ± 0.1	0.02 ± 0.01	1.0 ± 0.9	0.02 ± 0.03
tZ	31.8 ± 4.3	6.4 ± 1.1	5.3 ± 0.8	7.2 ± 1.1	11.8 ± 2.0	33.9 ± 4.5
tW	1.4 ± 0.8	0.2 ± 0.5	0.0 ± 0.2	0.7 ± 0.6	0.26 ± 0.42	0.39 ± 0.41
WtZ	2.3 ± 1.2	0.6 ± 0.3	0.3 ± 0.21	0.27 ± 0.2	1.1 ± 0.7	0.6 ± 0.5
VVV	12.4 ± 0.5	0.93 ± 0.06	0.35 ± 0.03	0.13 ± 0.02	0.14 ± 0.03	0.02 ± 0.01
VH	40 ± 6	2.6 ± 1.4	0.9 ± 0.8	0.7 ± 0.8	0.5 ± 0.6	0.0 ± 0.0
t <bar>t></bar>	12.1 ± 1.6	2.9 ± 0.6	2.5 ± 0.5	2.8 ± 0.5	11.2 ± 1.4	10.9 ± 1.5
t <bar>t>H</bar>	0.24 ± 0.03	0.05 ± 0.01	0.04 ± 0.01	0.06 ± 0.01	0.20 ± 0.03	0.13 ± 0.02
Total	5010 ± 260	227 ± 24	88 ± 12	57 ± 8	76 ± 16	53 ± 8

Table 15: Pre-fit yields in each of the 1-jet regions.

⁶⁴⁰ Here <85% includes jets that fail to pass the 85% WP, and 60% includes jets that pass the highest
⁶⁴¹ WP. The post-fit yields in each region are summarized in Table 16.

⁶⁴²

	1j, <85% WP	1j, 77%-85% WP	1j, 70%-77% WP	1j, 60%-70% WP	1j, 60% WP	tZ CR
WZ + b – 1j	8.1 ± 4.9	4.7 ± 2.0	4.6 ± 2.0	5.1 ± 2.1	18 ± 10	5.0 ± 2.5
WZ + c – 1j	260 ± 60	80 ± 14	43 ± 7	26 ± 5	7.4 ± 2.3	2.1 ± 0.7
WZ + l – 1j	3090 ± 130	90 ± 11	17.3 ± 2.8	4.9 ± 1.6	1.3 ± 0.4	0.23 ± 0.13
WZ + b – 2j	1.10 ± 0.37	0.44 ± 0.11	0.39 ± 0.06	0.62 ± 0.14	2.1 ± 0.5	0.59 ± 0.14
WZ + c – 2j	21 ± 5	5.6 ± 1.2	3.0 ± 0.7	2.0 ± 0.5	0.70 ± 0.20	0.30 ± 0.08
WZ + l – 2j	250 ± 60	5.7 ± 1.6	0.73 ± 0.53	0.31 ± 0.15	0.07 ± 0.06	0.01 ± 0.01
WZ – Other	13 ± 5	1.4 ± 0.4	0.42 ± 0.08	0.2 ± 0.01	0.30 ± 0.05	0.67 ± 0.15
Other VV	6.2 ± 0.6	0.92 ± 0.07	0.02 ± 0.01	0.01 ± 0.01	0.01 ± 0.01	0.01 ± 0.01
ZZ	346 ± 57	19 ± 5	4.3 ± 0.8	2.7 ± 0.5	2.4 ± 0.1	2.1 ± 0.6
t <bar>t>W</bar>	1.09 ± 0.21	0.2 ± 0.1	0.1 ± 0.1	0.4 ± 0.1	1.5 ± 0.3	0.1 ± 0.2
t <bar>t>Z</bar>	6.8 ± 1.2	1.4 ± 0.3	1.0 ± 0.2	1.2 ± 0.2	4.4 ± 0.7	3.2 ± 0.5
rare Top	0.14 ± 0.04	0.04 ± 0.02	0.04 ± 0.0	0.1 ± 0.03	0.14 ± 0.04	0.15 ± 0.05
t <bar>t>WW</bar>	0.04 ± 0.03	0.01 ± 0.02	0.01 ± 0.01	0.01 ± 0.01	0.01 ± 0.02	0.01 ± 0.01
Z + jets	169 ± 37	8.9 ± 1.9	3.7 ± 0.8	3.3 ± 0.7	3.2 ± 0.7	0.8 ± 0.2
W + jets	0.01 ± 0.01					
V + γ	46 ± 28	1.9 ± 2.4	0.1 ± 0.1	0.0 ± 0.2	1.0 ± 0.9	0.0 ± 0.0
tZ	31 ± 4	6.0 ± 1.0	5.3 ± 0.8	7.2 ± 1.0	11.8 ± 1.8	33.9 ± 4.5
tW	1.37 ± 0.82	0.18 ± 0.26	0.01 ± 0.12	0.67 ± 0.64	0.26 ± 0.42	0.39 ± 0.41
WtZ	2.3 ± 1.2	0.6 ± 0.3	0.3 ± 0.2	0.3 ± 0.2	1.1 ± 0.6	0.6 ± 0.3
VVV	12.4 ± 0.4	0.9 ± 0.1	0.4 ± 0.1	0.13 ± 0.02	0.14 ± 0.03	0.02 ± 0.01
VH	40 ± 6	2.6 ± 1.4	0.9 ± 0.8	0.7 ± 0.8	0.4 ± 0.6	0.01 ± 0.01
t <bar>t></bar>	12.1 ± 1.6	2.9 ± 0.6	2.5 ± 0.5	2.8 ± 0.5	11.2 ± 1.5	10.9 ± 1.4
t <bar>t>H</bar>	0.24 ± 0.03	0.05 ± 0.01	0.04 ± 0.01	0.06 ± 0.01	0.20 ± 0.03	0.13 ± 0.02
Total	5100 ± 110	227 ± 12	87 ± 6	56.7 ± 4.4	76 ± 9	52.5 ± 4.2

Table 16: Post-fit yields in each of the 1-jet regions.

643 The impact of each NP is calculated by performing the fit with the parameter of interest held
 644 fixed, varied from its fitted value by its uncertainty, and calculating $\Delta\mu$ relative to the baseline
 645 fit. The impact of the most significant sources of systematic uncertainties on WZ + b and WZ +
 646 c with one associated jet is summarized in Tables 17–18.

Uncertainty Source	$\Delta\mu$	
WZ + 1-jet light cross-section	0.13	-0.15
WZ + 1-jet charm cross-section	-0.10	0.12
Jet Energy Scale	0.1	-0.13
Other Diboson + b cross-section	-0.09	0.09
tZ cross-section	-0.08	0.08
WZ 1-jet/2-jet Migration	0.08	-0.07
Jet Energy Resolution	-0.07	0.08
Luminosity	-0.06	0.07
Flavor tagging	0.05	0.05
t <bar>t} cross-section</bar>	-0.05	0.05
Total Systematic Uncertainty	0.28	0.33

Table 17: Summary of the most significant sources of systematic uncertainty on the measurement of WZ + b with exactly one associated jet.

Uncertainty Source	$\Delta\sigma/\sigma_{\text{nominal}}$	
WZ + c 1j/2j migration	0.12	-0.09
Flavor Tagging	0.09	0.08
WZ + b, 1-jet cross-section	-0.04	0.05
Luminosity	-0.04	0.04
Jet Energy Resolution	0.04	0.04
WZ + b, 2-jet cross-section	0.04	-0.03
WZ cross-section - QCD scale	-0.04	0.04
Jet Energy Scaling	0.04	0.02
WZ cross-section - PDF	-0.03	0.03
WZ + light, 1-jet cross-section	0.03	-0.03
total	0.1879	0.1753

Table 18: Summary of the most significant sources of systematic uncertainty on the measurement of WZ + c with exactly one associated jet.

647 The ranking and impact of those nuisance parameters with the largest contribution to the overall
648 uncertainty is shown in Figure 40.

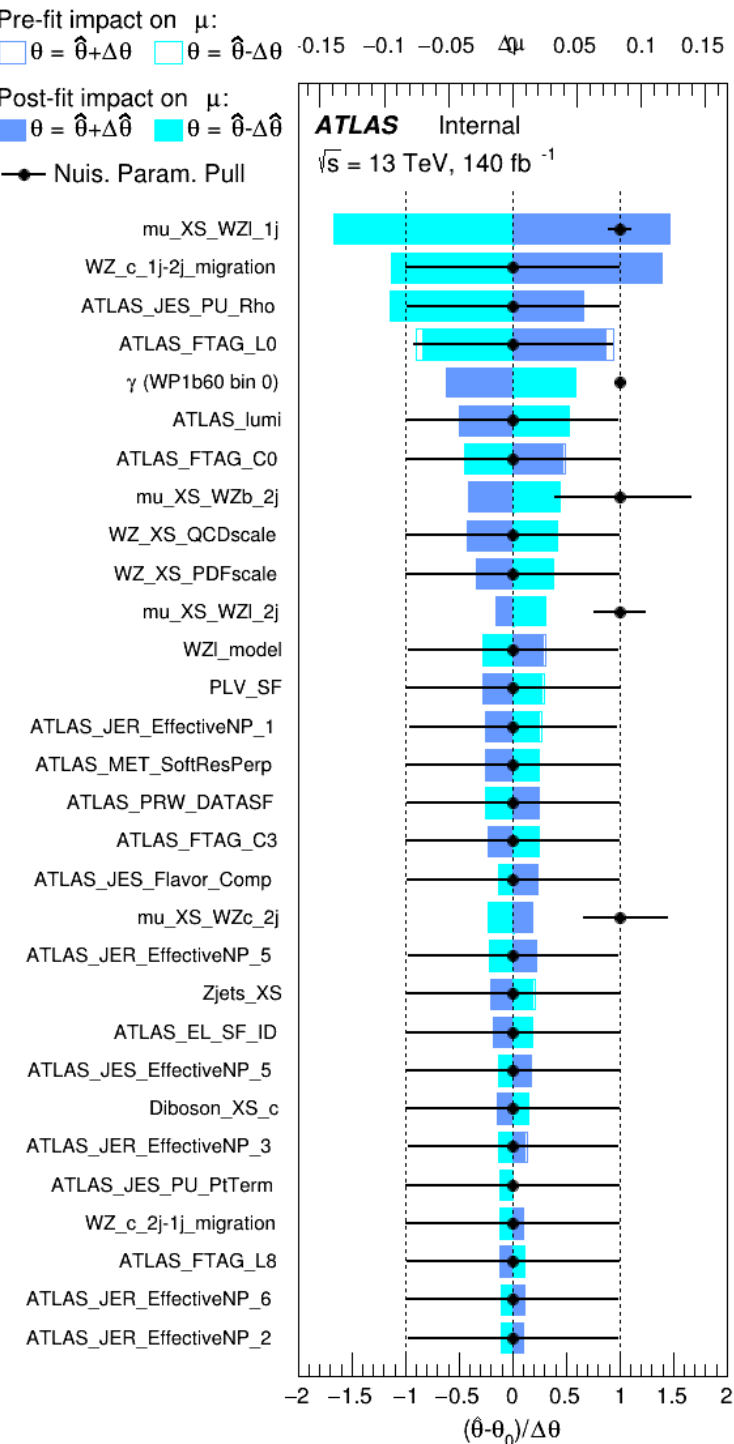


Figure 40: Impact of systematic uncertainties on the signal-strength of $WZ + b$ for events with exactly one jet

649 Here γ represents the impact of the statistical uncertainty of the MC prediction in that particular
 650 bin. The large impact of the Jet Energy Scale and Jet Flavor Tagging is unsurprising, as the
 651 definition of the fit regions depends heavily on the modeling of the jets. The other major sources
 652 of uncertainty come from background modelling and cross-section uncertainty.

653 Pre-fit yields in each of the 2-jet fit are shown in Table 19.

	2j, <85% WP	2j, 77%-85% WP	2j, 70%-77% WP	2j, 60%-70% WP	2j, 60% WP	tZ CR 2j
WZ + b - 2j	3.1 ± 1.6	6.7 ± 0.5	5.6 ± 0.4	8.0 ± 0.6	24 ± 2	5 ± 1
WZ + c - 2j	180 ± 20	54 ± 6	41 ± 3	24 ± 3	17 ± 2	7.0 ± 0.6
WZ + l - 2j	1250 ± 150	90 ± 14	18 ± 3	5.8 ± 1.4	1.4 ± 0.4	0.25 ± 0.15
WZ + b - 1j	3.4 ± 0.6	1.52 ± 0.35	1.58 ± 0.23	1.95 ± 0.39	7.8 ± 1.1	0.8 ± 0.6
WZ + c - 1j	56 ± 14	17.6 ± 4.0	8.6 ± 2.2	6.3 ± 1.8	3.0 ± 0.9	0.7 ± 0.2
WZ + l - 1j	427 ± 120	24 ± 7	4.7 ± 2.3	1.6 ± 0.7	0.3 ± 0.2	0.01 ± 0.01
WZ - Other	129 ± 29	6.1 ± 4.6	1.2 ± 0.3	0.3 ± 0.2	2.9 ± 0.5	3.6 ± 0.6
Other VV	7.63 ± 0.63	0.6 ± 0.5	0.16 ± 0.03	0.01 ± 0.01	0.1 ± 0.1	0.1 ± 0.1
ZZ	135 ± 20	14.1 ± 3.2	4.7 ± 0.8	4.0 ± 0.6	4.1 ± 0.7	3.1 ± 0.5
t \bar{t} W	0.8 ± 0.2	0.4 ± 0.1	0.5 ± 0.1	0.7 ± 0.2	4.3 ± 0.6	3.9 ± 0.6
t \bar{t} Z	14.7 ± 2.2	5.6 ± 0.8	4.5 ± 0.7	6.5 ± 1.1	25.4 ± 4.0	21.9 ± 3.4
rare Top	0.14 ± 0.04	0.07 ± 0.03	0.03 ± 0.02	0.09 ± 0.03	0.37 ± 0.07	0.6 ± 0.1
t \bar{t} WW	0.04 ± 0.03	0.02 ± 0.02	0.01 ± 0.01	0.01 ± 0.00	0.03 ± 0.03	0.01 ± 0.01
Z + jets	110.0 ± 22.9	9.6 ± 2.0	2.1 ± 0.50	1.6 ± 0.4	5.1 ± 1.1	1.5 ± 0.3
W + jets	0.0 ± 0.0	0.0 ± 0.0	0.0 ± 0.0	0.0 ± 0.0	0.0 ± 0.0	0.0 ± 0.0
V + γ	25 ± 18	0.5 ± 0.2	0.1 ± 0.1	0.1 ± 0.1	0.0 ± 0.02	0.05 ± 0.07
tZ	21.9 ± 2.9	9.6 ± 1.3	9.1 ± 1.0	10.0 ± 1.5	14.7 ± 3.2	60 ± 6
tW	0.9 ± 0.7	0.2 ± 0.3	0.0 ± 0.1	0.0 ± 0.0	0.8 ± 0.6	0.2 ± 0.2
WtZ	4.9 ± 2.5	1.5 ± 0.8	1.1 ± 0.6	1.3 ± 0.7	4.6 ± 2.4	3.3 ± 1.7
VVV	7.4 ± 0.3	1.0 ± 0.1	0.4 ± 0.1	0.2 ± 0.1	0.13 ± 0.03	0.04 ± 0.01
VH	19.5 ± 4.2	2.8 ± 1.6	0.7 ± 0.7	0.1 ± 0.2	0.0 ± 0.0	0.0 ± 0.0
t \bar{t}	0.7 ± 0.4	0.1 ± 0.1	0.05 ± 0.06	0.15 ± 0.13	0.8 ± 0.5	2.3 ± 1.2
t \bar{t}	6.8 ± 1.0	2.4 ± 0.5	1.8 ± 0.4	3.3 ± 0.6	8.4 ± 1.2	13.6 ± 1.7
t \bar{t} H	0.4 ± 0.1	0.2 ± 0.1	0.16 ± 0.02	0.23 ± 0.03	0.94 ± 0.11	1.03 ± 0.12
Total	2580 ± 160	229 ± 24	89 ± 13	69 ± 11	120 ± 15	108 ± 11

Table 19: Pre-fit yields in each of the 2-jet regions.

654 The post-fit yields in each region are summarized in Table 20.

	2j, <85% WP	2j, 77%-85% WP	2j, 70%-77% WP	2j, 60%-70% WP	2j, 60% WP	tZ CR 2j
WZ + b	13 ± 6	6.7 ± 2.9	5.8 ± 2.5	8.0 ± 3.5	31 ± 13	14 ± 5
WZ + c	260 ± 60	77 ± 15	41 ± 8	26 ± 5	10.9 ± 2.4	4.8 ± 1.1
WZ + l	1860 ± 90	90 ± 12	17.6 ± 2.8	5.8 ± 1.3	1.4 ± 0.4	0.3 ± 0.2
WZ + b - 1j	3.4 ± 0.6	1.52 ± 0.35	1.58 ± 0.23	1.95 ± 0.39	6.7 ± 1.1	1.9 ± 0.6
WZ + c - 1j	56 ± 14	17.6 ± 4.0	8.6 ± 2.2	6.3 ± 1.8	3.0 ± 0.9	0.7 ± 0.2
WZ + l - 1j	427 ± 120	24 ± 7	4.7 ± 2.3	1.6 ± 0.7	0.3 ± 0.2	0.01 ± 0.01
WZ - Other	129 ± 29	6.1 ± 4.6	1.2 ± 0.3	0.3 ± 0.2	2.9 ± 0.5	3.6 ± 0.6
Other VV	7.6 ± 0.6	0.3 ± 0.3	0.3 ± 0.1	0.1 ± 0.06	0.03 ± 0.02	0.1 ± 0.1
ZZ	145 ± 30	11.3 ± 4.4	2.7 ± 1.6	1.0 ± 0.3	4.0 ± 0.1	2.4 ± 0.1
t̄tW	0.8 ± 0.2	0.4 ± 0.1	0.54 ± 0.12	0.74 ± 0.15	4.3 ± 0.6	3.9 ± 0.6
t̄tZ	14.7 ± 2.2	5.6 ± 0.8	4.5 ± 0.7	6.5 ± 1.0	25.4 ± 3.9	21.9 ± 3.3
rare Top	0.14 ± 0.04	0.07 ± 0.03	0.03 ± 0.02	0.09 ± 0.03	0.4 ± 0.1	0.6 ± 0.1
t̄tWW	0.04 ± 0.03	0.02 ± 0.02	0.01 ± 0.01	0.01 ± 0.01	0.03 ± 0.03	0.01 ± 0.01
Z + jets	110 ± 23	9.6 ± 2.0	2.1 ± 0.5	1.6 ± 0.4	5.1 ± 1.1	1.5 ± 0.3
W + jets	0.0 ± 0.0					
V + γ	25 ± 19	0.5 ± 0.2	0.1 ± 0.1	0.13 ± 0.14	0.0 ± 0.02	0.05 ± 0.07
tZ	21.9 ± 2.7	9.6 ± 1.2	7.1 ± 0.9	10.0 ± 1.4	14.7 ± 3.0	60 ± 6
tW	0.1 ± 0.7	0.2 ± 0.3	0.0 ± 0.1	0.0 ± 0.0	0.8 ± 0.6	0.2 ± 0.2
WtZ	4.9 ± 2.5	1.5 ± 0.8	1.1 ± 0.6	1.3 ± 0.7	4.6 ± 2.3	3.3 ± 1.7
VVV	7.4 ± 0.3	1.0 ± 0.1	0.36 ± 0.03	0.19 ± 0.03	0.13 ± 0.03	0.04 ± 0.01
VH	19 ± 4	2.8 ± 1.6	0.7 ± 0.7	0.1 ± 0.2	0.0 ± 0.0	0.0 ± 0.0
t̄t	6.8 ± 1.0	2.4 ± 0.5	1.8 ± 0.4	3.3 ± 0.6	8.4 ± 1.2	13.6 ± 1.7
t̄tH	0.40 ± 0.05	0.19 ± 0.03	0.16 ± 0.02	0.23 ± 0.03	0.94 ± 0.11	1.03 ± 0.11
Total	2580 ± 60	229 ± 11	89 ± 6	69.1 ± 4.1	120 ± 10	108 ± 6

Table 20: Post-fit yields in each of the 2-jet regions.

655 The same set of systematic uncertainties consider for the 1-jet fit are included in the 2-jet fit as
 656 well. The impact of the most significant systematic uncertainties on WZ + b and c is summarized
 657 in Tables 21-22.

Uncertainty Source	$\Delta\mu$	
WZ + c 2-jet cross-section	-0.13	0.16
WZ + l 2-jet cross-section	0.12	-0.09
ttZ cross-section - QCD scale	-0.10	0.13
WZ + b 1-jet cross-section	-0.11	0.10
Jet Energy Scale	-0.11	0.11
Luminosity	-0.11	0.12
tZ cross-section	-0.11	0.11
WtZ cross-section	-0.07	0.07
Flavor tagging	0.05	0.05
Other VV + b cross-section	-0.05	0.05
Total	0.35	0.37

Table 21: Summary of the most significant sources of systematic uncertainty on the measurement of WZ + b 2-jet events.

Uncertainty Source	$\Delta\sigma/\sigma_{\text{nominal}}$	
WZ + c 1j/2j migration	-0.17	0.25
Flavor Tagging	0.14	0.13
WZ + b, 1-jet cross-section	-0.09	0.09
Jet Energy Scale	0.06	0.08
Jet Energy Resolution	0.05	0.05
WZ $\geq 3j/2j$ migration	-0.04	0.04
WZ + c 2j/1j migration	-0.04	0.04
WZ cross-section - QCD scale	-0.04	0.04
WZ + light modelling	0.04	-0.03
Luminosity	-0.03	0.03
total	0.2694	0.3274

Table 22: Summary of the most significant sources of systematic uncertainty on the measurement of WZ + c with 2 associated jets.

658 The ranking and impact of those nuisance parameters with the largest contribution to the overall
 659 uncertainty is shown in Figure 41.

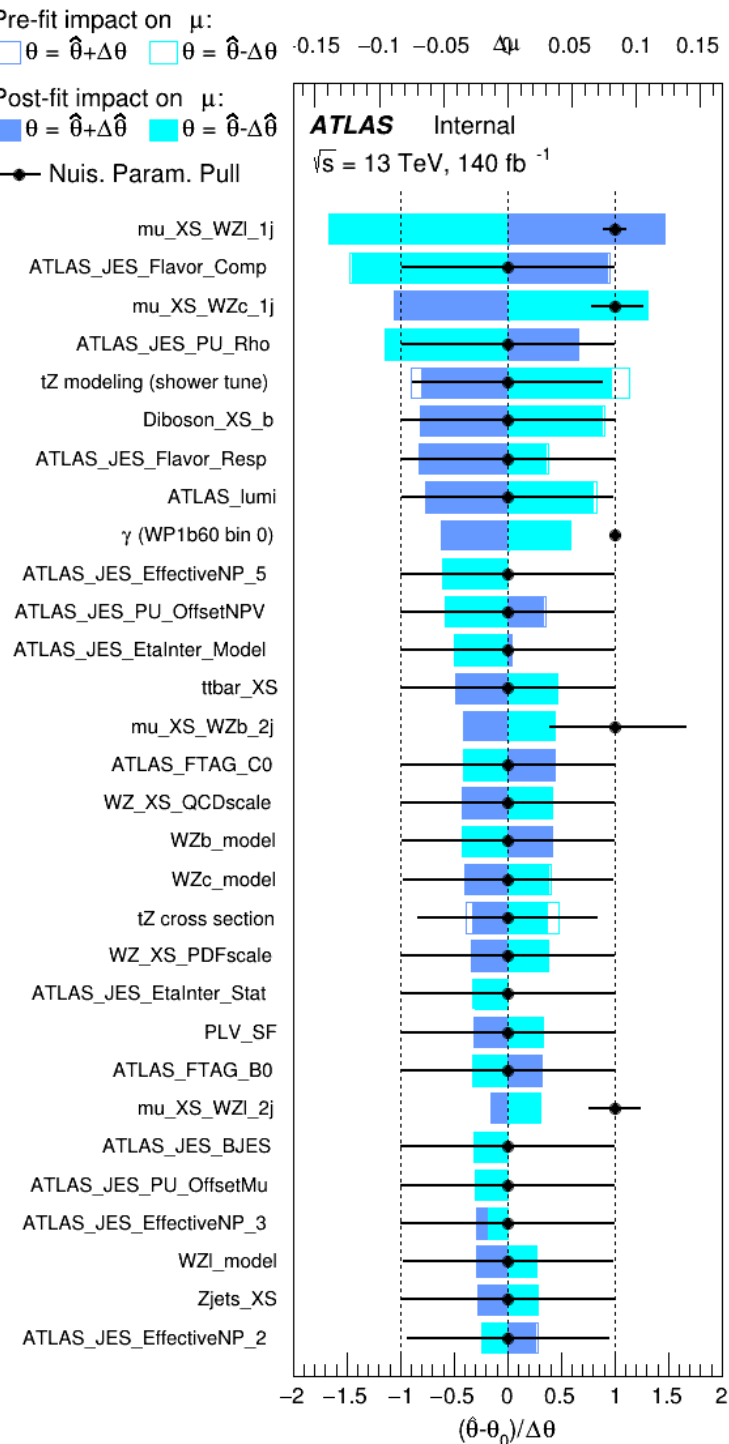


Figure 41: Impact of systematic uncertainties on the signal-strength of $WZ + b$ in 2-jet events.

660 The large impact of the Jet Energy Scale and Jet Flavor Tagging is unsurprising, as the shape of
661 the fit regions depends heavily on the modeling of the jets. The other major sources of uncertainty
662 come from background modelling and cross-section uncertainty.

663 **8.3 Inclusive 1+2 Jet Fit**

664 An alternative fit is performed which combines the WZ + 1-jet and WZ + 2-jet samples rather than
665 fitting them independently. This is done primarily as a cross-check of the nominal analysis, to
666 see if measuring 1-jet and 2-jet events separately and combining them gives drastically different
667 results than measuring them together.

668 For this study, three signal templates, WZ + b, WZ + charm and WZ + light, are fit to data, and
669 the systematics accounting for migrations between 1-jet and 2-jet bins are removed. All other
670 background and nuisance parameters remain the same as the nominal fit.

671 The measured μ value for WZ + b is $\mu = 1.00^{+0.30}_{-0.29}(\text{stat})^{+0.25}_{-23}(\text{sys})$, with a significance of 2.8σ ,
672 and the uncertainty on WZ + charm is $\mu = 1.00 \pm 0.12(\text{stat}) \pm 0.13(\text{sys})$. This is compared to
673 combined uncertainty of $\mu = 1.00^{+0.32}_{-0.30}(\text{stat})^{+0.24}_{-23}(\text{sys})$ for WZ + b when 1-jet and 2-jet events
674 are measured separately and then combined.

675 A post-fit summary plot of the fit regions is shown in Figure 42:

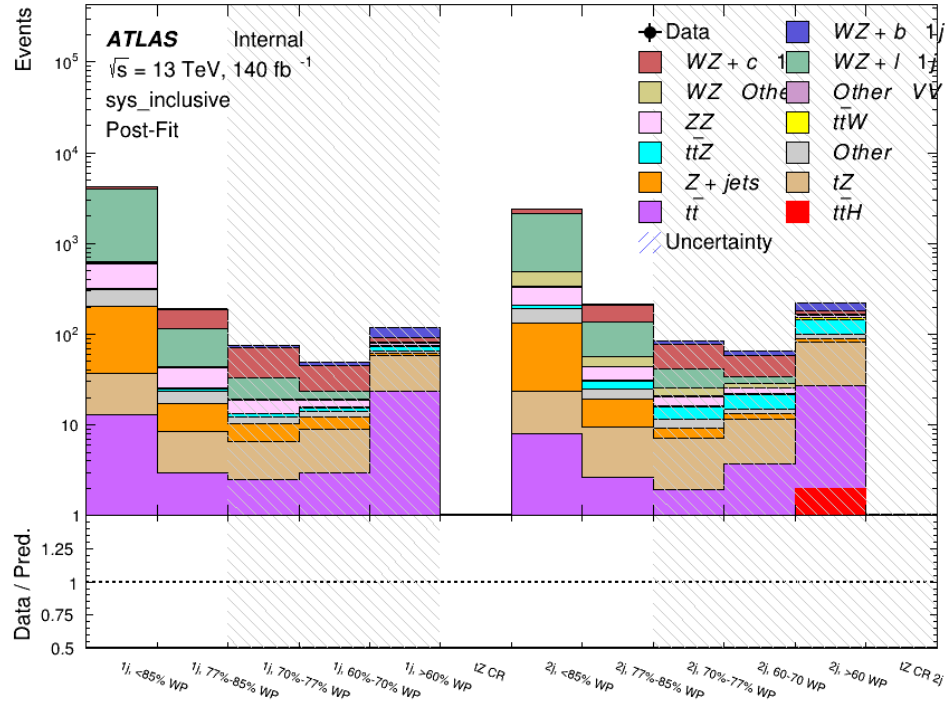


Figure 42: Post-fit summary of the 1-jet fit regions.

676 The impact of the most significant sources of systematic uncertainties on the measurement of
 677 WZ+b is summarized in Table 23.

Uncertainty Source	$\Delta\mu$
WZ + light cross-section	0.13 -0.12
WZ + charm cross-section	-0.10 0.12
Jet Energy Scale	0.08 0.13
tZ cross-section	-0.10 0.10
Jet Energy Resolution	-0.10 0.10
Luminosity	-0.08 0.09
Other Diboson + b cross-section	-0.07 0.07
Flavor tagging	0.05 0.05
t̄t cross-section	-0.05 0.05
WZ cross-section - QCD scale	-0.04 0.03
Total Systematic Uncertainty	0.28 0.32

Table 23: Summary of the most significant sources of systematic uncertainty on the measurement of WZ + b with one or two associated jets.

678 The ranking and impact of those nuisance parameters with the largest contribution to the overall
679 uncertainty is shown in Figure 43.

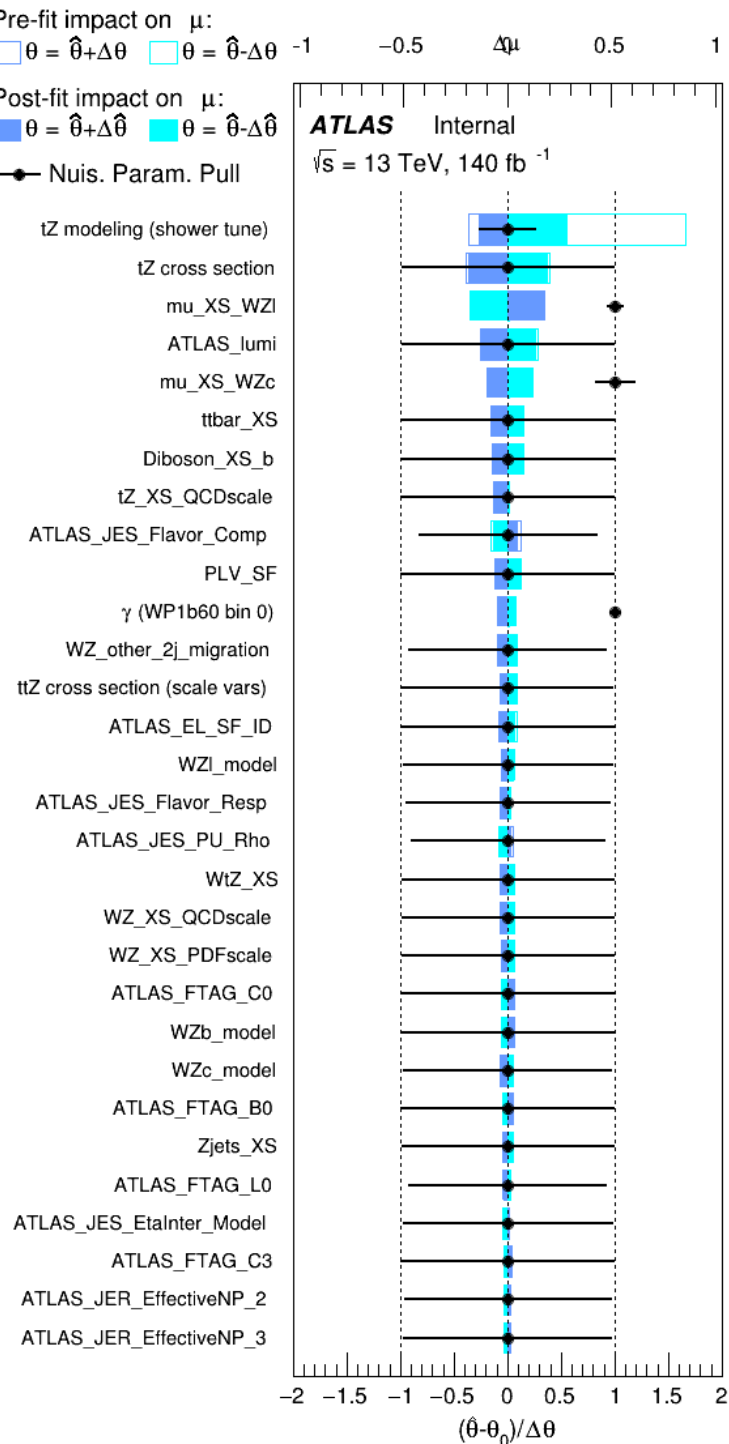


Figure 43: Impact of systematic uncertainties on the signal-strength of $WZ + b$ for events with one or two jets

680 **8.4 Alternative tZ Inclusive Fit**

681 **8.4.1 tZ Inclusive Fit**

682 While tZ is often considered as a distinct process from WZ + b, this could also be considered
683 part of the signal. Alternative studies are performed where, using the same framework as the
684 nominal analysis, a measurement of WZ + b is performed that includes tZ as part of WZ+b.

685 Because of this change, the tZ CR is no longer necessary, and only the five pseudo-continuous
686 b-tag regions are used in the fit. Further, systematics related to the tZ cross-section are removed
687 from the fit, as they are now encompassed by the normalization measurement of WZ + b. All
688 other systematic uncertainties are carried over from the nominal analysis.

689 An expected WZ + b cross-section of $4.1^{+0.78}_{-0.74}(\text{stat})^{+0.53}_{-0.52}(\text{sys}) \text{ fb}$ is extracted from the fit, with
690 an expected significance of 4.0σ .

691 The impact of the predominate systematics are summarized in Table 24.

Uncertainty Source	$\Delta\mu$	
WZ + light cross-section	0.08	-0.08
Jet Energy Scale	-0.06	0.08
Luminosity	-0.05	0.06
WZ + charm cross-section	-0.04	0.05
Other Diboson + b cross-section	-0.04	0.04
WZ cross-section - QCD scale	-0.04	0.03
t̄t cross-section	-0.03	0.03
Jet Energy Resolution	-0.03	0.03
Flavor tagging	-0.03	0.03
Z+jets cross section	-0.02	0.02
Total Systematic Uncertainty	-0.15	0.16

Table 24: Summary of the most significant sources of systematic uncertainty on the measurement of WZ + b with exactly one associated jet.

692 **8.4.2 Floating tZ**

693 In order to quantify the impact of the tZ uncertainty on the fit, an alternative fit strategy is
694 used where the tZ normalization is allowed to float. This normalization factor replaces the
695 cross-section uncertainty on tZ, and all other parameters of the fit remain the same.

696 An uncertainty of 17% on the normalization of tZ is extracted from the fit, compared to a theory
697 uncertainty of 15% applied to the tZ cross-section. The measured uncertainties on WZ remain
698 the same.

699 9 Conclusion

700 A measurement of WZ + heavy flavor is performed using 140 fb^{-1} of $\sqrt{s} = 13 \text{ TeV}$ proton-
 701 proton collision data collected by the ATLAS detector at the LHC. The expected cross-section
 702 of WZ+b with 1-jet is $1.74^{+0.82}_{-0.75}(\text{stat})^{+0.53}_{-0.48}(\text{sys}) \text{ fb}$, and $14.6 \pm 2.5(\text{stat}) \pm 2.3(\text{sys}) \text{ fb}$ for WZ
 703 + charm, with a correlation of -0.22 between them. An expected significance of 2.0 is observed
 704 for WZ + b in this region.

705 For the 2-jet regions, an expected significance of 1.7 is observed for WZ + b, with an ex-
 706 pected cross-section of $2.5^{+1.3}_{-1.3}(\text{stat})^{+0.95}_{-0.83}(\text{sys}) \text{ fb}$. For WZ + charm, a cross-section of
 707 $12.7 \pm 3.2(\text{stat}) \pm 2.7(\text{sys}) \text{ fb}$ is expected for 2-jet events. A correlation of -0.26 is observed
 708 for WZ+b and WZ + charm.

709 **This section will be include final results once unblinded.**

710 References

- 711 [1] ATLAS Collaboration. ‘Observation of electroweak $W^\pm Z$ boson pair production in asso-
 712 ciation with two jets in pp collisions at $\sqrt{s} = 13 \text{ TeV}$ with the ATLAS detector’. In: *Phys.*
 713 *Lett.* B793 (2019), pp. 469–492. doi: [10.1016/j.physletb.2019.05.012](https://doi.org/10.1016/j.physletb.2019.05.012). arXiv:
 714 [1812.09740 \[hep-ex\]](https://arxiv.org/abs/1812.09740).
- 715 [2] ATLAS Collaboration. ‘Luminosity determination in pp collisions at $\sqrt{s} = 7 \text{ TeV}$ using
 716 the ATLAS detector at the LHC’. In: *Eur. Phys. J. C* 71 (2011), p. 1630. doi: [10.1140/epjc/s10052-011-1630-5](https://doi.org/10.1140/epjc/s10052-011-1630-5). arXiv: [1101.2185 \[hep-ex\]](https://arxiv.org/abs/1101.2185).
- 718 [3] ATLAS Collaboration. ‘Performance of the ATLAS detector using first collision data’.
 719 In: *JHEP* 09 (2010), p. 056. doi: [10.1007/JHEP09\(2010\)056](https://doi.org/10.1007/JHEP09(2010)056). arXiv: [1005.5254 \[hep-ex\]](https://arxiv.org/abs/1005.5254).
- 721 [4] S. Agostinelli et al. ‘GEANT4: A Simulation toolkit’. In: *Nucl. Instrum. Meth.* A506
 722 (2003), pp. 250–303. doi: [10.1016/S0168-9002\(03\)01368-8](https://doi.org/10.1016/S0168-9002(03)01368-8).
- 723 [5] T. Gleisberg et al. ‘Event generation with SHERPA 1.1’. In: *JHEP* 02 (2009), p. 007. doi:
 724 [10.1088/1126-6708/2009/02/007](https://doi.org/10.1088/1126-6708/2009/02/007). arXiv: [0811.4622 \[hep-ph\]](https://arxiv.org/abs/0811.4622).
- 725 [6] R. D. Ball et al. ‘Parton distributions for the LHC Run II’. In: *JHEP* 04 (2015), p. 040.
 726 doi: [10.1007/JHEP04\(2015\)040](https://doi.org/10.1007/JHEP04(2015)040). arXiv: [1410.8849 \[hep-ph\]](https://arxiv.org/abs/1410.8849).
- 727 [7] H.-L. Lai et al. ‘New parton distributions for collider physics’. In: *Phys. Rev. D* 82 (2010),
 728 p. 074024. doi: [10.1103/PhysRevD.82.074024](https://doi.org/10.1103/PhysRevD.82.074024). arXiv: [1007.2241 \[hep-ph\]](https://arxiv.org/abs/1007.2241).
- 729 [8] J. Alwall et al. ‘The automated computation of tree-level and next-to-leading order dif-
 730 fferential cross sections, and their matching to parton shower simulations’. In: *JHEP* 07
 731 (2014), p. 079. doi: [10.1007/JHEP07\(2014\)079](https://doi.org/10.1007/JHEP07(2014)079). arXiv: [1405.0301 \[hep-ph\]](https://arxiv.org/abs/1405.0301).
- 732 [9] M. Bahr et al. ‘Herwig++ Physics and Manual’. In: *Eur. Phys. J. C* 58 (2008), p. 639. doi:
 733 [10.1140/epjc/s10052-008-0798-9](https://doi.org/10.1140/epjc/s10052-008-0798-9). arXiv: [0803.0883 \[hep-ph\]](https://arxiv.org/abs/0803.0883).

- 734 [10] R. D. Ball et al. ‘Parton distributions with LHC data’. In: *Nucl. Phys. B* 867 (2013), p. 244.
 735 doi: [10.1016/j.nuclphysb.2012.10.003](https://doi.org/10.1016/j.nuclphysb.2012.10.003). arXiv: [1207.1303 \[hep-ph\]](https://arxiv.org/abs/1207.1303).
- 736 [11] S. Frixione, G. Ridolfi and P. Nason. ‘A positive-weight next-to-leading-order Monte Carlo
 737 for heavy flavour hadroproduction’. In: *JHEP* 09 (2007), p. 126. doi: [10.1088/1126-6708/2007/09/126](https://doi.org/10.1088/1126-6708/2007/09/126). arXiv: [0707.3088 \[hep-ph\]](https://arxiv.org/abs/0707.3088).
- 738 [12] E. Re. ‘Single-top Wt-channel production matched with parton showers using the POWHEG
 739 method’. In: *Eur. Phys. J. C* 71 (2011), p. 1547. doi: [10.1140/epjc/s10052-011-1547-z](https://doi.org/10.1140/epjc/s10052-011-1547-z). arXiv: [1009.2450 \[hep-ph\]](https://arxiv.org/abs/1009.2450).
- 740 [13] ATLAS Collaboration. *Electron efficiency measurements with the ATLAS detector using
 741 the 2015 LHC proton–proton collision data*. ATLAS-CONF-2016-024. 2016. URL: <https://cds.cern.ch/record/2157687>.
- 742 [14] ATLAS Collaboration. ‘Measurement of the muon reconstruction performance of the
 743 ATLAS detector using 2011 and 2012 LHC proton–proton collision data’. In: *Eur. Phys.
 744 J. C* 74 (2014), p. 3130. doi: [10.1140/epjc/s10052-014-3130-x](https://doi.org/10.1140/epjc/s10052-014-3130-x). arXiv: [1407.3935 \[hep-ex\]](https://arxiv.org/abs/1407.3935).
- 745 [15] R. Narayan et al. *Measurement of the total and differential cross sections of a top-quark-
 746 antiquark pair in association with a W boson in proton-proton collisions at a centre-of-
 747 mass energy of 13 TeV with ATLAS detector at the Large Hadron Collider*. Tech. rep.
 748 ATL-COM-PHYS-2020-217. Geneva: CERN, Mar. 2020. URL: <https://cds.cern.ch/record/2712986>.
- 749 [16] ATLAS Collaboration. *Jet Calibration and Systematic Uncertainties for Jets Reconstruc-
 750 ted in the ATLAS Detector at $\sqrt{s} = 13$ TeV*. ATL-PHYS-PUB-2015-015. 2015. URL:
 751 <https://cds.cern.ch/record/2037613>.
- 752 [17] ATLAS Collaboration. *Selection of jets produced in 13 TeV proton–proton collisions with
 753 the ATLAS detector*. ATLAS-CONF-2015-029. 2015. URL: <https://cds.cern.ch/record/2037702>.
- 754 [18] ATLAS Collaboration. ‘Performance of pile-up mitigation techniques for jets in pp col-
 755 lisions at $\sqrt{s} = 8$ TeV using the ATLAS detector’. In: *Eur. Phys. J. C* 76 (2016), p. 581.
 756 doi: [10.1140/epjc/s10052-016-4395-z](https://doi.org/10.1140/epjc/s10052-016-4395-z). arXiv: [1510.03823 \[hep-ex\]](https://arxiv.org/abs/1510.03823).
- 757 [19] ATLAS Collaboration. ‘Performance of b -jet identification in the ATLAS experiment’. In:
 758 *Journal of Instrumentation* 11.04 (2016), P04008. URL: <http://stacks.iop.org/1748-0221/11/i=04/a=P04008>.
- 759 [20] ATLAS Collaboration. ‘Performance of missing transverse momentum reconstruction
 760 with the ATLAS detector using proton–proton collisions at $\sqrt{s} = 13$ TeV’. In: *The
 761 European Physical Journal C* 78.11 (Nov. 2018). ISSN: 1434-6052. doi: [10.1140/epjc/s10052-018-6288-9](https://doi.org/10.1140/epjc/s10052-018-6288-9). URL: <http://dx.doi.org/10.1140/epjc/s10052-018-6288-9>.
- 762 [21] ATLAS Collaboration. ‘Measurement of the fiducial and differential cross-section of a top
 763 quark pair in association with a Z boson at 13 TeV with the ATLAS detector’. In: ATL-
 764 COM-PHYS-2019-334 (Apr. 2019). URL: <https://cds.cern.ch/record/2672207>.

- 774 [22] T. Chen and C. Guestrin. ‘XGBoost: A Scalable Tree Boosting System’. In: *Proceedings*
 775 of the 22nd ACM SIGKDD International Conference on Knowledge Discovery and Data
 776 Mining. KDD ’16. San Francisco, California, USA: ACM, 2016, pp. 785–794. ISBN: 978-
 777 1-4503-4232-2. doi: [10.1145/2939672.2939785](https://doi.org/10.1145/2939672.2939785). URL: <http://doi.acm.org/10.1145/2939672.2939785>.
- 779 [23] R. Frederix et al. ‘The automation of next-to-leading order electroweak calculations’. In: *Journal of High Energy Physics* 2018.7 (July 2018). ISSN: 1029-8479. doi: [10.1007/jhep07\(2018\)185](https://doi.org/10.1007/jhep07(2018)185). URL: [http://dx.doi.org/10.1007/JHEP07\(2018\)185](http://dx.doi.org/10.1007/JHEP07(2018)185).
- 782 [24] 2021. URL: https://twiki.cern.ch/twiki/bin/view/AtlasProtected/BTagCalibrationRecommendationsRelease21#Tools_for_Flavor_Tagging_Calibra.
- 785 [25] ‘Luminosity determination in pp collisions at $\sqrt{s} = 13$ TeV using the ATLAS detector at
 786 the LHC’. In: (June 2019).
- 787 [26] ATLAS Collaboration. ‘The new LUCID-2 detector for luminosity measurement and
 788 monitoring in ATLAS’. In: *JINST* 13.07 (2018), P07017. doi: [10.1088/1748-0221/13/07/P07017](https://doi.org/10.1088/1748-0221/13/07/P07017).
- 790 [27] A. Collaboration. ‘Electron reconstruction and identification in the ATLAS experiment
 791 using the 2015 and 2016 LHC proton–proton collision data at $\sqrt{s} = 13$ TeV’. In: *The*
 792 *European Physical Journal C* 79.8 (Aug. 2019). ISSN: 1434-6052. doi: [10.1140/epjc/s10052-019-7140-6](https://doi.org/10.1140/epjc/s10052-019-7140-6). URL: <http://dx.doi.org/10.1140/epjc/s10052-019-7140-6>.
- 795 [28] ATLAS Collaboration. ‘Jet energy scale measurements and their systematic uncertainties
 796 in proton–proton collisions at $\sqrt{s} = 13$ TeV with the ATLAS detector’. In: *Phys. Rev.*
 797 *D* 96 (2017), p. 072002. doi: [10.1103/PhysRevD.96.072002](https://doi.org/10.1103/PhysRevD.96.072002). arXiv: [1703.09665](https://arxiv.org/abs/1703.09665) [hep-ex].
- 799 [29] ATLAS Collaboration. ‘Observation of the associated production of a top quark and a
 800 Z boson in pp collisions at $\sqrt{s}= 13$ TeV with the ATLAS detector’. In: *Journal of High*
 801 *Energy Physics* 2020.7 (July 2020). ISSN: 1029-8479. doi: [10.1007/jhep07\(2020\)124](https://doi.org/10.1007/jhep07(2020)124).
 802 URL: [http://dx.doi.org/10.1007/JHEP07\(2020\)124](http://dx.doi.org/10.1007/JHEP07(2020)124).

803 **A Appendices**

804 **A.1 Non-prompt lepton MVA**

805 A lepton MVA has been developed to better reject non-prompt leptons than standard cut-
 806 based selections based upon impact parameter, isolation and PID. The name of this MVA is
 807 **PromptLeptonVeto**. The full set of studies and a detailed explanation can be found in [15].

808 The decays of W and Z bosons are commonly selected by the identification of one or two electrons
 809 or muons. The negligible lifetimes of these bosons mean that the leptons produced in the decay
 810 originate from the interaction vertex and are thus labelled “prompt”. Analyses using these
 811 light leptons impose strict reconstruction quality, isolation and impact parameter requirements
 812 to remove “fake” leptons. A significant source of the fake light leptons is non-prompt leptons
 813 produced in decays of hadrons that contain bottom (b) or charm (c) quarks. Such hadrons
 814 typically have microscopically significant lifetimes that can be detected experimentally.

815 These non-prompt leptons can also pass the tight selection criteria. In analyses that involve top (t)
 816 quarks, which decay almost exclusively into a W boson and a b quark, non-prompt leptons from
 817 the semileptonic decay of bottom and charm hadrons can be a significant source of background
 818 events. This is particularly the case in the selection of same-sign dilepton and multilepton final
 819 states.

820 The main idea is to identify non-prompt light leptons using lifetime information associated with a
 821 track jet that matches the selected light lepton. This lifetime information is computed using tracks
 822 contained within the jet. Typically, lepton lifetime is determined using the impact parameter of the
 823 track reconstructed by the inner tracking detector which is matched to the reconstructed lepton.
 824 Using additional reconstructed charged particle tracks increases the precision of identifying the
 825 displaced decay vertex of bottom or charm hadrons that produced a non-prompt light lepton.
 826 The MVA also includes information related to the isolation of the lepton to reject non-prompt
 827 leptons.

828 **PromptLeptonVeto** is a gradient boosted BDT. The training of the BDT is performed on leptons
 829 selected from the POWHEG+PYTHIA6 non-allhad $t\bar{t}$ MC sample. Eight variables are used to train
 830 the BDT in order to discriminate between prompt and non-prompt leptons. The track jets that
 831 are matched to the non-prompt leptons correspond to jets initiated by b or c quarks, and may
 832 contain a displaced vertex. Consequently, three of the selected variables are used to identify
 833 b-tag jets by standard ATLAS flavour tagging algorithms. Two variables use the relationship
 834 between the track jet and lepton: the ratio of the lepton p_T with respect to the track jet p_T and
 835 ΔR between the lepton and the track jet axis. Finally three additional variables test whether the
 836 reconstructed lepton is isolated: the number of tracks collected by the track jet and the lepton
 837 track and calorimeter isolation variables. Table 25 describes the variables used to train the BDT
 838 algorithm. The choice of input variables has been extensively discussed with Egamma, Muon,
 839 Tracking, and Flavour Tagging CP groups.

840 The output distribution of the BDT is shown in Figure A.1.

Variable	Description
N_{track} in track jet	Number of tracks collected by the track jet
$\text{IP2 log}(P_b/P_{\text{light}})$	Log-likelihood ratio between the b and light jet hypotheses with the IP2D algorithm
$\text{IP3 log}(P_b/P_{\text{light}})$	Log-likelihood ratio between the b and light jet hypotheses with the IP3D algorithm
$N_{\text{TrkAtVtx}} \text{ SV} + \text{JF}$	Number of tracks used in the secondary vertex found by the SV1 algorithm in addition to the number of tracks from secondary vertices found by the JetFitter algorithm with at least two tracks
$p_T^{\text{lepton}}/p_T^{\text{track jet}}$	The ratio of the lepton p_T and the track jet p_T
$\Delta R(\text{lepton}, \text{track jet})$	ΔR between the lepton and the track jet axis
$p_T^{\text{VarCone30}}/p_T$	Lepton track isolation, with track collecting radius of $\Delta R < 0.3$
$E_T^{\text{TopoCone30}}/p_T$	Lepton calorimeter isolation, with topological cluster collecting radius of $\Delta R < 0.3$

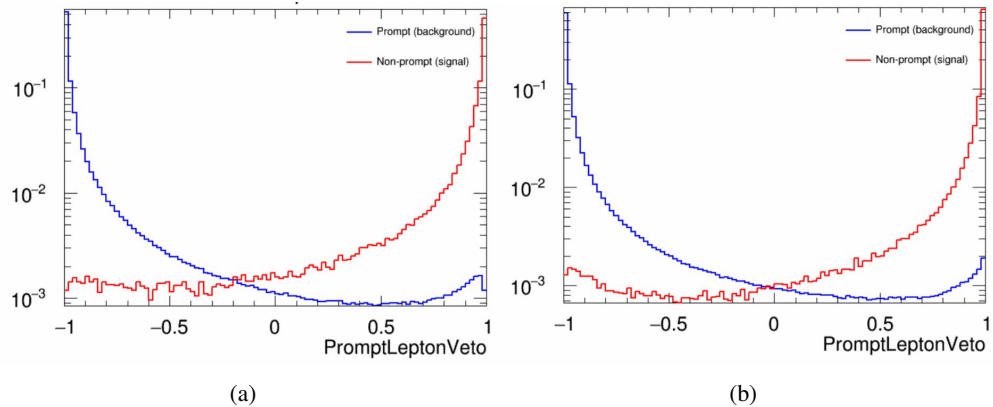
Table 25: A table of the variables used in the training of **PromptLeptonVeto** (PLV).

Figure 44: Distribution of the PLV BDT discriminant for (a) electrons and (b) muons.

841 The ROC curve for the BDT response, compared to the standard **FixedCutTight** WP, is
 842 shown in figure A.1, which shows a clear improvement when using this alternative identification
 843 algorithm.

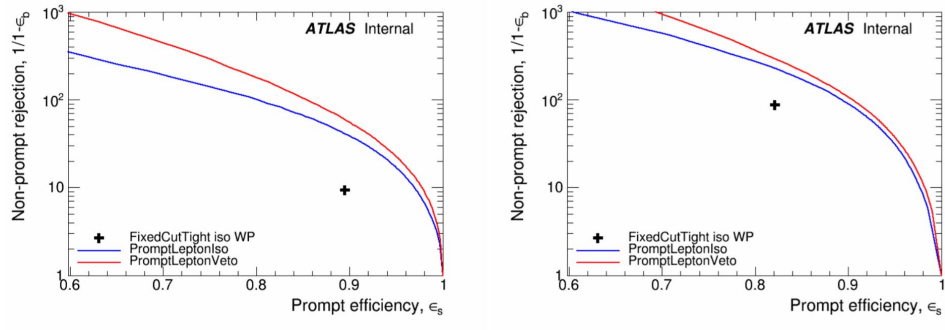


Figure 45: ROC curves for the PLV as well as the performance of the standard FixedCutTight WP for (left) electrons and (right) muons. Plot also includes curves for PROMPTLEPTONIso, which is not considered in this analysis.

844 Cutoff values of -0.7 for electrons and -0.5 for muons are chosen as the WPs for this MVA, based
 845 on an optimisation of S/\sqrt{B} performed in the preselection regions of the $t\bar{t}H$ – ML analysis,
 846 which have a signature similar to that of this analysis.

847 The efficiency of the tight PromptLeptonVeto working point is measured using the tag and
 848 probe method with $Z \rightarrow \ell^+ \ell^-$ events. Such calibrations are performed by analysers from this
 849 analysis in communication with the Egamma and Muon combined performance groups. The
 850 scale factor is approximately 0.92 for $10 < p_T < 15$ GeV, and averages 0.98 to 0.99 for higher
 851 p_T leptons. An extra systematic is applied to muons within $\Delta R < 0.6$ of a calorimeter jet,
 852 since there is a strong dependence on the scale factor due to the presence of these jets. For
 853 electrons, the dominant systematic is coming from pile-up dependence. Overall the systematics
 854 are a maximum of 3% at low p_T and decreasing at a function of p_T .

855 A.2 Non-prompt CR Modelling

856 In order to further validate the modeling in each of the non-prompt CRs, additional kinematic
 857 plots are made in the $Z+jets$ CR and $t\bar{t}$ CR in each of the continuous b-tag regions, after the
 858 correction factors detailed in Section 6.3 have been applied.

859 In the case of the $Z+jets$ CR, the p_T spectrum of the lepton originating from the W candidate is
 860 shown, as this is the distribution used to extract the scale factor applied to $Z+jets$. These plots
 861 are shown in Figures 46 and 47.

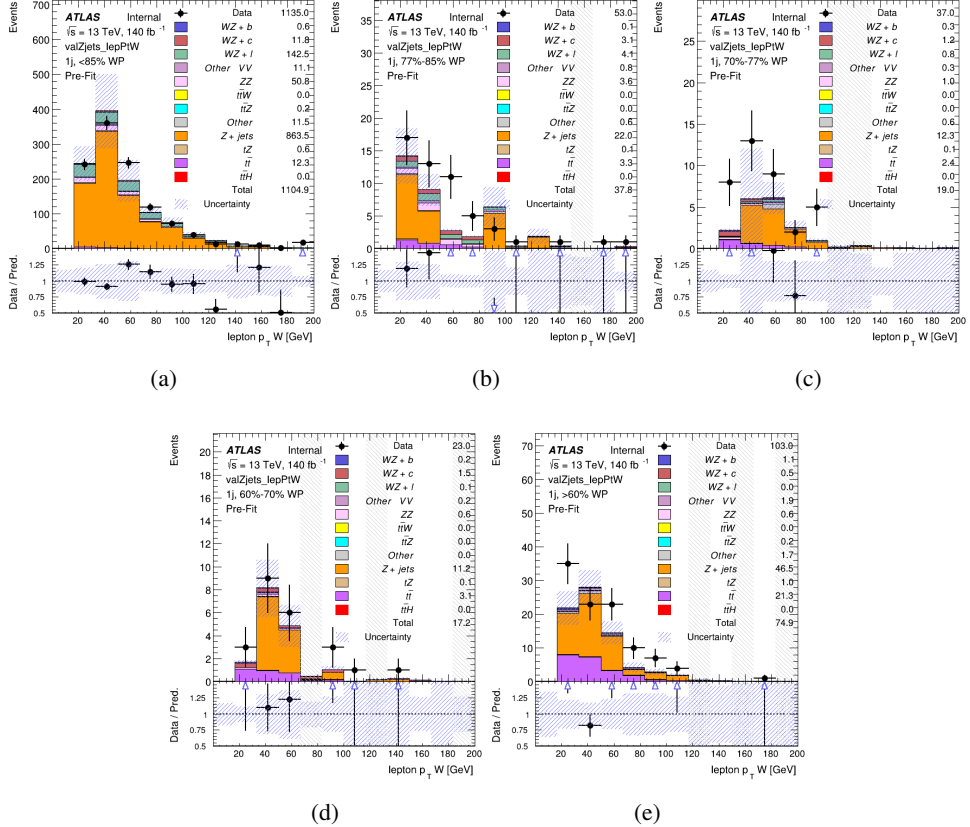


Figure 46: Comparisons between the data and MC distributions of the p_T of the lepton originating from the W-candidate in the Z+jets CR for each of the 1-jet b-tag working point regions

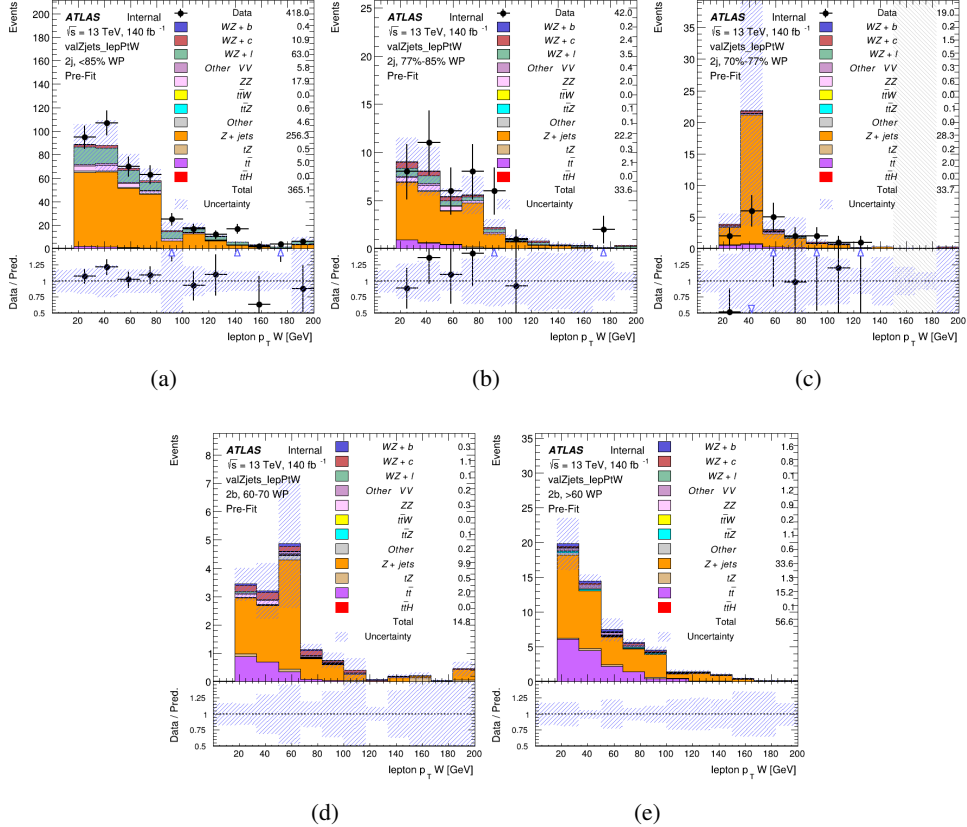


Figure 47: Comparisons between the data and MC distributions of the p_T of the lepton originating from the W-candidate in the Z+jets CR for each of the 2-jet b-tag working point regions

862 The same is shown for the $t\bar{t}$ CR, but the p_T of the OS lepton is used instead as a representation
 863 of the modeling, as the lepton from the W is not well defined for $t\bar{t}$ events. These plots are shown
 864 in Figures 48 and 49.

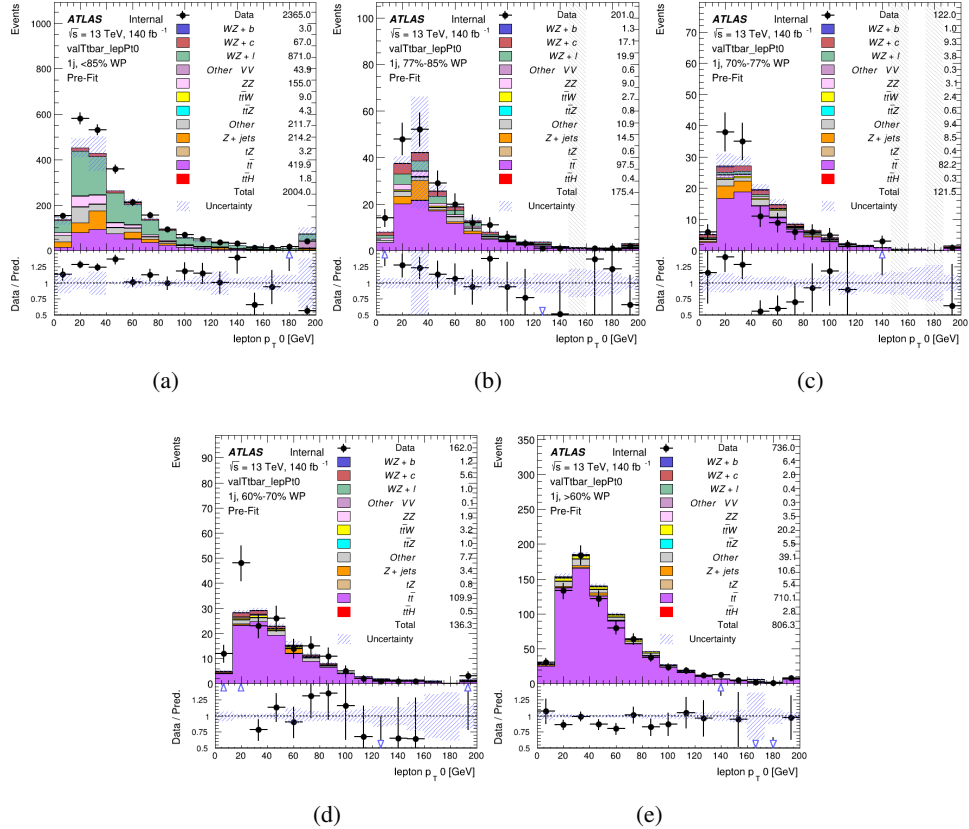


Figure 48: Comparisons between the data and MC distributions of the p_T of the OS lepton in the $t\bar{t}$ CR for each of the 1-jet b-tag working point regions

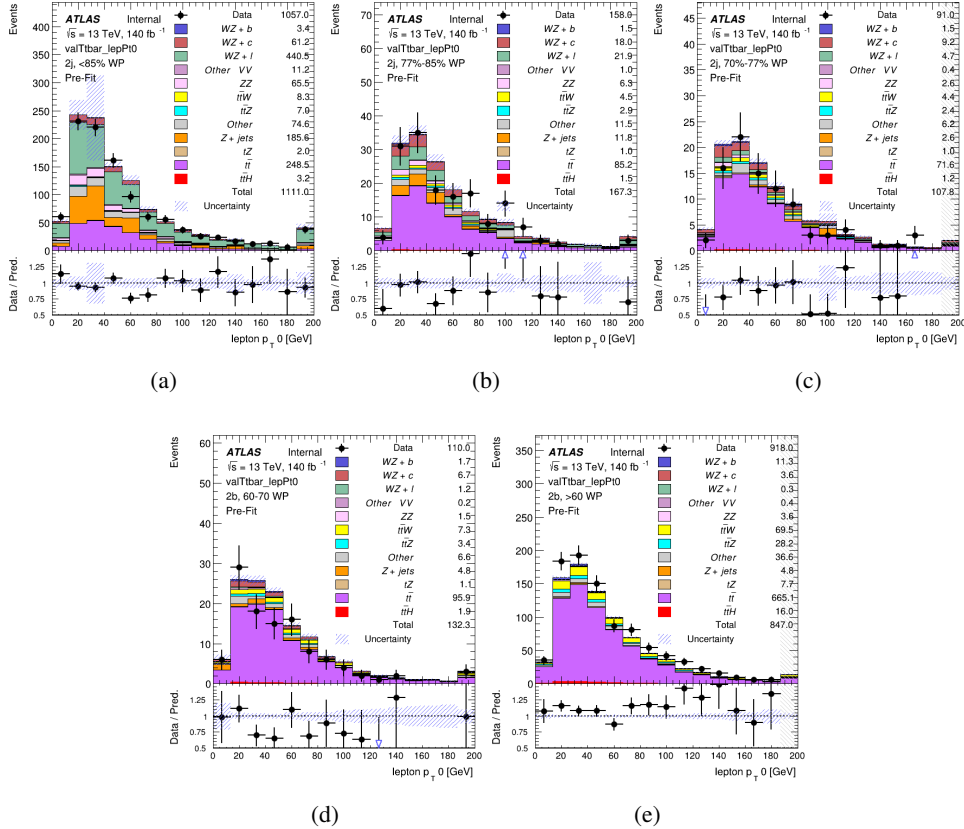


Figure 49: Comparisons between the data and MC distributions of the p_T of the OS lepton in the $t\bar{t}$ CR for each of the 2-jet b-tag working point regions

865 A.3 DSID list

Data:

```
data15_13TeV.AllYear.physics_Main.PhysCont.DAOD_HIGG8D1.grp15_v01_p4134
data16_13TeV.AllYear.physics_Main.PhysCont.DAOD_HIGG8D1.grp16_v01_p4134
data17_13TeV.AllYear.physics_Main.PhysCont.DAOD_HIGG8D1.grp17_v01_p4134
data18_13TeV.AllYear.physics_Main.PhysCont.DAOD_HIGG8D1.grp18_v01_p4134
```

mc16a:

```
mc16_13TeV.361603.PowhegPy8EG_CT10nloME_AZNLOCTEQ6L1_ZZllll_mll4.deriv.DAOD_HIGG8D1.e4475_s3126_r9364_r9315_p4133
mc16_13TeV.361602.PowhegPy8EG_CT10nloME_AZNLOCTEQ6L1_WZlvvv_mll4.deriv.DAOD_HIGG8D1.e4054_s3126_r9364_r9315_p4133
mc16_13TeV.361604.PowhegPy8EG_CT10nloME_AZNLOCTEQ6L1_ZZvvll_mll4.deriv.DAOD_HIGG8D1.e4475_s3126_r9364_r9315_p4133
mc16_13TeV.361600.PowhegPy8EG_CT10nloME_AZNLOCTEQ6L1_WWlvvv.deriv.DAOD_HIGG8D1.e4616_s3126_r9364_r9315_p4133
mc16_13TeV.361605.PowhegPy8EG_CT10nloME_AZNLOCTEQ6L1_ZZvvvv_mll4.deriv.DAOD_HIGG8D1.e4054_s3126_s3136_r9364_r9315_p4133
mc16_13TeV.361601.PowhegPy8EG_CT10nloME_AZNLOCTEQ6L1_WZlvvll_mll4.deriv.DAOD_HIGG8D1.e4475_s3126_r9364_r9315_p4133
mc16_13TeV.364286.Sherpa_222_NNPDF30NNLO_llvvjj_ss_EW4.deriv.DAOD_HIGG8D1.e6055_e5984_s3126_r9364_r9315_p3983 mc16_13TeV.364285.Sherpa_222_NNPDF30NNLO_llvvjj_ss_EW4.deriv.DAOD_HIGG8D1.e7421_e5984_s3126_r9364_r9315_p4133
mc16_13TeV.364740.MGPy8EG_NNPDF30NLO_A14NNPDF23LO_llvlij_EW6_OFPlus.deriv.DAOD_HIGG8D1.e7421_e5984_s3126_r9364_r9315_p4133
mc16_13TeV.364742.MGPy8EG_NNPDF30NLO_A14NNPDF23LO_llvlij_EW6_SFPlus.deriv.DAOD_HIGG8D1.e7421_e5984_s3126_r9364_r9315_p4133
mc16_13TeV.364253.Sherpa_222_NNPDF30NNLO_llvv.deriv.DAOD_HIGG8D1.e5916_s3126_r9364_r9315_p4133
mc16_13TeV.364250.Sherpa_222_NNPDF30NNLO_llll.deriv.DAOD_HIGG8D1.e5894_s3126_r9364_r9315_p4133
mc16_13TeV.364254.Sherpa_222_NNPDF30NNLO_llvv.deriv.DAOD_HIGG8D1.e5916_s3126_r9364_r9315_p4133
```

mc16_13TeV.364255.Sherpa_222_NNPDF30NNLO_lvyy.deriv.DAOD_HIGG8D1.e5916_s3126_r9364_r9315_p4133
 mc16_13TeV.410155.aMcAtNloPythia8EvtGen_MEN30NLO_A14N23LO_ttW.deriv.DAOD_HIGG8D1.e5070_s3126_r9364_r9315_p4133
 mc16_13TeV.410156.aMcAtNloPythia8EvtGen_MEN30NLO_A14N23LO_ttZnuu.deriv.DAOD_HIGG8D1.e5070_s3126_r9364_r9315_p4133
 mc16_13TeV.410157.aMcAtNloPythia8EvtGen_MEN30NLO_A14N23LO_ttZqq.deriv.DAOD_HIGG8D1.e5070_s3126_r9364_r9315_p4133
 mc16_13TeV.410218.aMcAtNloPythia8EvtGen_MEN30NLO_A14N23LO_ttee.deriv.DAOD_HIGG8D1.e5070_s3126_r9364_r9315_p4133
 mc16_13TeV.410219.aMcAtNloPythia8EvtGen_MEN30NLO_A14N23LO_ttmumu.deriv.DAOD_HIGG8D1.e5070_s3126_r9364_r9315_p4133
 mc16_13TeV.410220.aMcAtNloPythia8EvtGen_MEN30NLO_A14N23LO_ttautau.deriv.DAOD_HIGG8D1.e5070_s3126_r9364_r9315_p4133
 mc16_13TeV.412063.aMcAtNloPythia8EvtGen_tllq_NNPDF30_nf4_A4.deriv.DAOD_TOPQ1.e7054_e5984_s3126_r9364_r9315_p4174
 mc16_13TeV.410276.aMcAtNloPythia8EvtGen_MEN30NLO_A14N23LO_ttee_mll_1_5.deriv.DAOD_HIGG8D1.e6087_e5984_s3126_r9364_r9315_p4133
 mc16_13TeV.410277.aMcAtNloPythia8EvtGen_MEN30NLO_A14N23LO_ttmumu_mll_1_5.deriv.DAOD_HIGG8D1.e6087_e5984_s3126_r9364_r9315_p4133
 mc16_13TeV.410278.aMcAtNloPythia8EvtGen_MEN30NLO_A14N23LO_ttautau_mll_1_5.deriv.DAOD_HIGG8D1.e6087_e5984_s3126_r9364_r9315_p4133
 mc16_13TeV.410397.MadGraphPythia8EvtGen_ttbar_wbee_MEN30LO_A14N23LO.deriv.DAOD_HIGG8D1.e6086_e5984_s3126_r9364_r9315_p4133
 mc16_13TeV.410398.MadGraphPythia8EvtGen_ttbar_wbmumu_MEN30LO_A14N23LO.deriv.DAOD_HIGG8D1.e6086_e5984_s3126_r9364_r9315_p4133
 mc16_13TeV.410399.MadGraphPythia8EvtGen_ttbar_wbtautau_MEN30LO_A14N23LO.deriv.DAOD_HIGG8D1.e6086_e5984_s3126_r9364_r9315_p4133
 mc16_13TeV.410658.PhPy8EG_A14_tchan_BW50_lept_top.deriv.DAOD_HIGG8D1.e6671_e5984_s3126_r9364_r9315_p4133
 mc16_13TeV.410659.PhPy8EG_A14_tchan_BW50_lept_antitop.deriv.DAOD_HIGG8D1.e6671_e5984_s3126_r9364_r9315_p4133
 mc16_13TeV.410644.PowhegPythia8EvtGen_A14_singletop_schan_lept_top.deriv.DAOD_HIGG8D1.e6527_e5984_s3126_r9364_r9315_p4133
 mc16_13TeV.410645.PowhegPythia8EvtGen_A14_singletop_schan_lept_antitop.deriv.DAOD_HIGG8D1.e6527_e5984_s3126_r9364_r9315_p4133
 mc16_13TeV.304014.MadGraphPythia8EvtGen_A14NNPDF23_3top_SM.deriv.DAOD_HIGG8D1.e4324_s3126_r9364_r9315_p4133
 mc16_13TeV.410080.MadGraphPythia8EvtGen_A14NNPDF23_4topSM.deriv.DAOD_HIGG8D1.e4111_s3126_r9364_r9315_p4133
 mc16_13TeV.410081.MadGraphPythia8EvtGen_A14NNPDF23_ttbarWW.deriv.DAOD_HIGG8D1.e4111_s3126_r9364_r9315_p4133
 mc16_13TeV.364100.Sherpa_221_NNPDF30NNLO_Zmumu_MAXHTPTV0_70_CVetoBVeto.deriv.DAOD_HIGG8D1.e5271_s3126_r9364_r9315_p4133
 mc16_13TeV.364101.Sherpa_221_NNPDF30NNLO_Zmumu_MAXHTPTV0_70_CFilterBVeto.deriv.DAOD_HIGG8D1.e5271_s3126_r9364_r9315_p4133
 mc16_13TeV.364102.Sherpa_221_NNPDF30NNLO_Zmumu_MAXHTPTV0_70_BFilter.deriv.DAOD_HIGG8D1.e5271_s3126_r9364_r9315_p4133
 mc16_13TeV.364103.Sherpa_221_NNPDF30NNLO_Zmumu_MAXHTPTV70_140_CVetoBVeto.deriv.DAOD_HIGG8D1.e5271_s3126_r9364_r9315_p4133
 mc16_13TeV.364104.Sherpa_221_NNPDF30NNLO_Zmumu_MAXHTPTV70_140_CFilterBVeto.deriv.DAOD_HIGG8D1.e5271_s3126_r9364_r9315_p4133
 mc16_13TeV.364106.Sherpa_221_NNPDF30NNLO_Zmumu_MAXHTPTV140_280_CVetoBVeto.deriv.DAOD_HIGG8D1.e5271_s3126_r9364_r9315_p4133
 mc16_13TeV.364107.Sherpa_221_NNPDF30NNLO_Zmumu_MAXHTPTV140_280_CFilterBVeto.deriv.DAOD_HIGG8D1.e5271_s3126_r9364_r9315_p4133
 mc16_13TeV.364108.Sherpa_221_NNPDF30NNLO_Zmumu_MAXHTPTV140_280_BFilter.deriv.DAOD_HIGG8D1.e5271_s3126_r9364_r9315_p4133
 mc16_13TeV.364109.Sherpa_221_NNPDF30NNLO_Zmumu_MAXHTPTV280_500_CVetoBVeto.deriv.DAOD_HIGG8D1.e5271_s3126_r9364_r9315_p4133
 mc16_13TeV.364110.Sherpa_221_NNPDF30NNLO_Zmumu_MAXHTPTV280_500_CFilterBVeto.deriv.DAOD_HIGG8D1.e5271_s3126_r9364_r9315_p4133
 mc16_13TeV.364111.Sherpa_221_NNPDF30NNLO_Zmumu_MAXHTPTV280_500_BFilter.deriv.DAOD_HIGG8D1.e5271_e5984_s3126_r9364_r9315_p4133
 mc16_13TeV.364111.Sherpa_221_NNPDF30NNLO_Zmumu_MAXHTPTV280_500_BFilter.deriv.DAOD_HIGG8D1.e5271_s3126_r9364_r9315_p4133
 mc16_13TeV.364112.Sherpa_221_NNPDF30NNLO_Zmumu_MAXHTPTV500_1000.deriv.DAOD_HIGG8D1.e5271_s3126_r9364_r9315_p4133
 mc16_13TeV.364113.Sherpa_221_NNPDF30NNLO_Zmumu_MAXHTPTV1000_E_CMS.deriv.DAOD_HIGG8D1.e5271_s3126_r9364_r9315_p4133
 mc16_13TeV.364114.Sherpa_221_NNPDF30NNLO_Zee_MAXHTPTV0_70_CVetoBVeto.deriv.DAOD_HIGG8D1.e5299_s3126_r9364_r9315_p4133
 mc16_13TeV.364115.Sherpa_221_NNPDF30NNLO_Zee_MAXHTPTV0_70_CFilterBVeto.deriv.DAOD_HIGG8D1.e5299_s3126_r9364_r9315_p4133
 mc16_13TeV.364116.Sherpa_221_NNPDF30NNLO_Zee_MAXHTPTV0_70_BFilter.deriv.DAOD_HIGG8D1.e5299_s3126_r9364_r9315_p4133
 mc16_13TeV.364117.Sherpa_221_NNPDF30NNLO_Zee_MAXHTPTV70_140_CVetoBVeto.deriv.DAOD_HIGG8D1.e5299_s3126_r9364_r9315_p4133
 mc16_13TeV.364118.Sherpa_221_NNPDF30NNLO_Zee_MAXHTPTV70_140_CFilterBVeto.deriv.DAOD_HIGG8D1.e5299_s3126_r9364_r9315_p4133
 mc16_13TeV.364119.Sherpa_221_NNPDF30NNLO_Zee_MAXHTPTV70_140_BFilter.deriv.DAOD_HIGG8D1.e5299_s3126_r9364_r9315_p4133
 mc16_13TeV.364120.Sherpa_221_NNPDF30NNLO_Zee_MAXHTPTV140_280_CVetoBVeto.deriv.DAOD_HIGG8D1.e5299_s3126_r9364_r9315_p4133
 mc16_13TeV.364121.Sherpa_221_NNPDF30NNLO_Zee_MAXHTPTV140_280_CFilterBVeto.deriv.DAOD_HIGG8D1.e5299_s3126_r9364_r9315_p4133
 mc16_13TeV.364122.Sherpa_221_NNPDF30NNLO_Zee_MAXHTPTV140_280_BFilter.deriv.DAOD_HIGG8D1.e5299_s3126_r9364_r9315_p4133
 mc16_13TeV.364123.Sherpa_221_NNPDF30NNLO_Zee_MAXHTPTV280_500_CVetoBVeto.deriv.DAOD_HIGG8D1.e5299_s3126_r9364_r9315_p4133
 mc16_13TeV.364124.Sherpa_221_NNPDF30NNLO_Zee_MAXHTPTV280_500_CFilterBVeto.deriv.DAOD_HIGG8D1.e5299_s3126_r9364_r9315_p4133
 mc16_13TeV.364125.Sherpa_221_NNPDF30NNLO_Zee_MAXHTPTV280_500_BFilter.deriv.DAOD_HIGG8D1.e5299_s3126_r9364_r9315_p4133
 mc16_13TeV.364126.Sherpa_221_NNPDF30NNLO_Zee_MAXHTPTV280_500_BFilter.deriv.DAOD_HIGG8D1.e5299_s3126_r9364_r9315_p4133
 mc16_13TeV.364127.Sherpa_221_NNPDF30NNLO_Zee_MAXHTPTV1000_E_CMS.deriv.DAOD_HIGG8D1.e5299_s3126_r9364_r9315_p4133
 mc16_13TeV.364128.Sherpa_221_NNPDF30NNLO_Ztautau_MAXHTPTV0_70_CVetoBVeto.deriv.DAOD_HIGG8D1.e5307_s3126_r9364_r9315_p4133
 mc16_13TeV.364129.Sherpa_221_NNPDF30NNLO_Ztautau_MAXHTPTV0_70_CFilterBVeto.deriv.DAOD_HIGG8D1.e5307_s3126_r9364_r9315_p4133
 mc16_13TeV.364130.Sherpa_221_NNPDF30NNLO_Ztautau_MAXHTPTV0_70_BFilter.deriv.DAOD_HIGG8D1.e5307_s3126_r9364_r9315_p4133
 mc16_13TeV.364131.Sherpa_221_NNPDF30NNLO_Ztautau_MAXHTPTV70_140_CVetoBVeto.deriv.DAOD_HIGG8D1.e5307_s3126_r9364_r9315_p4133
 mc16_13TeV.364132.Sherpa_221_NNPDF30NNLO_Ztautau_MAXHTPTV70_140_CFilterBVeto.deriv.DAOD_HIGG8D1.e5307_s3126_r9364_r9315_p4133
 mc16_13TeV.364133.Sherpa_221_NNPDF30NNLO_Ztautau_MAXHTPTV70_140_BFilter.deriv.DAOD_HIGG8D1.e5307_s3126_r9364_r9315_p4133
 mc16_13TeV.364134.Sherpa_221_NNPDF30NNLO_Ztautau_MAXHTPTV140_280_CVetoBVeto.deriv.DAOD_HIGG8D1.e5307_s3126_r9364_r9315_p4133
 mc16_13TeV.364135.Sherpa_221_NNPDF30NNLO_Ztautau_MAXHTPTV140_280_CFilterBVeto.deriv.DAOD_HIGG8D1.e5307_s3126_r9364_r9315_p4133
 mc16_13TeV.364136.Sherpa_221_NNPDF30NNLO_Ztautau_MAXHTPTV140_280_BFilter.deriv.DAOD_HIGG8D1.e5307_s3126_r9364_r9315_p4133
 mc16_13TeV.364137.Sherpa_221_NNPDF30NNLO_Ztautau_MAXHTPTV280_500_CVetoBVeto.deriv.DAOD_HIGG8D1.e5307_e5984_s3126_r9364_r9315_p4133
 mc16_13TeV.364138.Sherpa_221_NNPDF30NNLO_Ztautau_MAXHTPTV280_500_CFilterBVeto.deriv.DAOD_HIGG8D1.e5313_s3126_r9364_r9315_p4133

mc16_13TeV.364189.Sherpa_221_NNPDF30NNLO_Wtaunu_MAXHTPTV70_140_BFilter.deriv.DAOD_HIGG8D1.e5340_s3126_r9364_r9315_p4133
 mc16_13TeV.364190.Sherpa_221_NNPDF30NNLO_Wtaunu_MAXHTPTV140_280_CVetoBVeto.deriv.DAOD_HIGG8D1.e5340_e5984_s3126_r9364_r9315_p4133
 mc16_13TeV.364190.Sherpa_221_NNPDF30NNLO_Wtaunu_MAXHTPTV140_280_CVetoBVeto.deriv.DAOD_HIGG8D1.e5340_s3126_r9364_r9315_p4133
 mc16_13TeV.364191.Sherpa_221_NNPDF30NNLO_Wtaunu_MAXHTPTV140_280_CFilterBVeto.deriv.DAOD_HIGG8D1.e5340_s3126_r9364_r9315_p4133
 mc16_13TeV.364191.Sherpa_221_NNPDF30NNLO_Wtaunu_MAXHTPTV140_280_CFilterBVeto.deriv.DAOD_HIGG8D1.e5340_e5984_s3126_s3136_r9364_r9315_p4133
 mc16_13TeV.364192.Sherpa_221_NNPDF30NNLO_Wtaunu_MAXHTPTV140_280_BFilter.deriv.DAOD_HIGG8D1.e5340_s3126_r9364_r9315_p4133
 mc16_13TeV.364193.Sherpa_221_NNPDF30NNLO_Wtaunu_MAXHTPTV280_500_CVetoBVeto.deriv.DAOD_HIGG8D1.e5340_s3126_r9364_r9315_p4133
 mc16_13TeV.364193.Sherpa_221_NNPDF30NNLO_Wtaunu_MAXHTPTV280_500_CVetoBVeto.deriv.DAOD_HIGG8D1.e5340_e5984_s3126_s3136_r9364_r9315_p4133
 mc16_13TeV.364194.Sherpa_221_NNPDF30NNLO_Wtaunu_MAXHTPTV280_500_CFilterBVeto.deriv.DAOD_HIGG8D1.e5340_s3126_r9364_r9315_p4133
 mc16_13TeV.364194.Sherpa_221_NNPDF30NNLO_Wtaunu_MAXHTPTV280_500_CFilterBVeto.deriv.DAOD_HIGG8D1.e5340_e5984_s3126_s3136_r9364_r9315_p4133
 mc16_13TeV.364195.Sherpa_221_NNPDF30NNLO_Wtaunu_MAXHTPTV280_500_BFilter.deriv.DAOD_HIGG8D1.e5340_s3126_r9364_r9315_p4133
 mc16_13TeV.364196.Sherpa_221_NNPDF30NNLO_Wtaunu_MAXHTPTV500_1000.deriv.DAOD_HIGG8D1.e5340_s3126_r9364_r9315_p4133
 mc16_13TeV.364197.Sherpa_221_NNPDF30NNLO_Wtaunu_MAXHTPTV1000_E_CMS.deriv.DAOD_HIGG8D1.e5340_s3126_r9364_r9315_p4133
 mc16_13TeV.364500.Sherpa_222_NNPDF30NNLO_eegamma_pty_7_15.deriv.DAOD_HIGG8D1.e5928_e5984_s3126_r9364_r9315_p4133
 mc16_13TeV.364501.Sherpa_222_NNPDF30NNLO_eegamma_pty_15_35.deriv.DAOD_HIGG8D1.e5928_e5984_s3126_r9364_r9315_p4133
 mc16_13TeV.364502.Sherpa_222_NNPDF30NNLO_eegamma_pty_35_70.deriv.DAOD_HIGG8D1.e5928_e5984_s3126_r9364_r9315_p4133
 mc16_13TeV.364503.Sherpa_222_NNPDF30NNLO_eegamma_pty_70_140.deriv.DAOD_HIGG8D1.e5928_e5984_s3126_r9364_r9315_p4133
 mc16_13TeV.364504.Sherpa_222_NNPDF30NNLO_eegamma_pty_140_E_CMS.deriv.DAOD_HIGG8D1.e5928_e5984_s3126_r9364_r9315_p4133
 mc16_13TeV.364505.Sherpa_222_NNPDF30NNLO_mumugamma_pty_7_15.deriv.DAOD_HIGG8D1.e5928_e5984_s3126_r9364_r9315_p4133
 mc16_13TeV.364506.Sherpa_222_NNPDF30NNLO_mumugamma_pty_15_35.deriv.DAOD_HIGG8D1.e5988_e5984_s3126_r9364_r9315_p4133
 mc16_13TeV.364507.Sherpa_222_NNPDF30NNLO_mumugamma_pty_35_70.deriv.DAOD_HIGG8D1.e5928_e5984_s3126_r9364_r9315_p4133
 mc16_13TeV.364508.Sherpa_222_NNPDF30NNLO_mumugamma_pty_70_140.deriv.DAOD_HIGG8D1.e5928_e5984_s3126_r9364_r9315_p4133
 mc16_13TeV.364509.Sherpa_222_NNPDF30NNLO_mumugamma_pty_140_E_CMS.deriv.DAOD_HIGG8D1.e5928_e5984_s3126_r9364_r9315_p4133
 mc16_13TeV.364510.Sherpa_222_NNPDF30NNLO_tautaugamma_pty_7_15.deriv.DAOD_HIGG8D1.e5928_s3126_r9364_r9315_p4133
 mc16_13TeV.364511.Sherpa_222_NNPDF30NNLO_tautaugamma_pty_15_35.deriv.DAOD_HIGG8D1.e5928_s3126_r9364_r9315_p4133
 mc16_13TeV.364512.Sherpa_222_NNPDF30NNLO_tautaugamma_pty_35_70.deriv.DAOD_HIGG8D1.e5928_s3126_r9364_r9315_p4133
 mc16_13TeV.364513.Sherpa_222_NNPDF30NNLO_tautaugamma_pty_70_140.deriv.DAOD_HIGG8D1.e5982_s3126_r9364_r9315_p4133
 mc16_13TeV.364514.Sherpa_222_NNPDF30NNLO_tautaugamma_pty_140_E_CMS.deriv.DAOD_HIGG8D1.e5928_s3126_r9364_r9315_p4133
 mc16_13TeV.364521.Sherpa_222_NNPDF30NNLO_enugamma_pty_7_15.deriv.DAOD_HIGG8D1.e5928_s3126_r9364_r9315_p4133
 mc16_13TeV.364522.Sherpa_222_NNPDF30NNLO_enugamma_pty_15_35.deriv.DAOD_HIGG8D1.e5928_s3126_r9364_r9315_p4133
 mc16_13TeV.364523.Sherpa_222_NNPDF30NNLO_enugamma_pty_35_70.deriv.DAOD_HIGG8D1.e5928_s3126_r9364_r9315_p4133
 mc16_13TeV.364524.Sherpa_222_NNPDF30NNLO_enugamma_pty_70_140.deriv.DAOD_HIGG8D1.e5928_s3126_r9364_r9315_p4133
 mc16_13TeV.364525.Sherpa_222_NNPDF30NNLO_enugamma_pty_140_E_CMS.deriv.DAOD_HIGG8D1.e5928_s3126_r9364_r9315_p4133
 mc16_13TeV.364525.Sherpa_222_NNPDF30NNLO_enugamma_pty_140_E_CMS.deriv.DAOD_HIGG8D1.e5928_e5984_s3126_r9364_r9315_p4133
 mc16_13TeV.364526.Sherpa_222_NNPDF30NNLO_munugamma_pty_7_15.deriv.DAOD_HIGG8D1.e5928_s3126_r9364_r9315_p4133
 mc16_13TeV.364527.Sherpa_222_NNPDF30NNLO_munugamma_pty_15_35.deriv.DAOD_HIGG8D1.e5928_s3126_r9364_r9315_p4133
 mc16_13TeV.364528.Sherpa_222_NNPDF30NNLO_munugamma_pty_35_70.deriv.DAOD_HIGG8D1.e5928_s3126_r9364_r9315_p4133
 mc16_13TeV.364529.Sherpa_222_NNPDF30NNLO_munugamma_pty_70_140.deriv.DAOD_HIGG8D1.e5928_s3126_r9364_r9315_p4133
 mc16_13TeV.364530.Sherpa_222_NNPDF30NNLO_munugamma_pty_140_E_CMS.deriv.DAOD_HIGG8D1.e5928_s3126_r9364_r9315_p4133
 mc16_13TeV.364530.Sherpa_222_NNPDF30NNLO_munugamma_pty_140_E_CMS.deriv.DAOD_HIGG8D1.e5928_e5984_s3126_r9364_r9315_p4133
 mc16_13TeV.364531.Sherpa_222_NNPDF30NNLO_taunugamma_pty_7_15.deriv.DAOD_HIGG8D1.e5928_s3126_r9364_r9315_p4133
 mc16_13TeV.364532.Sherpa_222_NNPDF30NNLO_taunugamma_pty_15_35.deriv.DAOD_HIGG8D1.e5928_s3126_r9364_r9315_p4133
 mc16_13TeV.364533.Sherpa_222_NNPDF30NNLO_taunugamma_pty_35_70.deriv.DAOD_HIGG8D1.e5928_s3126_r9364_r9315_p4133
 mc16_13TeV.364534.Sherpa_222_NNPDF30NNLO_taunugamma_pty_70_140.deriv.DAOD_HIGG8D1.e5928_s3126_r9364_r9315_p4133
 mc16_13TeV.364535.Sherpa_222_NNPDF30NNLO_taunugamma_pty_140_E_CMS.deriv.DAOD_HIGG8D1.e5928_s3126_r9364_r9315_p4133
 mc16_13TeV.364535.Sherpa_222_NNPDF30NNLO_taunugamma_pty_140_E_CMS.deriv.DAOD_HIGG8D1.e5928_e5984_s3126_r9364_r9315_p4133
 mc16_13TeV.410560.MadGraphPythia8EvtGen_A14_Z_4fl_tchan_noAllHad.deriv.DAOD_HIGG8D1.e5803_s3126_r9364_r9315_p4133
 mc16_13TeV.410013.PowhegPythiaEvtGen_P2012_Wt_inclusive_top.deriv.DAOD_HIGG8D1.e3753_s3126_r9364_r9315_p4133
 mc16_13TeV.410014.PowhegPythiaEvtGen_P2012_Wt_inclusive_antitop.deriv.DAOD_HIGG8D1.e3753_s3126_r9364_r9315_p4133
 mc16_13TeV.410408.aMcAtNloPythia8EvtGen_tWZ_Tzoll_minDR1.deriv.DAOD_HIGG8D1.e6423_e5984_s3126_r9364_r9315_p4133
 mc16_13TeV.364242.Sherpa_222_NNPDF30NNLO_WWW_31v_EW6.deriv.DAOD_HIGG8D1.e5887_s3126_r9364_r9315_p4133
 mc16_13TeV.364243.Sherpa_222_NNPDF30NNLO_WWW_412v_EW6.deriv.DAOD_HIGG8D1.e5887_s3126_r9364_r9315_p4133
 mc16_13TeV.364244.Sherpa_222_NNPDF30NNLO_WWW_214v_EW6.deriv.DAOD_HIGG8D1.e5887_s3126_r9364_r9315_p4133
 mc16_13TeV.364245.Sherpa_222_NNPDF30NNLO_WZZ_51v_EW6.deriv.DAOD_HIGG8D1.e5887_s3126_r9364_r9315_p4133
 mc16_13TeV.364246.Sherpa_222_NNPDF30NNLO_WZZ_313v_EW6.deriv.DAOD_HIGG8D1.e5887_s3126_r9364_r9315_p4133
 mc16_13TeV.364247.Sherpa_222_NNPDF30NNLO_ZZZ_610v_EW6.deriv.DAOD_HIGG8D1.e5887_s3126_r9364_r9315_p4133
 mc16_13TeV.364248.Sherpa_222_NNPDF30NNLO_ZZZ_412v_EW6.deriv.DAOD_HIGG8D1.e5887_s3126_r9364_r9315_p4133
 mc16_13TeV.364249.Sherpa_222_NNPDF30NNLO_ZZZ_214v_EW6.deriv.DAOD_HIGG8D1.e5887_s3126_r9364_r9315_p4133
 mc16_13TeV.342284.Pythia8EvtGen_A14NNPDF23LO_WH125_inc.deriv.DAOD_HIGG8D1.e4246_s3126_r9364_r9315_p4133
 mc16_13TeV.342285.Pythia8EvtGen_A14NNPDF23LO_ZH125_inc.deriv.DAOD_HIGG8D1.e4246_s3126_r9364_r9315_p4133
 mc16_13TeV.341998.aMcAtNloHppEG_UEEE5_CTEQ6L1_CT10ME_tWH125_gamgam_yt_plus1.deriv.DAOD_HIGG8D1.e4394_e5984_s3126_r9364_r9315_p4133
 mc16_13TeV.410389.MadGraphPythia8EvtGen_A14NNPDF23_ttgamma_nonallhadronic.deriv.DAOD_HIGG8D1.e6155_e5984_s3126_r9364_r9315_p4133

mc16_13TeV.410470.PhPy8EG_A14_ttbar_hdamp258p75_nonallhad.deriv.DAOD_HIGG8D1.e6337_e5984_s3126_r9364_r9315_p4133
 mc16_13TeV.410472.PhPy8EG_A14_ttbar_hdamp258p75_dil.deriv.DAOD_HIGG8D1.e6348_e5984_s3126_r9364_r9315_p4133
 mc16_13TeV.346343.PhPy8EG_A14NNPDF23_NNPDF30ME_ttH125_allhad.deriv.DAOD_HIGG8D1.e7148_e5984_s3126_r9364_r9315_p4133
 mc16_13TeV.346344.PhPy8EG_A14NNPDF23_NNPDF30ME_ttH125_semilep.deriv.DAOD_HIGG8D1.e7148_e5984_s3126_r9364_r9315_p4133
 mc16_13TeV.346345.PhPy8EG_A14NNPDF23_NNPDF30ME_ttH125_dilep.deriv.DAOD_HIGG8D1.e7148_e5984_s3126_r9364_r9315_p4133

 mc16d:
 mc16_13TeV.364253.Sherpa_222_NNPDF30NNLO_lllv.deriv.DAOD_HIGG8D1.e5916_e5984_s3126_r10201_r10210_p4133
 mc16_13TeV.364250.Sherpa_222_NNPDF30NNLO_llll.deriv.DAOD_HIGG8D1.e5984_e5984_s3126_r10201_r10210_p4133
 mc16_13TeV.364254.Sherpa_222_NNPDF30NNLO_llvv.deriv.DAOD_HIGG8D1.e5916_e5984_s3126_r10201_r10210_p4133
 mc16_13TeV.364255.Sherpa_222_NNPDF30NNLO_lvvv.deriv.DAOD_HIGG8D1.e5916_e5984_s3126_r10201_r10210_p4133
 mc16_13TeV.410155.aMcAtNloPythia8EvtGen_MEN30NLO_A14N23LO_ttW.deriv.DAOD_HIGG8D1.e5070_e5984_s3126_r10201_r10210_p4133
 mc16_13TeV.410156.aMcAtNloPythia8EvtGen_MEN30NLO_A14N23LO_ttZnunu.deriv.DAOD_HIGG8D1.e5070_e5984_s3126_r10201_r10210_p4133
 mc16_13TeV.410157.aMcAtNloPythia8EvtGen_MEN30NLO_A14N23LO_ttZqq.deriv.DAOD_HIGG8D1.e5070_e5984_s3126_r10201_r10210_p4133
 mc16_13TeV.410218.aMcAtNloPythia8EvtGen_MEN30NLO_A14N23LO_ttee.deriv.DAOD_HIGG8D1.e5070_e5984_s3126_r10201_r10210_p4133
 mc16_13TeV.410219.aMcAtNloPythia8EvtGen_MEN30NLO_A14N23LO_ttmumu.deriv.DAOD_HIGG8D1.e5070_e5984_s3126_r10201_r10210_p4133
 mc16_13TeV.410220.aMcAtNloPythia8EvtGen_MEN30NLO_A14N23LO_ttautau.deriv.DAOD_HIGG8D1.e5070_e5984_s3126_r10201_r10210_p4133
 mc16_13TeV.410276.aMcAtNloPythia8EvtGen_MEN30NLO_A14N23LO_ttautau_mll_1_5.deriv.DAOD_HIGG8D1.e6087_e5984_s3126_r10201_r10210_p4133
 mc16_13TeV.410277.aMcAtNloPythia8EvtGen_MEN30NLO_A14N23LO_ttautau_mll_1_5.deriv.DAOD_HIGG8D1.e6087_e5984_s3126_r10201_r10210_p4133
 mc16_13TeV.410278.aMcAtNloPythia8EvtGen_MEN30NLO_A14N23LO_ttautau_mll_1_5.deriv.DAOD_HIGG8D1.e6087_e5984_s3126_r10201_r10210_p4133
 mc16_13TeV.410397.MadGraphPythia8EvtGen_ttbar_wbee_MEN30LO_A14N23LO.deriv.DAOD_HIGG8D1.e6086_e5984_s3126_r10201_r10210_p4133
 mc16_13TeV.410398.MadGraphPythia8EvtGen_ttbar_wbmumu_MEN30LO_A14N23LO.deriv.DAOD_HIGG8D1.e6086_e5984_s3126_r10201_r10210_p4133
 mc16_13TeV.410399.MadGraphPythia8EvtGen_ttbar_wbtautau_MEN30LO_A14N23LO.deriv.DAOD_HIGG8D1.e6086_e5984_s3126_r10201_r10210_p4133
 mc16_13TeV.410658.PhPy8EG_A14_tchan_BW50_lept_top.deriv.DAOD_HIGG8D1.e6671_e5984_s3126_r10201_r10210_p4133
 mc16_13TeV.410659.PhPy8EG_A14_tchan_BW50_lept_antitop.deriv.DAOD_HIGG8D1.e6671_e5984_s3126_r10201_r10210_p4133
 mc16_13TeV.410644.PowhegPythia8EvtGen_A14_singleton_schan_lept_top.deriv.DAOD_HIGG8D1.e6527_e5984_s3126_r10201_r10210_p4133
 mc16_13TeV.410645.PowhegPythia8EvtGen_A14_singleton_schan_lept_antitop.deriv.DAOD_HIGG8D1.e6527_s3126_r10201_r10210_p4133
 mc16_13TeV.412063.aMcAtNloPythia8EvtGen_tllq_NNPDF30_nf4_A14.deriv.DAOD_TOPQ1.e7054_e5984_s3126_r10201_r10210_p4174
 mc16_13TeV.304014.MadGraphPythia8EvtGen_A14NNPDF23_3top_SM.deriv.DAOD_HIGG8D1.e4324_e5984_s3126_r10201_r10210_p4133
 mc16_13TeV.410080.MadGraphPythia8EvtGen_A14NNPDF23_4topSM.deriv.DAOD_HIGG8D1.e4111_e5984_s3126_r10201_r10210_p4133
 mc16_13TeV.410081.MadGraphPythia8EvtGen_A14NNPDF23_ttbarWW.deriv.DAOD_HIGG8D1.e4111_e5984_s3126_r10201_r10210_p4133
 mc16_13TeV.364100.Sherpa_221_NNPDF30NNLO_Zmumu_MAXHTPTV0_70_CVetoBVeto.deriv.DAOD_HIGG8D1.e5271_s3126_r10201_r10210_p4133
 mc16_13TeV.364101.Sherpa_221_NNPDF30NNLO_Zmumu_MAXHTPTV0_70_CFilterBVeto.deriv.DAOD_HIGG8D1.e5271_s3126_r10201_r10210_p4133
 mc16_13TeV.364101.Sherpa_221_NNPDF30NNLO_Zmumu_MAXHTPTV0_70_CFilterBVeto.deriv.DAOD_HIGG8D1.e5271_s3126_r10201_r10210_p4133
 mc16_13TeV.364102.Sherpa_221_NNPDF30NNLO_Zmumu_MAXHTPTV0_70_BFilter.deriv.DAOD_HIGG8D1.e5271_s3126_r10201_r10210_p4133
 mc16_13TeV.364103.Sherpa_221_NNPDF30NNLO_Zmumu_MAXHTPTV70_140_CVetoBVeto.deriv.DAOD_HIGG8D1.e5271_s3126_r10201_r10210_p4133
 mc16_13TeV.364104.Sherpa_221_NNPDF30NNLO_Zmumu_MAXHTPTV70_140_CFilterBVeto.deriv.DAOD_HIGG8D1.e5271_s3126_r10201_r10210_p4133
 mc16_13TeV.364106.Sherpa_221_NNPDF30NNLO_Zmumu_MAXHTPTV140_280_CVetoBVeto.deriv.DAOD_HIGG8D1.e5271_s3126_r10201_r10210_p4133
 mc16_13TeV.364107.Sherpa_221_NNPDF30NNLO_Zmumu_MAXHTPTV140_280_CFilterBVeto.deriv.DAOD_HIGG8D1.e5271_s3126_r10201_r10210_p4133
 mc16_13TeV.364108.Sherpa_221_NNPDF30NNLO_Zmumu_MAXHTPTV140_280_BFilter.deriv.DAOD_HIGG8D1.e5271_s3126_r10201_r10210_p4133
 mc16_13TeV.364108.Sherpa_221_NNPDF30NNLO_Zmumu_MAXHTPTV140_280_BFilter.deriv.DAOD_HIGG8D1.e5271_s3126_r10201_r10210_p4133
 mc16_13TeV.364109.Sherpa_221_NNPDF30NNLO_Zmumu_MAXHTPTV280_500_CVetoBVeto.deriv.DAOD_HIGG8D1.e5271_s3126_r10201_r10210_p4133
 mc16_13TeV.364109.Sherpa_221_NNPDF30NNLO_Zmumu_MAXHTPTV280_500_CVetoBVeto.deriv.DAOD_HIGG8D1.e5271_s3126_r10201_r10210_p4133
 mc16_13TeV.364110.Sherpa_221_NNPDF30NNLO_Zmumu_MAXHTPTV280_500_CFilterBVeto.deriv.DAOD_HIGG8D1.e5271_s3126_r10201_r10210_p4133
 mc16_13TeV.364111.Sherpa_221_NNPDF30NNLO_Zmumu_MAXHTPTV280_500_BFilter.deriv.DAOD_HIGG8D1.e5271_s3126_r10201_r10210_p4133
 mc16_13TeV.364111.Sherpa_221_NNPDF30NNLO_Zmumu_MAXHTPTV280_500_BFilter.deriv.DAOD_HIGG8D1.e5271_s3126_r10201_r10210_p4133
 mc16_13TeV.364112.Sherpa_221_NNPDF30NNLO_Zmumu_MAXHTPTV280_500_BFilter.deriv.DAOD_HIGG8D1.e5271_s3126_r10201_r10210_p4133
 mc16_13TeV.364112.Sherpa_221_NNPDF30NNLO_Zmumu_MAXHTPTV280_500_BFilter.deriv.DAOD_HIGG8D1.e5271_s3126_r10201_r10210_p4133
 mc16_13TeV.364113.Sherpa_221_NNPDF30NNLO_Zmumu_MAXHTPTV1000_E_CMS.deriv.DAOD_HIGG8D1.e5271_s3126_r10201_r10210_p4133
 mc16_13TeV.364114.Sherpa_221_NNPDF30NNLO_Zee_MAXHTPTV0_70_CVetoBVeto.deriv.DAOD_HIGG8D1.e5299_s3126_r10201_r10210_p4133
 mc16_13TeV.364115.Sherpa_221_NNPDF30NNLO_Zee_MAXHTPTV0_70_CFilterBVeto.deriv.DAOD_HIGG8D1.e5299_e5984_s3126_r10201_r10210_p4133
 mc16_13TeV.364116.Sherpa_221_NNPDF30NNLO_Zee_MAXHTPTV0_70_BFilter.deriv.DAOD_HIGG8D1.e5299_e5984_s3126_r10201_r10210_p4133
 mc16_13TeV.364117.Sherpa_221_NNPDF30NNLO_Zee_MAXHTPTV70_140_CVetoBVeto.deriv.DAOD_HIGG8D1.e5299_e5984_s3126_r10201_r10210_p4133
 mc16_13TeV.364118.Sherpa_221_NNPDF30NNLO_Zee_MAXHTPTV70_140_CFilterBVeto.deriv.DAOD_HIGG8D1.e5299_e5984_s3126_r10201_r10210_p4133
 mc16_13TeV.364119.Sherpa_221_NNPDF30NNLO_Zee_MAXHTPTV70_140_BFilter.deriv.DAOD_HIGG8D1.e5299_e5984_s3126_r10201_r10210_p4133
 mc16_13TeV.364120.Sherpa_221_NNPDF30NNLO_Zee_MAXHTPTV140_280_CVetoBVeto.deriv.DAOD_HIGG8D1.e5299_e5984_s3126_r10201_r10210_p4133
 mc16_13TeV.364121.Sherpa_221_NNPDF30NNLO_Zee_MAXHTPTV140_280_CFilterBVeto.deriv.DAOD_HIGG8D1.e5299_e5984_s3126_r10201_r10210_p4133
 mc16_13TeV.364122.Sherpa_221_NNPDF30NNLO_Zee_MAXHTPTV140_280_BFilter.deriv.DAOD_HIGG8D1.e5299_e5984_s3126_r10201_r10210_p4133
 mc16_13TeV.364123.Sherpa_221_NNPDF30NNLO_Zee_MAXHTPTV280_500_CVetoBVeto.deriv.DAOD_HIGG8D1.e5299_e5984_s3126_r10201_r10210_p4133
 mc16_13TeV.364124.Sherpa_221_NNPDF30NNLO_Zee_MAXHTPTV280_500_CFilterBVeto.deriv.DAOD_HIGG8D1.e5299_e5984_s3126_r10201_r10210_p4133
 mc16_13TeV.364125.Sherpa_221_NNPDF30NNLO_Zee_MAXHTPTV280_500_BFilter.deriv.DAOD_HIGG8D1.e5299_e5984_s3126_r10201_r10210_p4133
 mc16_13TeV.364126.Sherpa_221_NNPDF30NNLO_Zee_MAXHTPTV500_1000.deriv.DAOD_HIGG8D1.e5299_e5984_s3126_r10201_r10210_p4133

mc16_13TeV.364506.Sherpa_222_NNPDF30NNLO_mumugamma_pty_15_35.deriv.DAOD_HIGG8D1.e5928_e5984_s3126_r10201_r10210_p4133
mc16_13TeV.364507.Sherpa_222_NNPDF30NNLO_mumugamma_pty_35_70.deriv.DAOD_HIGG8D1.e5928_e5984_s3126_r10201_r10210_p4133
mc16_13TeV.364508.Sherpa_222_NNPDF30NNLO_mumugamma_pty_70_140.deriv.DAOD_HIGG8D1.e5928_e5984_s3126_r10201_r10210_p4133
mc16_13TeV.364509.Sherpa_222_NNPDF30NNLO_mumugamma_pty_140_E_CMS.deriv.DAOD_HIGG8D1.e5928_e5984_s3126_r10201_r10210_p4133
mc16_13TeV.364510.Sherpa_222_NNPDF30NNLO_tautaugamma_pty_7_15.deriv.DAOD_HIGG8D1.e5928_e5984_s3126_r10201_r10210_p4133
mc16_13TeV.364511.Sherpa_222_NNPDF30NNLO_tautaugamma_pty_15_35.deriv.DAOD_HIGG8D1.e5928_e5984_s3126_r10201_r10210_p4133
mc16_13TeV.364512.Sherpa_222_NNPDF30NNLO_tautaugamma_pty_35_70.deriv.DAOD_HIGG8D1.e5928_e5984_s3126_r10201_r10210_p4133
mc16_13TeV.364513.Sherpa_222_NNPDF30NNLO_tautaugamma_pty_70_140.deriv.DAOD_HIGG8D1.e5928_e5984_s3126_r10201_r10210_p4133
mc16_13TeV.364513.Sherpa_222_NNPDF30NNLO_tautaugamma_pty_70_140.deriv.DAOD_HIGG8D1.e5928_e5984_s3126_r10201_r10210_p4133
mc16_13TeV.364514.Sherpa_222_NNPDF30NNLO_tautaugamma_pty_140_E_CMS.deriv.DAOD_HIGG8D1.e5928_e5984_s3126_r10201_r10210_p4133
mc16_13TeV.364521.Sherpa_222_NNPDF30NNLO_enugamma_pty_7_15.deriv.DAOD_HIGG8D1.e5928_e5984_s3126_r10201_r10210_p4133
mc16_13TeV.364522.Sherpa_222_NNPDF30NNLO_enugamma_pty_15_35.deriv.DAOD_HIGG8D1.e5928_e5984_s3126_r10201_r10210_p4133
mc16_13TeV.364523.Sherpa_222_NNPDF30NNLO_enugamma_pty_35_70.deriv.DAOD_HIGG8D1.e5928_e5984_s3126_r10201_r10210_p4133
mc16_13TeV.364524.Sherpa_222_NNPDF30NNLO_enugamma_pty_70_140.deriv.DAOD_HIGG8D1.e5928_e5984_s3126_r10201_r10210_p4133
mc16_13TeV.364525.Sherpa_222_NNPDF30NNLO_enugamma_pty_140_E_CMS.deriv.DAOD_HIGG8D1.e5928_e5984_s3126_r10201_r10210_p4133
mc16_13TeV.364526.Sherpa_222_NNPDF30NNLO_munugamma_pty_7_15.deriv.DAOD_HIGG8D1.e5928_e5984_s3126_r10201_r10210_p4133
mc16_13TeV.364527.Sherpa_222_NNPDF30NNLO_munugamma_pty_15_35.deriv.DAOD_HIGG8D1.e5928_e5984_s3126_r10201_r10210_p4133
mc16_13TeV.364528.Sherpa_222_NNPDF30NNLO_munugamma_pty_35_70.deriv.DAOD_HIGG8D1.e5928_e5984_s3126_r10201_r10210_p4133
mc16_13TeV.364529.Sherpa_222_NNPDF30NNLO_munugamma_pty_70_140.deriv.DAOD_HIGG8D1.e5928_e5984_s3126_r10201_r10210_p4133
mc16_13TeV.364530.Sherpa_222_NNPDF30NNLO_munugamma_pty_140_E_CMS.deriv.DAOD_HIGG8D1.e5928_e5984_s3126_r10201_r10210_p4133
mc16_13TeV.364531.Sherpa_222_NNPDF30NNLO_taunugamma_pty_7_15.deriv.DAOD_HIGG8D1.e5928_e5984_s3126_r10201_r10210_p4133
mc16_13TeV.364532.Sherpa_222_NNPDF30NNLO_taunugamma_pty_15_35.deriv.DAOD_HIGG8D1.e5928_e5984_s3126_r10201_r10210_p4133
mc16_13TeV.364533.Sherpa_222_NNPDF30NNLO_taunugamma_pty_35_70.deriv.DAOD_HIGG8D1.e5928_e5984_s3126_r10201_r10210_p4133
mc16_13TeV.364534.Sherpa_222_NNPDF30NNLO_taunugamma_pty_70_140.deriv.DAOD_HIGG8D1.e5928_e5984_s3126_r10201_r10210_p4133
mc16_13TeV.364535.Sherpa_222_NNPDF30NNLO_taunugamma_pty_140_E_CMS.deriv.DAOD_HIGG8D1.e5928_e5984_s3126_r10201_r10210_p4133
mc16_13TeV.410056.MadGraphPythiaEvtGen_A14_iZ_4fl_tchan_noAllHad.deriv.DAOD_HIGG8D1.e5803_e5984_s3126_r10201_r10210_p4133
mc16_13TeV.410013.PowhegPythiaEvtGen_P2012_Wt_inclusive_top.deriv.DAOD_HIGG8D1.e3753_s3126_r10201_r10210_p4133
mc16_13TeV.410014.PowhegPythiaEvtGen_P2012_Wt_inclusive_antitop.deriv.DAOD_HIGG8D1.e3753_s3126_r10201_r10210_p4133
mc16_13TeV.410408.aMcAtNloPythia8EvtGen_tWZ_Ztoll_minDR1.deriv.DAOD_HIGG8D1.e6423_e5984_s3126_r10201_r10210_p4133
mc16_13TeV.364242.Sherpa_222_NNPDF30NNLO_WWW_313v_EW6.deriv.DAOD_HIGG8D1.e5887_e5984_s3126_r10201_r10210_p4133
mc16_13TeV.364243.Sherpa_222_NNPDF30NNLO_WWW_412v_EW6.deriv.DAOD_HIGG8D1.e5887_e5984_s3126_r10201_r10210_p4133
mc16_13TeV.364244.Sherpa_222_NNPDF30NNLO_WWW_214v_EW6.deriv.DAOD_HIGG8D1.e5887_e5984_s3126_r10201_r10210_p4133
mc16_13TeV.364245.Sherpa_222_NNPDF30NNLO_WZZ_511v_EW6.deriv.DAOD_HIGG8D1.e5887_e5984_s3126_r10201_r10210_p4133
mc16_13TeV.364246.Sherpa_222_NNPDF30NNLO_WZZ_313v_EW6.deriv.DAOD_HIGG8D1.e5887_e5984_s3126_r10201_r10210_p4133
mc16_13TeV.364247.Sherpa_222_NNPDF30NNLO_ZZZ_610v_EW6.deriv.DAOD_HIGG8D1.e5887_e5984_s3126_r10201_r10210_p4133
mc16_13TeV.364248.Sherpa_222_NNPDF30NNLO_ZZZ_412v_EW6.deriv.DAOD_HIGG8D1.e5887_e5984_s3126_r10201_r10210_p4133
mc16_13TeV.364249.Sherpa_222_NNPDF30NNLO_ZZZ_214v_EW6.deriv.DAOD_HIGG8D1.e5887_e5984_s3126_r10201_r10210_p4133
mc16_13TeV.342284.Pythia8EvtGen_A14NNPDF23LO_WH125_inc.deriv.DAOD_HIGG8D1.e4246_e5984_s3126_r10201_r10210_p4133
mc16_13TeV.342285.Pythia8EvtGen_A14NNPDF23LO_ZH125_inc.deriv.DAOD_HIGG8D1.e4246_e5984_s3126_r10201_r10210_p4133
mc16_13TeV.341998.aMcAtNloHppEG_UEEE5_CTEQ6L1_CT10ME_tWH125_gamgam_yt_plus1.deriv.DAOD_HIGG8D1.e4394_e5984_s3126_r10201_r10210_p4133
mc16_13TeV.410470.PhPy8EG_A14_ttbar_hdamp258p75_nonallhad.deriv.DAOD_HIGG8D1.e6337_e5984_s3126_r10201_r10210_p4133
mc16_13TeV.410472.PhPy8EG_A14_ttbar_hdamp258p75_dil.deriv.DAOD_HIGG8D1.e6348_e5984_s3126_r10201_r10210_p4133
mc16_13TeV.346343.PhPy8EG_A14NNPDF23_NNPDF30ME_ttH125_allhad.deriv.DAOD_HIGG8D1.e7148_e5984_s3126_r10201_r10210_p4133
mc16_13TeV.346344.PhPy8EG_A14NNPDF23_NNPDF30ME_ttH125_semilep.deriv.DAOD_HIGG8D1.e7148_e5984_a875_r10201_r10210_p4133
mc16_13TeV.346345.PhPy8EG_A14NNPDF23_NNPDF30ME_ttH125_dilep.deriv.DAOD_HIGG8D1.e7148_e5984_a875_r10201_r10210_p4133

mc16e:

mc16_13TeV.361605.PowhegPy8EG_CT10nloME_AZNLOCTEQ6L1_ZZvvvv_mll4.deriv.DAOD_HIGG8D1.e4054_e5984_s3126_r10724_r10726_p4133
mc16_13TeV.361602.PowhegPy8EG_CT10nloME_AZNLOCTEQ6L1_WZlvvv_mll4.deriv.DAOD_HIGG8D1.e4054_e5984_s3126_r10724_r10726_p4133
mc16_13TeV.361601.PowhegPy8EG_CT10nloME_AZNLOCTEQ6L1_WZlavl_mll4.deriv.DAOD_HIGG8D1.e4475_e5984_s3126_r10724_r10726_p4133
mc16_13TeV.361600.PowhegPy8EG_CT10nloME_AZNLOCTEQ6L1_WWlvlv.deriv.DAOD_HIGG8D1.e4616_e5984_s3126_r10724_r10726_p4133
mc16_13TeV.361603.PowhegPy8EG_CT10nloME_AZNLOCTEQ6L1_ZZllll_mll4.deriv.DAOD_HIGG8D1.e4475_e5984_s3126_r10724_r10726_p4133
mc16_13TeV.361604.PowhegPy8EG_CT10nloME_AZNLOCTEQ6L1_ZZvvll_mll4.deriv.DAOD_HIGG8D1.e4475_e5984_s3126_r10724_r10726_p4133
mc16_13TeV.364288.Sherpa_222_NNPDF30NNLO_llll_lowMllPtComplement.deriv.DAOD_HIGG8D1.e6096_s3126_r10724_p3983 mc16_13TeV.364287.Sherpa_222_NNPDF30NNLO_llll_lowMllPtComplement.deriv.DAOD_HIGG8D1.e6096_s3126_r10724_p3983
mc16_13TeV.364285.Sherpa_222_NNPDF30NNLO_llvjj_EW6.deriv.DAOD_HIGG8D1.e6055_s3126_r10724_p3983
mc16_13TeV.364284.Sherpa_222_NNPDF30NNLO_llvjj_EW6.deriv.DAOD_HIGG8D1.e6055_s3126_r10724_p3983
mc16_13TeV.364283.Sherpa_222_NNPDF30NNLO_lllijj_EW6.deriv.DAOD_HIGG8D1.e6055_s3126_r10724_p3983
mc16_13TeV.364739.MGPy8EG_NNPDF30NLO_A14NNPDF23LO_lvjlljjEW6_OFMinus.deriv.DAOD_HIGG8D1.e7421_e5984_s3126_r10724_r10726_p4133
mc16_13TeV.364742.MGPy8EG_NNPDF30NLO_A14NNPDF23LO_lvjlljjEW6_SFPlus.deriv.DAOD_HIGG8D1.e7421_e5984_s3126_r10724_r10726_p4133
mc16_13TeV.364740.MGPy8EG_NNPDF30NLO_A14NNPDF23LO_lvjlljjEW6_OFPlus.deriv.DAOD_HIGG8D1.e7421_e5984_s3126_r10724_r10726_p4133
mc16_13TeV.364741.MGPy8EG_NNPDF30NLO_A14NNPDF23LO_lvjlljjEW6_SFMinus.deriv.DAOD_HIGG8D1.e7421_e5984_s3126_r10724_r10726_p4133
mc16_13TeV.364253.Sherpa_222_NNPDF30NNLO_llv.deriv.DAOD_HIGG8D1.e5916_e5984_s3126_r10724_r10726_p4133

mc16_13TeV.364250.Sherpa_222_NNPDF30NNLO_llll.deriv.DAOD_HIGG8D1.e5894_e5984_s3126_r10724_r10726_p4133
 mc16_13TeV.364254.Sherpa_222_NNPDF30NNLO_llvv.deriv.DAOD_HIGG8D1.e5916_e5984_s3126_r10724_r10726_p4133
 mc16_13TeV.364255.Sherpa_222_NNPDF30NNLO_lvvv.deriv.DAOD_HIGG8D1.e5916_e5984_s3126_r10724_r10726_p4133
 mc16_13TeV.410155.aMcAtNloPythia8EvtGen_MEN30NLO_A14N23LO_ttW.deriv.DAOD_HIGG8D1.e5070_e5984_s3126_r10724_r10726_p4133
 mc16_13TeV.410156.aMcAtNloPythia8EvtGen_MEN30NLO_A14N23LO_ttZnunu.deriv.DAOD_HIGG8D1.e5070_e5984_s3126_r10724_r10726_p4133
 mc16_13TeV.410157.aMcAtNloPythia8EvtGen_MEN30NLO_A14N23LO_ttZqq.deriv.DAOD_HIGG8D1.e5070_e5984_s3126_r10724_r10726_p4133
 mc16_13TeV.410218.aMcAtNloPythia8EvtGen_MEN30NLO_A14N23LO_ttee.deriv.DAOD_HIGG8D1.e5070_e5984_s3126_r10724_r10726_p4133
 mc16_13TeV.410219.aMcAtNloPythia8EvtGen_MEN30NLO_A14N23LO_ttmumu.deriv.DAOD_HIGG8D1.e5070_e5984_s3126_r10724_r10726_p4133
 mc16_13TeV.410220.aMcAtNloPythia8EvtGen_MEN30NLO_A14N23LO_ttautau.deriv.DAOD_HIGG8D1.e5070_e5984_s3126_r10724_r10726_p4133
 mc16_13TeV.410276.aMcAtNloPythia8EvtGen_MEN30NLO_A14N23LO_ttee_mll_1_5.deriv.DAOD_HIGG8D1.e6087_e5984_s3126_r10724_r10726_p4133
 mc16_13TeV.410277.aMcAtNloPythia8EvtGen_MEN30NLO_A14N23LO_ttmumu_mll_1_5.deriv.DAOD_HIGG8D1.e6087_e5984_s3126_r10724_r10726_p4133
 mc16_13TeV.410278.aMcAtNloPythia8EvtGen_MEN30NLO_A14N23LO_ttautau_mll_1_5.deriv.DAOD_HIGG8D1.e6087_e5984_s3126_r10724_r10726_p4133
 mc16_13TeV.410397.MadGraphPythia8EvtGen_ttbar_wbee_MEN30NLO_A14N23LO.deriv.DAOD_HIGG8D1.e6086_e5984_s3126_r10724_r10726_p4133
 mc16_13TeV.410398.MadGraphPythia8EvtGen_ttbar_wbmumu_MEN30NLO_A14N23LO.deriv.DAOD_HIGG8D1.e6086_e5984_s3126_r10724_r10726_p4133
 mc16_13TeV.410399.MadGraphPythia8EvtGen_ttbar_wbtautau_MEN30NLO_A14N23LO.deriv.DAOD_HIGG8D1.e6086_e5984_s3126_r10724_r10726_p4133
 mc16_13TeV.410658.PhPy8EG_A14_tchan_BW50_lept_top.deriv.DAOD_HIGG8D1.e6671_e5984_s3126_s3136_r10724_r10726_p4133
 mc16_13TeV.410659.PhPy8EG_A14_tchan_BW50_lept_antitop.deriv.DAOD_HIGG8D1.e6671_e5984_s3126_s3136_r10724_r10726_p4133
 mc16_13TeV.410644.PowhegPythia8EvtGen_A14_singletop_schan_lept_top.deriv.DAOD_HIGG8D1.e6527_e5984_s3126_r10724_r10726_p4133
 mc16_13TeV.410645.PowhegPythia8EvtGen_A14_singletop_schan_lept_antitop.deriv.DAOD_HIGG8D1.e6527_e5984_s3126_r10724_r10726_p4133
 mc16_13TeV.412063.aMcAtNloPythia8EvtGen_tllq_NNPDF30_nf4_A14.deriv.DAOD_TOPQ1.e7054_e5984_s3126_r10724_r10726_p4174
 mc16_13TeV.304014.MadGraphPythia8EvtGen_A14NNPDF23_3top_SM.deriv.DAOD_HIGG8D1.e4324_e5984_s3126_r10724_r10726_p4133
 mc16_13TeV.410080.MadGraphPythia8EvtGen_A14NNPDF23_4topSM.deriv.DAOD_HIGG8D1.e4111_e5984_s3126_r10724_r10726_p4133
 mc16_13TeV.410081.MadGraphPythia8EvtGen_A14NNPDF23_ttbarWW.deriv.DAOD_HIGG8D1.e4111_e5984_s3126_r10724_r10726_p4133
 mc16_13TeV.364100.Sherpa_221_NNPDF30NNLO_Zmumu_MAXHPTV0_70_CVetoBVeto.deriv.DAOD_HIGG8D1.e5271_e5984_s3126_s3136_r10724_r10726_p4133
 mc16_13TeV.364100.Sherpa_221_NNPDF30NNLO_Zmumu_MAXHPTV0_70_CVetoBVeto.deriv.DAOD_HIGG8D1.e5271_e5984_s3126_r10724_r10726_p4133
 mc16_13TeV.364101.Sherpa_221_NNPDF30NNLO_Zmumu_MAXHPTV0_70_CFilterBVeto.deriv.DAOD_HIGG8D1.e5271_e5984_s3126_r10724_r10726_p4133
 mc16_13TeV.364102.Sherpa_221_NNPDF30NNLO_Zmumu_MAXHPTV0_70_BFilter.deriv.DAOD_HIGG8D1.e5271_e5984_s3126_s3136_r10724_r10726_p4133
 mc16_13TeV.364102.Sherpa_221_NNPDF30NNLO_Zmumu_MAXHPTV0_70_BFilter.deriv.DAOD_HIGG8D1.e5271_e5984_s3126_r10724_r10726_p4133
 mc16_13TeV.364103.Sherpa_221_NNPDF30NNLO_Zmumu_MAXHPTV70_140_CVetoBVeto.deriv.DAOD_HIGG8D1.e5271_e5984_s3126_r10724_r10726_p4133
 mc16_13TeV.364103.Sherpa_221_NNPDF30NNLO_Zmumu_MAXHPTV70_140_CVetoBVeto.deriv.DAOD_HIGG8D1.e5271_e5984_s3126_s3136_r10724_r10726_p4133
 mc16_13TeV.364104.Sherpa_221_NNPDF30NNLO_Zmumu_MAXHPTV70_140_CFilterBVeto.deriv.DAOD_HIGG8D1.e5271_e5984_s3126_r10724_r10726_p4133
 mc16_13TeV.364104.Sherpa_221_NNPDF30NNLO_Zmumu_MAXHPTV70_140_CFilterBVeto.deriv.DAOD_HIGG8D1.e5271_e5984_s3126_s3136_r10724_r10726_p4133
 mc16_13TeV.364106.Sherpa_221_NNPDF30NNLO_Zmumu_MAXHPTV140_280_CVetoBVeto.deriv.DAOD_HIGG8D1.e5271_e5984_s3126_s3136_r10724_r10726_p4133
 mc16_13TeV.364106.Sherpa_221_NNPDF30NNLO_Zmumu_MAXHPTV140_280_CVetoBVeto.deriv.DAOD_HIGG8D1.e5271_e5984_s3126_r10724_r10726_p4133
 mc16_13TeV.364107.Sherpa_221_NNPDF30NNLO_Zmumu_MAXHPTV140_280_CFilterBVeto.deriv.DAOD_HIGG8D1.e5271_e5984_s3126_r10724_r10726_p4133
 mc16_13TeV.364107.Sherpa_221_NNPDF30NNLO_Zmumu_MAXHPTV140_280_CFilterBVeto.deriv.DAOD_HIGG8D1.e5271_e5984_s3126_s3136_r10724_r10726_p4133
 mc16_13TeV.364108.Sherpa_221_NNPDF30NNLO_Zmumu_MAXHPTV140_280_BFilter.deriv.DAOD_HIGG8D1.e5271_e5984_s3126_r10724_r10726_p4133
 mc16_13TeV.364109.Sherpa_221_NNPDF30NNLO_Zmumu_MAXHPTV280_500_CVetoBVeto.deriv.DAOD_HIGG8D1.e5271_e5984_s3126_r10724_r10726_p4133
 mc16_13TeV.364110.Sherpa_221_NNPDF30NNLO_Zmumu_MAXHPTV280_500_CFilterBVeto.deriv.DAOD_HIGG8D1.e5271_e5984_s3126_r10724_r10726_p4133
 mc16_13TeV.364110.Sherpa_221_NNPDF30NNLO_Zmumu_MAXHPTV280_500_CFilterBVeto.deriv.DAOD_HIGG8D1.e5271_e5984_s3126_s3136_r10724_r10726_p4133
 mc16_13TeV.364111.Sherpa_221_NNPDF30NNLO_Zmumu_MAXHPTV280_500_BFilter.deriv.DAOD_HIGG8D1.e5271_e5984_s3126_s3136_r10724_r10726_p4133
 mc16_13TeV.364111.Sherpa_221_NNPDF30NNLO_Zmumu_MAXHPTV280_500_BFilter.deriv.DAOD_HIGG8D1.e5271_e5984_s3126_r10724_r10726_p4133
 mc16_13TeV.364112.Sherpa_221_NNPDF30NNLO_Zmumu_MAXHPTV500_1000.deriv.DAOD_HIGG8D1.e5271_e5984_s3126_r10724_r10726_p4133
 mc16_13TeV.364113.Sherpa_221_NNPDF30NNLO_Zmumu_MAXHPTV1000_E_CMS.deriv.DAOD_HIGG8D1.e5271_e5984_s3126_r10724_r10726_p4133
 mc16_13TeV.364113.Sherpa_221_NNPDF30NNLO_Zmumu_MAXHPTV1000_E_CMS.deriv.DAOD_HIGG8D1.e5271_e5984_s3126_s3136_r10724_r10726_p4133
 mc16_13TeV.364114.Sherpa_221_NNPDF30NNLO_Zee_MAXHPTV0_70_CVetoBVeto.deriv.DAOD_HIGG8D1.e5299_e5984_s3126_s3136_r10724_r10726_p4133
 mc16_13TeV.364114.Sherpa_221_NNPDF30NNLO_Zee_MAXHPTV0_70_CVetoBVeto.deriv.DAOD_HIGG8D1.e5299_e5984_s3126_r10724_r10726_p4133
 mc16_13TeV.364115.Sherpa_221_NNPDF30NNLO_Zee_MAXHPTV0_70_CFilterBVeto.deriv.DAOD_HIGG8D1.e5299_e5984_s3126_s3136_r10724_r10726_p4133
 mc16_13TeV.364115.Sherpa_221_NNPDF30NNLO_Zee_MAXHPTV0_70_CFilterBVeto.deriv.DAOD_HIGG8D1.e5299_e5984_s3126_r10724_r10726_p4133
 mc16_13TeV.364116.Sherpa_221_NNPDF30NNLO_Zee_MAXHPTV0_70_BFilter.deriv.DAOD_HIGG8D1.e5299_e5984_s3126_r10724_r10726_p4133
 mc16_13TeV.364117.Sherpa_221_NNPDF30NNLO_Zee_MAXHPTV70_140_CVetoBVeto.deriv.DAOD_HIGG8D1.e5299_e5984_s3126_s3136_r10724_r10726_p4133
 mc16_13TeV.364117.Sherpa_221_NNPDF30NNLO_Zee_MAXHPTV70_140_CVetoBVeto.deriv.DAOD_HIGG8D1.e5299_e5984_s3126_r10724_r10726_p4133
 mc16_13TeV.364118.Sherpa_221_NNPDF30NNLO_Zee_MAXHPTV70_140_CFilterBVeto.deriv.DAOD_HIGG8D1.e5299_e5984_s3126_s3136_r10724_r10726_p4133
 mc16_13TeV.364118.Sherpa_221_NNPDF30NNLO_Zee_MAXHPTV70_140_CFilterBVeto.deriv.DAOD_HIGG8D1.e5299_e5984_s3126_r10724_r10726_p4133
 mc16_13TeV.364119.Sherpa_221_NNPDF30NNLO_Zee_MAXHPTV70_140_BFilter.deriv.DAOD_HIGG8D1.e5299_e5984_s3126_r10724_r10726_p4133
 mc16_13TeV.364120.Sherpa_221_NNPDF30NNLO_Zee_MAXHPTV140_280_CVetoBVeto.deriv.DAOD_HIGG8D1.e5299_e5984_s3126_r10724_r10726_p4133
 mc16_13TeV.364121.Sherpa_221_NNPDF30NNLO_Zee_MAXHPTV140_280_CFilterBVeto.deriv.DAOD_HIGG8D1.e5299_e5984_s3126_r10724_r10726_p4133
 mc16_13TeV.364122.Sherpa_221_NNPDF30NNLO_Zee_MAXHPTV140_280_BFilter.deriv.DAOD_HIGG8D1.e5299_e5984_s3126_s3136_r10724_r10726_p4133
 mc16_13TeV.364122.Sherpa_221_NNPDF30NNLO_Zee_MAXHPTV140_280_BFilter.deriv.DAOD_HIGG8D1.e5299_e5984_s3126_r10724_r10726_p4133
 mc16_13TeV.364123.Sherpa_221_NNPDF30NNLO_Zee_MAXHPTV280_500_CVetoBVeto.deriv.DAOD_HIGG8D1.e5299_e5984_s3126_r10724_r10726_p4133
 mc16_13TeV.364124.Sherpa_221_NNPDF30NNLO_Zee_MAXHPTV280_500_CFilterBVeto.deriv.DAOD_HIGG8D1.e5299_e5984_s3126_r10724_r10726_p4133
 mc16_13TeV.364125.Sherpa_221_NNPDF30NNLO_Zee_MAXHPTV280_500_BFilter.deriv.DAOD_HIGG8D1.e5299_e5984_s3126_s3136_r10724_r10726_p4133

mc16_13TeV.364513.Sherpa_222_NNPDF30NNLO_tautaugamma_pty_70_140.deriv.DAOD_HIGG8D1.e5982_e5984_s3126_r10724_r10726_p4133
 mc16_13TeV.364514.Sherpa_222_NNPDF30NNLO_tautaugamma_pty_140_E_CMS.deriv.DAOD_HIGG8D1.e5928_e5984_s3126_r10724_r10726_p4133
 mc16_13TeV.364522.Sherpa_222_NNPDF30NNLO_enugamma_pty_15_35.deriv.DAOD_HIGG8D1.e5928_e5984_s3126_r10724_r10726_p4133
 mc16_13TeV.364523.Sherpa_222_NNPDF30NNLO_enugamma_pty_35_70.deriv.DAOD_HIGG8D1.e5928_e5984_s3126_r10724_r10726_p4133
 mc16_13TeV.364524.Sherpa_222_NNPDF30NNLO_enugamma_pty_70_140.deriv.DAOD_HIGG8D1.e5928_e5984_s3126_r10724_r10726_p4133
 mc16_13TeV.364525.Sherpa_222_NNPDF30NNLO_enugamma_pty_140_E_CMS.deriv.DAOD_HIGG8D1.e5928_e5984_s3126_r10724_r10726_p4133
 mc16_13TeV.364527.Sherpa_222_NNPDF30NNLO_munugamma_pty_15_35.deriv.DAOD_HIGG8D1.e5928_e5984_s3126_r10724_r10726_p4133
 mc16_13TeV.364528.Sherpa_222_NNPDF30NNLO_munugamma_pty_35_70.deriv.DAOD_HIGG8D1.e5928_e5984_s3126_r10724_r10726_p4133
 mc16_13TeV.364529.Sherpa_222_NNPDF30NNLO_munugamma_pty_70_140.deriv.DAOD_HIGG8D1.e5928_e5984_s3126_r10724_r10726_p4133
 mc16_13TeV.364530.Sherpa_222_NNPDF30NNLO_munugamma_pty_140_E_CMS.deriv.DAOD_HIGG8D1.e5928_e5984_s3126_r10724_r10726_p4133
 mc16_13TeV.364532.Sherpa_222_NNPDF30NNLO_taunugamma_pty_15_35.deriv.DAOD_HIGG8D1.e5928_e5984_s3126_r10724_r10726_p4133
 mc16_13TeV.364533.Sherpa_222_NNPDF30NNLO_taunugamma_pty_35_70.deriv.DAOD_HIGG8D1.e5928_e5984_s3126_r10724_r10726_p4133
 mc16_13TeV.364534.Sherpa_222_NNPDF30NNLO_taunugamma_pty_70_140.deriv.DAOD_HIGG8D1.e5928_e5984_s3126_r10724_r10726_p4133
 mc16_13TeV.364535.Sherpa_222_NNPDF30NNLO_taunugamma_pty_140_E_CMS.deriv.DAOD_HIGG8D1.e5928_e5984_s3126_r10724_r10726_p4133
 mc16_13TeV.410560.MadGraphPythia8EvtGen_A14_tZ_4fl_tchan_noAllHad.deriv.DAOD_HIGG8D1.e5803_e5984_s3126_r10724_r10726_p4133
 mc16_13TeV.410408.aMcAtNloPythia8EvtGen_tWZ_Ztoll_minDR1.deriv.DAOD_HIGG8D1.e6423_e5984_s3126_r10724_r10726_p4133
 mc16_13TeV.364242.Sherpa_222_NNPDF30NNLO_WWW_3l3v_EW6.deriv.DAOD_HIGG8D1.e5887_e5984_s3126_r10724_r10726_p4133
 mc16_13TeV.364243.Sherpa_222_NNPDF30NNLO_WWZ_4l2v_EW6.deriv.DAOD_HIGG8D1.e5887_e5984_s3126_r10724_r10726_p4133
 mc16_13TeV.364244.Sherpa_222_NNPDF30NNLO_WWZ_2l4v_EW6.deriv.DAOD_HIGG8D1.e5887_e5984_s3126_r10724_r10726_p4133
 mc16_13TeV.364245.Sherpa_222_NNPDF30NNLO_WZZ_5l1v_EW6.deriv.DAOD_HIGG8D1.e5887_e5984_s3126_r10724_r10726_p4133
 mc16_13TeV.364246.Sherpa_222_NNPDF30NNLO_WZZ_3l3v_EW6.deriv.DAOD_HIGG8D1.e5887_e5984_s3126_r10724_r10726_p4133
 mc16_13TeV.364247.Sherpa_222_NNPDF30NNLO_ZZZ_6l0v_EW6.deriv.DAOD_HIGG8D1.e5887_e5984_s3126_r10724_r10726_p4133
 mc16_13TeV.364248.Sherpa_222_NNPDF30NNLO_ZZZ_4l2v_EW6.deriv.DAOD_HIGG8D1.e5887_e5984_s3126_r10724_r10726_p4133
 mc16_13TeV.364249.Sherpa_222_NNPDF30NNLO_ZZZ_2l4v_EW6.deriv.DAOD_HIGG8D1.e5887_e5984_s3126_r10724_r10726_p4133
 mc16_13TeV.342284.Pythia8EvtGen_A14NNPDF23LO_WH125_inc.deriv.DAOD_HIGG8D1.e4246_e5984_s3126_r10724_r10726_p4133
 mc16_13TeV.342285.Pythia8EvtGen_A14NNPDF23LO_ZH125_inc.deriv.DAOD_HIGG8D1.e4246_e5984_s3126_r10724_r10726_p4133
 mc16_13TeV.341998.aMcAtNloHppEG_UEEE5_CTEQ6L1_CT10ME_tWH125_gamgam_yt_plus1.deriv.DAOD_HIGG8D1.e4394_e5984_s3126_r10724_r10726_p4133
 mc16_13TeV.410389.MadGraphPythia8EvtGen_A14NNPDF23_ttgamma_nonallhadronic.deriv.DAOD_HIGG8D1.e6155_e5984_s3126_r10724_r10726_p4133
 mc16_13TeV.410470.PhPy8EG_A14_ttbar_hdamp258p75_nonallhad.deriv.DAOD_HIGG8D1.e6337_e5984_s3126_r10724_r10726_p4133
 mc16_13TeV.410472.PhPy8EG_A14_ttbar_hdamp258p75_dil.deriv.DAOD_HIGG8D1.e6348_e5984_s3126_r10724_r10726_p4133
 mc16_13TeV.346343.PhPy8EG_A14NNPDF23_NNPDF30ME_ttH125_allhad.deriv.DAOD_HIGG8D1.e7148_e5984_s3126_r10724_r10726_p4133
 mc16_13TeV.346343.PhPy8EG_A14NNPDF23_NNPDF30ME_ttH125_allhad.deriv.DAOD_HIGG8D1.e7148_e5984_a875_r10724_r10726_p4133
 mc16_13TeV.346344.PhPy8EG_A14NNPDF23_NNPDF30ME_ttH125_semilep.deriv.DAOD_HIGG8D1.e7148_e5984_a875_r10724_r10726_p4133
 mc16_13TeV.346344.PhPy8EG_A14NNPDF23_NNPDF30ME_ttH125_semilep.deriv.DAOD_HIGG8D1.e7148_e5984_s3126_r10724_r10726_p4133
 mc16_13TeV.346345.PhPy8EG_A14NNPDF23_NNPDF30ME_ttH125_dilep.deriv.DAOD_HIGG8D1.e7148_e5984_a875_r10724_r10726_p4133
 mc16_13TeV.346345.PhPy8EG_A14NNPDF23_NNPDF30ME_ttH125_dilep.deriv.DAOD_HIGG8D1.e7148_e5984_s3126_r10724_r10726_p4133